UNIVERSITÀ DEGLI STUDI DI VERONA

DEPARTMENT OF

BIOTECHNOLOGY

GRADUATE SCHOOL OF

NATURAL SCIENCES AND ENGINEERING

DOCTORAL PROGRAM IN

BIOTECHNOLOGY

Cycle / year **XXX /2014**

TITLE OF THE DOCTORAL THESIS

$FePO_4$ NANOPARTICLES AS A SOURCE OF NUTRIENTS FOR PLANTS: SYNTHESIS AND EVALUATION OF THEIR EFFECTS ON HYDROPONICALLY GROWN CUCUMBER AND MAIZE SEEDLINGS

S.S.D. AGR/13

Coordinator: **Prof. MASSIMO DELLEDONNE**

Tutor: **Prof. ZENO VARANINI**

Doctoral Student: **Dott. DAVIDE SEGA**

RIASSUNTO

Nanoparticelle di $FePO_4$ come fonte di nutrienti per le piante: sintesi e valutazione dei loro effetti su piantine di cetriolo e mais cresciute in idroponica.

L'efficienza d'uso dei nutrienti (NUE) delle colture è generalmente bassa, in particolare se riferita all'assorbimento di nutrienti attraverso i fertilizzanti. Una strategia per migliorare la NUE potrebbe essere lo sviluppo di nuovi e più efficienti fertilizzanti. A questo proposito le nanotecnologie potrebbero offrire un'interessante opportunità. I nanomateriali sono ampiamente utilizzati in campo medico e farmaceutico, ma la loro applicazione in agricoltura, e in particolare nella nutrizione vegetale, è agli albori.

In questo lavoro di tesi è stato da prima valutato un metodo di laboratorio per la produzione in continuo di nanoparticelle di $FePO_4$ ($FePO_4$ NPs), basato sulla miscelazione estremamente fine e rapida di una soluzione di $FeCl_3$ con una soluzione di K_2HPO_4 in una camera di miscelazione. Il sistema di prova è stato in grado di produrre particelle di $FePO_4$ più piccole di 100 nm, raggiungendo la soglia di almeno 50% delle particelle più piccole di 100 nm, valore raccomandato dall' Unione Europea per la definizione di nano materiale. È stato poi costruito un prototipo per la sintesi in continuo di $FePO_4$ NPs, utilizzando due pompe dosatrici per il pompaggio delle soluzioni, e un giunto miscelante da HPLC come camera di miscelazione. Il sistema è in grado di produrre 15 $L \cdot h^{-1}$ di sospensione di $FePO_4$ NPs grezza. È stata inoltre ottimizzata la purificazione attraverso dialisi, assieme ad un metodo di stabilizzazione delle NPs, con citrato (cappaggio), basato sull'addizione di citrato di potassio tribasico emiscelazione vigorosa con vortex, al fine di ridurre l'aggregazione e la sedimentazione delle particelle sul lungo termine.

Le $FePO_4$ NPs sono state testate per la loro efficacia come fonte di P e Fe su due colture cresciute in idroponica, cetriolo (*Cucumis sativus*) e mais (*Zea mays*). Gli esperimenti sono stati ideati al fine di valutare le $FePO_4$ NPs come fonte di entrambi i nutrienti, oppure come fonte di solo P o solo Fe. Per questa ragione, come controlli negativi sono state usate piante cresciute senza P (-P), senza Fe (-Fe), o senza entrambi i nutrienti (-P-Fe). Inoltre, al fine di capire se la dimensione delle particelle di $FePO_4$ potesse causare differenti effetti sulle piante, sono stati inclusi negli esperimenti dei trattamenti con $FePO_4$ non nanometrico (bulk $FePO_4$). I risultati mostrano che le $FePO_4$ NPs migliorano la disponibilità di P e Fe, rispetto alla controparte non nano, come suggerito dai valori di indice SPAD delle foglie e dalla determinazione della concentrazione dei nutrienti nei tessuti vegetali.

Osservazioni di microscopia elettronica a trasmissione (TEM) su radici di cetriolo trattate con $FePO_4$ NPs hanno rivelato che queste particelle non entrano nella pianta, suggerendo come meccanismo di cessione dei nutrienti la dissoluzione nell'apoplasto. L'analisi di espressione genica di *AtPHR1*, un regolatore chiave della risposta alla P carenza in Arabidopsis, ha messo in luce in cetriolo una sovra regolazione di *Csa3M608690* in piante cresciute con $FePO_4$ NPs. Il comportamento trascrizionale di *Csa1M024210*, omologo di *AtBTS*, suggerisce

che le piante cresciute con entrambe le forme di $FePO_4$ sono, rispetto al Fe, in buono stato nutrizionale, confermando quindi i parametri fisiologici. Per mais, la modulazione negativa del gene *ZmFER-Like*, in risposta a tutti i trattamenti, suggerisce un ruolo minore di questo gene nella regolazione dell'omeostasi del Fe in questa specie, mentre la sovraregolazione di *ZmIRO2* in piante cresciute con entrambe le forme di $FePO_4$ conferma lo stato nutrizionale sub-ottimale di queste piante.

ABSTRACT

$FePO_4$ nanoparticles as a source of nutrients for plants: synthesis and evaluation of their effects on hydroponically grown cucumber and maize seedlings.

The nutrient use efficiency (NUE) of crops is typically low, in particular referring to the uptake of nutrients applied through fertilizers. A strategy to improve the NUE could be the development of new and more efficient fertilizers. A promising field in order to achieve this goal could be the use of nanotechnology. Nanomaterials are widely used in medical and pharmaceutical fields, but their application in agriculture and in particular in plant nutrition is at its infancy.
A continuous method of $FePO_4$ nanoparticles ($FePO_4$ NPs) synthesis based on the extremely fine and rapid mixing of a $FeCl_3$ solution with a K_2HPO_4 solution in a mixing chamber was tested for its effectiveness with a laboratory-made system. The proof-of-concept could produce $FePO_4$ particles smaller than 100 nm, reaching the threshold of 50% of particles smaller of 100 nm, a value that is recommended by the European Union for the definition of nanomaterial. A pilot plant for the continuous $FePO_4$ NPs synthesis was set up, using two dosing pumps for solutions pumping, and an HPLC mixing tee as mixing chamber. The system could produce 15 $L \cdot h^{-1}$ of raw $FePO_4$ NPs suspension. Purification through dyalisis was optimized, together with a stabilization method of $FePO_4$ NPs, called citrate capping, based on the adding of tribasic potassium citrate and thorough vortexing, in order to reduce aggregation and sedimentation of particles on long time periods.
$FePO_4$ NPs were then tested for their effectiveness as source of P and Fe on two hydroponically grown crop species, cucumber (*Cucumis sativus*) and maize (*Zea mays*). The experiments were designed in order to evaluate the effect of $FePO_4$ NPs as source of both nutrients, or source of sole P and Fe. For this reason, as negative controls were used plants grown without P (-P), without Fe (-Fe), or without both nutrients (-P-Fe). In addition, in order to analyze if the size of $FePO_4$ particles could cause different effects on plants, we included in the experiment a treatment with non-nanometric $FePO_4$ (bulk $FePO_4$). The results showed that nano-sized $FePO_4$ improved the availability of P and Fe, if compared to the non-nano counterpart, as demonstrated by SPAD indexes of leaves and the determination of nutrients concentrations in tissues.
Transmission Electron Microscopy (TEM) observations on cucumber roots treated with $FePO_4$ NPs revealed that these particles did not enter into the plant, suggesting as mechanism of delivery of nutrients the dissolution in the apoplast.
Gene expression analysis of homologs of *AtPHR1*, a key regulator of the response to P starvation in Arabidopsis, revealed in cucumber an upregulation of *Csa3M608690* in plants grown with $FePO_4$ NPs. The transcriptional behavior of *Csa1M024210*, homologs of *AtBTS*, suggested that plants grown with both forms of $FePO_4$ are, with respect of Fe, in good nutritional conditions thus confirming physiological parameters. For maize, the negative modulation of *ZmFER-Like* gene in response to all treatments suggested a minor role of this gene in the regulation of Fe homeostasis in this plant species, while the upregulation of

ZmIRO2 in plants grown with both forms of $FePO_4$ confirmed the sub-optimal nutritional state of the plants.

INDEX

1 INTRODUCTION

1.1 Foreword

World population is estimated to increase up to 8.6 billion in 2030, and to further increase to 9.8 billion to 2050, reaching 11.2 billion in 2100 (United Nations, 2017). The main contributors to such an increase in population will be African countries, followed by Asian ones (Figure 1).

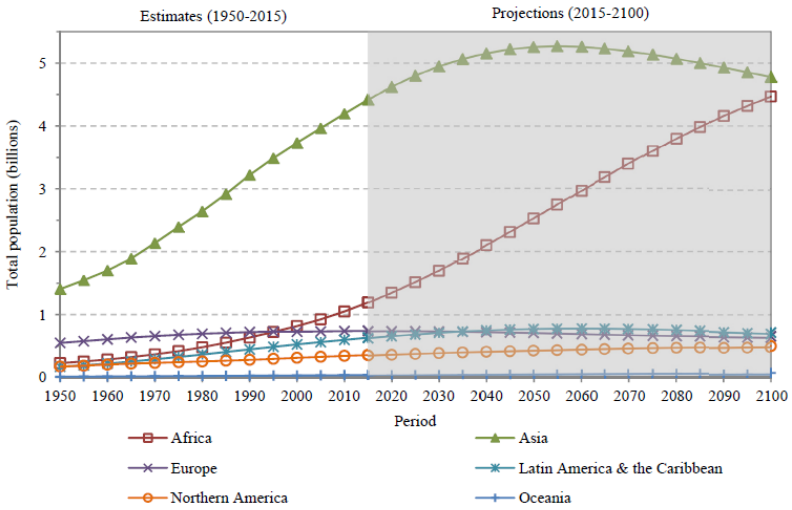

Figure 1: Projection of population by region to 2100 (United Nations, 2017).

However, the increase in population is not the only factor that will affect food demand. It is also estimated that developing countries will face a significant transition from a mainly rural population to a mainly urban one. Higher incomes will promote a rise in the demand of animal proteins like meat and dairy products, and all these factors will cause a further considerable increase in the demand of agricultural production. In order to meet these requires, global agricultural production will need to increase of about 50 percent within the year 2050. In detail, Sub-Saharan Africa and South Asia agriculture production will need to more than double, while the production of the rest of the world will have to be one third more than in 2012 (FAO, 2017).

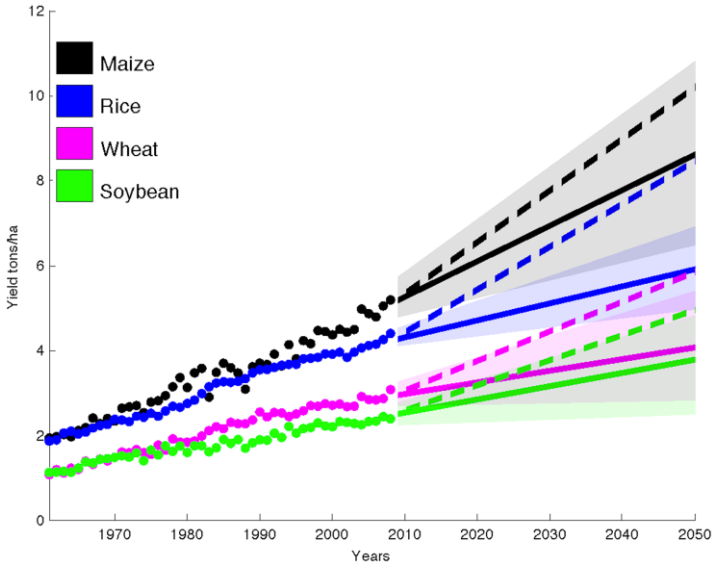

Figure 2: Global projections of crops yield with an average annual increase of 2.4% (dashed line) and with the actual trend (solid line) without variations in land used for cultivation (Ray et al., 2013)**.**

Nevertheless as shown in Figure 2, actual trends in crops yield increase are not enough to satisfy the need estimated in 2050,. To meet the future demand, crops yield will have to increase at 2.4% per year for the main four crops (maize, rice, wheat and soybean), value that is barely reached in some countries for some crops, whereas in other cases even decreases of yields are reported (Ray et al., 2013).

Moreover, environmental issues impose to avoid the expansion of agricultural land at the expense of forests and wild lands, and cultivable soil area balance is negative due to soil desertification, erosion, salinization, compaction and urbanization. For this and other factors, the average per capita cultivated area is decreasing being estimated to be around 0.2 hectares, while it was 0.27 hectares at the early 2000s (FAO, 2017).

The importance of exploring and apply innovation and techniques that can improve crops yield is therefore evident; about half of the worldwide crop yield increase and productivity during the last five decades can be ascribed to genetic improvement, while the other half to farming practices (Baligar et al., 2001), including irrigation, pests control and the use of chemical fertilizers (Figure 3) (Tilman et al.2002).

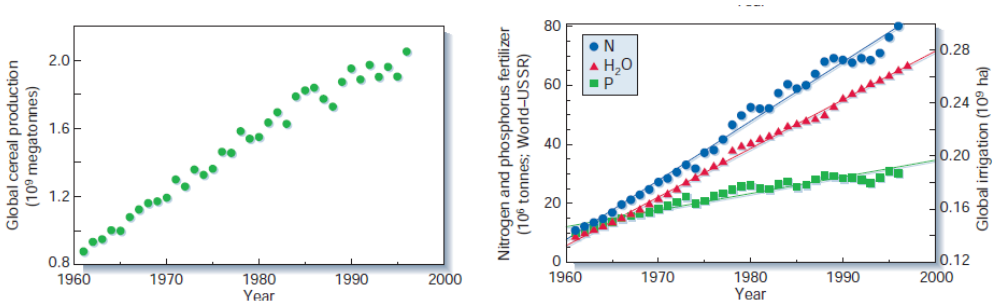

Figure 3: Correlation between the increase of global cereal production (left panel) and the application of irrigation, and nitrogen and phosphorus fertilizers (right panel). Adapted from Tilman et al. (2002)**.**

The importance of fertilizers in crop production is well known and established, and modern cultivation cannot be competitive without them. On the other hand, Nutrient Use Efficiency (NUE) of fertilizers is low, with values lower than 50% for nitrogen, around 40% for potassium and around 10-20% for phosphorus (Baligar et al., 2001). These values show how the efficiency of fertilizers represents a limit both for the economy and the sustainability of crops production. In principle crop NUE could be ameliorated through genetic improvement. However this requires a deep understanding of the mechanisms underlying the acquisition of nutrients from soil and their distribution within the plant. On the other hand, also fertilizers could be a matter of improvement, optimizing for example their nutrients release and availability, and new fields such as nanotechnology can help us in reaching this aim.

1.2 Plant mineral nutrition

As autotrophic organisms, plants need for their growth and development light, water, carbon dioxide and a series of nutrient elements. The essential nutrients for plants growth are 17, with C, H and O that are mainly absorbed through air and water, while the other 14 essential nutrients are absorbed through soil solution, and are generally defined as macronutrients or micronutrients, according to their relative concentration in plants tissues:

- macronutrients (N, P, K, S, Ca, Mg): those elements that are required and present in high concentration;
- micronutrients (Fe, Mn, B, Zn, Cu, Mo, Cl, Ni) that are required in very low concentrations or in traces.

The requisites for defining essential an element were defined by Arnon and Stout, (1939) in the following way: a) when the element is absent the plant cannot complete its lifecycle; b) the function of the element is specific, and cannot be replaced by another element; c) the element is directly involved in plant metabolism, or is required for a specific metabolic step, such as an enzyme reaction.
More recently, Nielsen (1984) proposed another definition: a nutrient is defined essential if its reduction under a certain concentration into a given tissue, determines a damage of a physiological function that is function of the concentration, and disappears once the element is re-supplied.
Beyond their relative concentration in tissues, mineral nutrients can also be classified according to their biological function.
Mengel and Kirkby (2001) proposed a classification that divides nutrients in 4 groups, and also includes the non-essential elements Na and Si:

- group 1: C, H, O, N e S; major constituents of sugars, proteins, lipids and nucleotides; their assimilation occurs through oxidation and reduction reactions
- group 2: P, B e Si; esterification with alcohol groups; phosphates are involved in energy transfer reactions.
- group 2: K, Ca, Mg, Cl, Mn e Na; establishing and controlling of the osmotic and electrochemical potentials, bridging of reaction partners.
- group 4: Fe, Cu, Zn e Mo; prosthetic group of enzymes and mediators of electron transport reactions through valence change.

The main source of these elements for plants is soil, where they are present with different relative amounts and availability, depending on soil nature and composition. In fact, the presence in the soil of a given element is not sufficient for its absorption, but it has to be available, which means that it has to be able to reach and interact with roots. Each nutrient can be present in various forms, that can affect its bioavailability. If plants can not acquire a nutrient element in an amount that is enough to sustain its requirements, deficiency symptoms appear. In particular, P and Fe are essential mineral nutrients that are often scarcely available

for plants. Iron is present in the soil in high total amounts, but it is scarcely available in aerobic soils. It is estimated that Fe deficiency occurs in about 30% of soils (Mori, 1999a) while P deficiency occurs in almost 65% of soils (Mori, 1999b; Kochian et al., 2004a), and for these reason are often limiting factors for agricultural productivity.

1.3 Phosporous

1.3.1 The role of phosphorous in plants

Phosphorous (P) is an essential macronutrient for plants, that represents about 0.2-1% of plants dry matter, and is absorbed as inorganic phosphate (Pi). It is important for plant physiology and nutrition because it is both a structural element and a mediator of energy transfer.
Pi can be considered a structural element of nucleic acids, those, as components of DNA and RNA, are fundamental in the conservation and translation of the genetic information. In both DNA and RNA, Pi acts as a bridge between ribonucleoside units allowing the formation of these macromolecules.
As bridging element, Pi is also fundamental in phospholipids, where it is esterified with a diglyceride on one side, and with another molecule (alcohol, amine or amino acid) on the other. This makes phospholipids amphipathic, with long lipophilic tales and polar regions, and this structure determines their function, making stable biomembranes.
Phosphate esters bonds and anhydrid bond are mediators of the cellular energy transfer. The energy liberated during glycolysis, aerobic respiration, or photosynthesis is used for the synthesis of anhydrid bond, and upon hydrolysis 30 kJ per mole ATP are released. This energy can be transferred to other compounds through phosphorylation reactions, activating them. In other reactions inorganic pyrophosphate (PPi) is released, and is the adenosine group that remains bound to the substrate. PPi release is fundamental in many biosynthetic processes such as coenzyme A acylation, adenosine phosphosulphate formation, sucrose formation in the cytosol and of starch in chloroplasts (Marschner's, 2012). Moreover, many enzymatic activities are modulated by phosphorylation mediated by kinase proteins (Budde and Chollet, 1988).
Pi compartmentation between cytosol and chloroplast is essential for the regulation of metabolic pathways of these subcellular compartments. Pi concentration in chloroplasts stroma influences photosynthesis: under full light a Pi concentration of 2.0-2.5 mM for the maximum photosynthesis is needed, while it is almost completely inhibited when Pi concentration goes lower than 1.4-1.0 mM (Robinson and Giersch, 1987; Heber *et al.*, 1989).

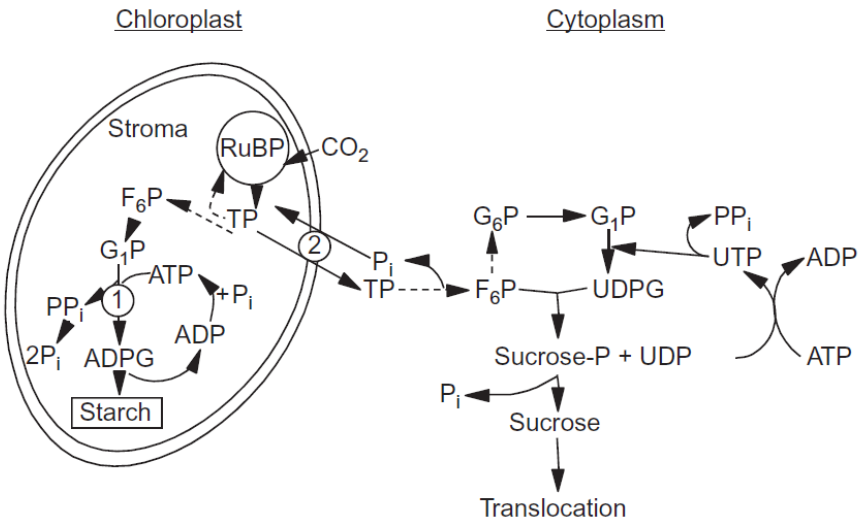

Figure 4: Involvement and regulatory role of P in starch synthesis and carbohydrate transport in a leaf cell. (1) ADP-glucose pyrophosphatase; (2) Phosphate translocator; TP: triosephosphate; GAP: glyceraldehydes-3-P; DHAP: dihydroxyacetone P; F6P: fructose-6-P; G6P: glucose-6-P. (Marschner, 2012).

On the other hand, a cytosolic increase of Pi concentration up to 1 mM stimulates net photosynthesis, but lowers the incorporation into starch of fixed carbon. In fact, at high stromal Pi concentrations (5 mM), starch synthesis is inhibited due to two different mechanisms that are present in chloroplasts: the first is that the key enzyme of starch synthesis into chloroplasts, ADP-glucose pyrophosphorylase is inhibited by Pi, and stimulated by triose phosphates. In fact, when the Pi/triose phosphates ratio is high the enzyme is inactivated (Portis, 1982). The second mechanism, regulated by Pi, is the release of triose phosphates from chloroplast, mediated by a Pi transporter located in the inner membrane (Heldt et al., 1991). In this way, an high cytosolic Pi concentration causes a lowering of triose phosphates concentration in the stroma, which are needed both as substrates and as activators for starch synthesis.

In older leaves, the major part of P is stored in the vacuole, that can contain up to 85-95% of total cellular P as Pi (Lauer et al., 1989). On the contrary, in P-deficient plants the major part of Pi is located in cytosol and chloroplasts, but at very low concentrations (Lauer and Blevins, 1989). As consequence, the inhibition of triose phosphates export from chloroplast causes an accumulation of starch in this organelle: it is one of the major symptoms observed in P-deficient plants.

Sugars and starch accumulation in leaves of P-deficient plants can also be caused by limited sucrose exportation, as consequence of a lack of ATP. In fact, sucrose is loaded to the phloem through cotransport with protons, and the proton gradient is generated by plasma membrane (PM) H^+-ATPases. The main forms of P stored in seeds are the salts of phytic acids, phytates (Lott et al., 2009). Phytic acids can form low solubility salts with various cations, such as Ca^{2+}, Mg^{2+}, K^+, and also Fe^{3+} and Zn^{2+} (Wang et al., 2008), and represents in seeds also the main storage form of K^+ and Mg^{2+}, and also Ca^{2+} and Zn^{2+} (Ockenden et al., 2004; Lott et al., 2009).

Also in pollen grains the major storage form of P are phytates of K^+-Mg^{2+}-Ca^{2+}, that are degraded during germination (Scott and Loewus, 1986; Baldi et al., 1987).

Phytate function is to be a source of P for membrane lipids and nucleic acids synthesis (Lott and Vollmer, 1973).

1.3.2 The behavior of P in the soil

P is present in the soil mainly in 4 forms: in solution, adsorbed to inorganic colloids surface, precipitated as crystalline or amorphous phosphates, and as component of soil organic matter. P concentrations in soil solution, as $H_2PO_4^-$ /HPO_4^{2-} are very low (0.1-10 μM) because different reactions are involved in its precipitation and retention. The majority of phosphate ions in soil is specifically adsorbed mainly on Fe and Al oxides and colloidal hydroxides, a process that limits its availability. Moreover, considerable amounts of PO_4^{3-} can precipitate as salts (see below). About 50-80% of soil P is present as organic form, and a prerequisite for its absorption is the activity of phosphatases, which are mainly released from roots and can hydrolyze it. For these reasons, even if P represents about 0.1% of the soil solid fraction P is often a limiting element for plants growth and development (Barber, 1984; Maathuis, 2009). Overall, the main factor affecting P availability in soil is pH. In fact, in acidic soils (pH<5.5) Pi availability decreases due to the precipitation as variscite ($AlPO_4 \cdot H_2O$) and/or strengite ($FePO_4 \cdot 2H_2O$), and at pH> 7 it can precipitate as tricalcic phosphate ($Ca_3(PO_4)_2$). Furthermore, in this last condition it can also be adsorbed on calcite. Therefore, the highest availability is reported for soils having pH values around 5.5-6.5.

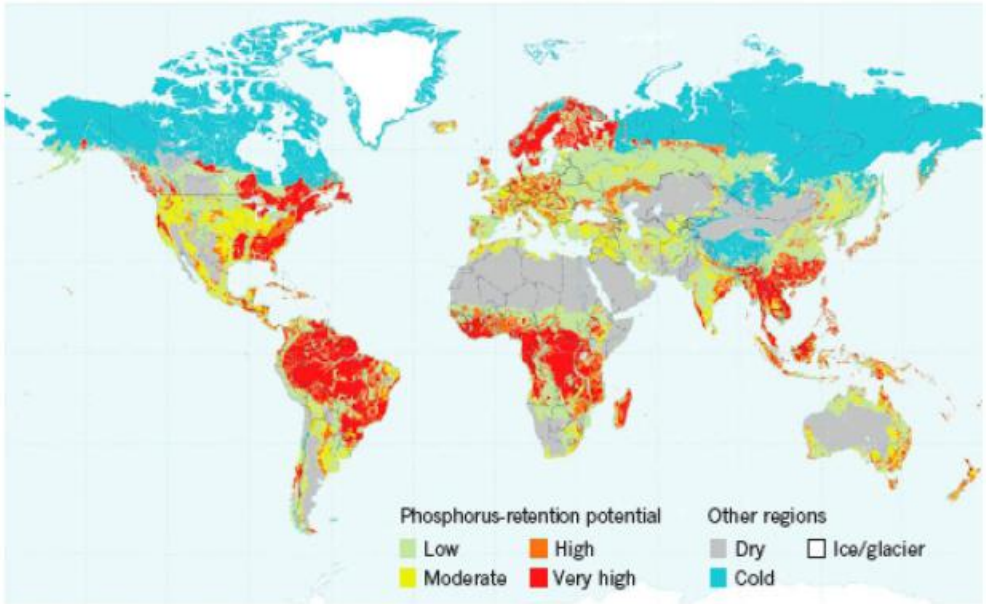

Figure 5: Map representing the phosphorous retention potential of soils on earth. (https://www.nrcs.usda.gov/wps/portal/nrcs/detail/soils/use/?cid=nrcs142p2_054014)

In soil, phosphate anion moves towards roots mainly through diffusion only for few millimeters: a limited mobility if compared to K^+ and NO_3^- (Hendriks et al., 1981).

For all these reasons, P fertilization fixes only temporarily the problem of its low availability. When P fertilizers are applied, only 10-25% is absorbed by plants, and the major part of it is retained by soil.

1.3.3 Symptoms and responses to P deficiency in plants

P deficiency in plants causes evident morphological modifications. The first and more visible symptom is an alteration of the shoot/root ratio, in favor of the latter, in order to increase soil exploration. The development of lateral roots is promoted, together with root hair production, reducing the development of the aerial part (Freeden et al., 1989; Lynch et al., 1991). P is a mobile element in plant, and if present in limiting amounts transferred from older to younger leaves. So older leaves exhibit first the deficiency symptoms. The inhibition of leaf expansion occurs, while chlorophyll production remains constant, conferring to the leaf a dark green coloration (Hecht-Buchholz, 1967), together with a purpling of leaf margins caused by anthocyanins accumulation (Figure 6).

Figure 6: Severe P deficiency in maize plant. (http://www.greenersideoflife.com)

A peculiar example of an efficient plant for P acquisition is white lupin (*Lupinus albus* L.): it forms dense root zones called cluster roots, that are effective in modifying rizospheric soil and solubilize P (Figure 7).

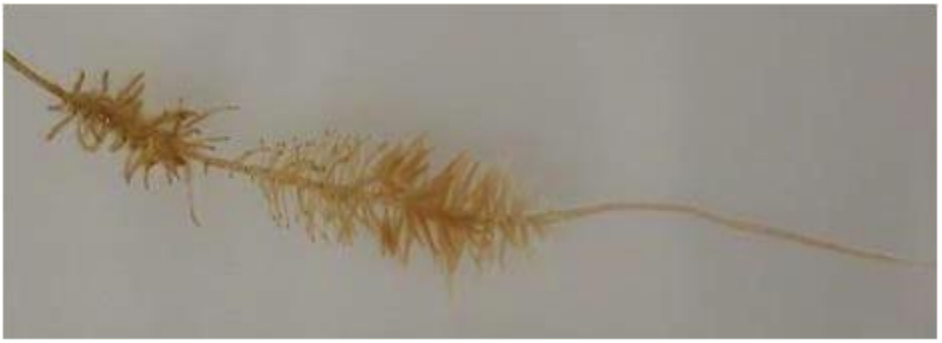

Figure 7: Cluster roots of 4-week-old white lupin, grown under phosphate starvation (Tomasi et al., 2008).

At the physiological level, P-deficiency causes several responses. P-deficient plants release as roots exudates high amounts of organic acids, that chelate Ca, Fe and Al, thereby releasing phosphate that is bound to these elements in soil minerals. Exudation of organic acids is tightly linked to protons extrusion, that balances the negative charges of the carboxylates (Tomasi et al., 2009). Also hydrolytic enzymes such as phosphatases and phytases can be extruded, in fact their role is to release P that is bound to the soil organic fraction. The exudation of these enzymes is finely regulated, and the expression of genes codifying for them is inversely proportional to the concentration of available P (Wasaki et al., 2003). Together with carboxylic acids, some plants, such as white lupin, release isoflavonoids, that can help P-acquisition both directly by mobilizing inorganic phosphorus and indirectly by reducing the microbial citrate mineralization and the activity of enzymes involved in microbial P acquisition, so acting in a synergic way with the other responses (Tomasi et al., 2008).

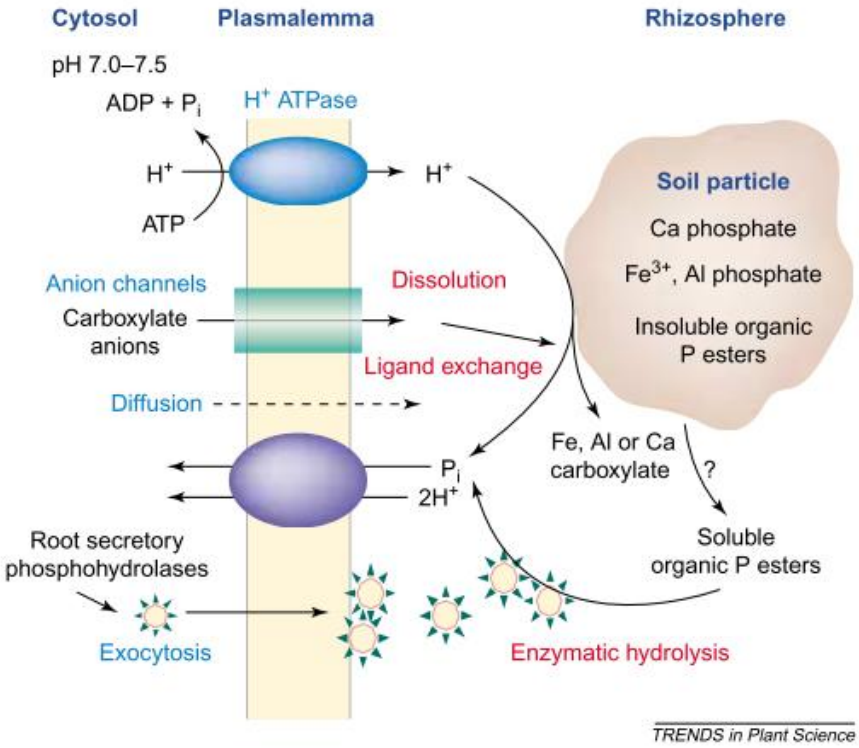

Figure 8: Model for root-induced chemical phosphate mobilization in the rhizosphere by exudation of carboxylates, protons and root secretory phosphohydrolases (Neumann and Martinoia, 2002).

Under Pi limiting condition one striking feature is that plants strongly induce the expression of high affinity phosphate transporters. Being Pi concentration in the soil solution (0.1-10 μM) much lower than those whitin the cell (2-20 mM), the anion has to be absorbed against the electrochemical gradient, through co-transport with two protons by specific transporters, belonging to PHT1 family (Schachtman et al. 1998; Hinsinger 2001). These are transmembrane transporters with 12 alpha-helixes whose expression raises when the available Pi in soil and Pi pool in plant tissues are low. Another transporter playing an important role in the

economy of Pi distribution is PHO1.H1. that loads Pi into the xylem. Its gene is strongly upregulated in P deficiency conditions (Hamburger et al., 2002).
The responses of plants to low P availability are controlled at the transcriptional level. In *Arabidopsis thaliana* PHR1 (Phosphate Response 1) and its homolog PHL1 (PHR1-Like) are important MYB-related transcription factors that are key regulators of the response to P-shortage (Sun et al., 2016). The overexpression of the genes codifying for PHR1 and PHL1 promotes the expression of effector genes as *AtPHT1* and *AtPHO1.H* (Briat et al., 2015), and enhances the tolerance to P deficiency (Nilsson et al., 2007; Matsui et al., 2013). PHR1 is also a major regulator in the change of primary and secondary metabolism (Pant, et al., 2015), membrane lipids remodeling (Pant, et al., 2015) and in the adaptation to high-light conditions in P-deficient plants (Nilsson et al., 2012).

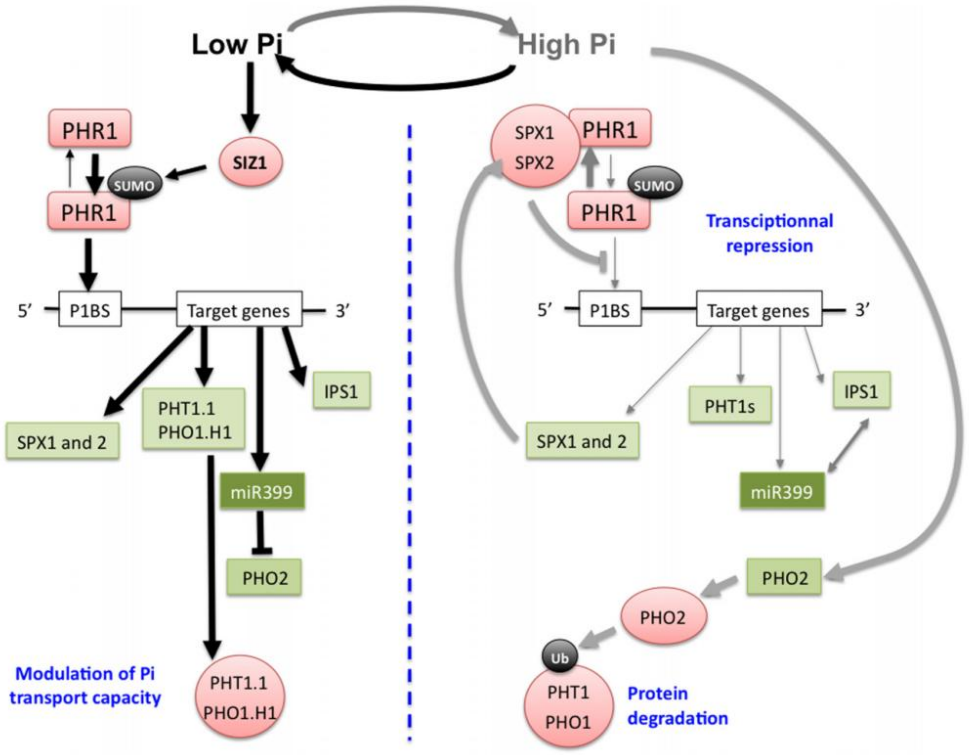

Figure 9: Schematic representation of the regulatory pathways required for plant adaptation to Pi deficiency, and the role of PHR1 (Briat et al., 2015).

In rice two orthologs of AtPHR1 are known: OsPHR1 and OsPHR2, the latter is also involved in the adaptation of root structure under P-deficiency condition (Zhou et al., 2008). In the maize genome two homolgous genes of *AtPHR1* were identified (*GRMZM2G006477* and *GRMZM2G162409*) suggesting a conserved response mechanism between monocotyledons and dicotyledons (Calderon-Vazquez et al., 2011).
Another strategy that plants evolved for enhancing P uptake is mycorrhizae formation, the association between a fungus and the plant. A detailed description of this biological process is beyond the scope of this work. However, the interaction with mycorrhizae is advantageous not only in enhancing P absorption,

but also for Ca, N and Zn uptake and in the tolerance to other abiotic stresses (Marschner, 2012).

1.3.4 Problems and perspectives of P nutrition

Considering the behavior of P in the soil system and the high level of diffusion of soils with a large P retention potential on earth, it is reasonable that this nutrient causes losses of production in almost 65% of cultivated lands. Moreover, the use efficiency of applied P fertilizers is around 10-20%. These data are worsened by the fact that the main source of P fertilizers (phosphorite) are not abundant. The US geological Survey estimated that there are 15 billions of metric tons of easily to extract phosphorite (US. Geological Survey, 2017) and 90% of these reservoirs are concentrated and controlled by five countries (China, Morocco, South Africa, United States and Giordan). It is so evident that it will be necessary to use reservoirs of minor quality, such as those located in Australia, Namibia and Perù, that need higher extraction costs and will so affect the price of fertilizers (Cordell et al., 2009). On the other hand, on the long term other alternatives will have to be developed, given that it is estimated the run out of reservoirs within 2100 (Rosemarin et al., 2009).

1.4 Iron

1.4.1 The role of iron in plants

Iron (Fe) is an essential micronutrient for plants, the more abundant in plant tissues among micronutrients reaching concentrations up to 100 ppm, and it is also the second abundant metal on the earth crust (5%), preceded by Al. (Marschner, 2012). This element can be considered both as a structural component and as a cofactor of the protein systems where it is inserted. Its main feature, as transition element, is the capacity of changing oxidation state between Fe^{2+} and Fe^{3+}. The redox potential of Fe(II)/Fe(III) couple varies depending on the ligand, thus explaining the importance of Fe in biological redox systems.
Cytochromes, the most known heme-proteins containing a Fe-porphyrin complex as prosthetic group, are key components of the redox systems in chloroplasts, mitochondria and nitrate reductase, allowing the transfer of electrons and redox potential. Moreover, plants utilize a diverse array of cytochrome P450 monooxygenases (P450s) in their biosynthetic and detoxification pathways, so plants account for more than 300 enzymes of this class (Schuler, 1996). Other heme-proteins containing Fe are catalases, and peroxidases. Catalase facilitate detoxification of H_2O_2 to water and O_2 according to the reaction:

$$2H_2O_2 \rightarrow 2H_2O+O_2$$

Peroxidases are present in various forms in many compartments. Ascorbate peroxidase, for example, detoxifies H_2O_2 in chloroplasts, while peroxidases in root cell wall catalyze the polymerization of phenols to lignin.

Fe is also part of Fe-S clusters of the non-heme Fe-S proteins and the most known of them is ferredoxin. Ferredoxin has many roles in cellular metabolism: it is responsible of the reduction of $NADP^+$ to NADPH at the end of photosynthesis; it is the source of electrons for the reduction of nitrite to ammonia operated by nitrite reductase, fundamental step nitrate assimilation, the same occurs for sulfite reductase in sulfate assimilation. Ferredoxin is also the electron donor glutamine oxoglutarateaminotransferase (GOGAT), a key enzyme for N assimilation. Other important Fe-S proteins are the isoenzymes of superoxide dismutase (SOD) which contain Fe as component of the prosthetic group (FeSOD) (Marschner, 2012). SODs detoxify superoxide free radicals by formation of H_2O_2 and can contain Cu, Zn, Mn instead of Fe as metal components (Fridovich, 1983; Sevilla et al., 1984), but in the chloroplast FeSOD is the main isoenzyme.
Fe is not only a structural component of heme, but it has also a crucial role in its biosynthesis (Figure 8); it regulates the enzymes aminolevulinic acid synthase (ALA synthase) and coproporphyrinogen oxidase.

1.4.2 The behavior of Fe in soil

Although Fe is the second abundant metal on earth crust and represents about 5% of soil dry weight, in aerated soils the concentration of Fe in solution is low, due to its precipitation as hydroxides, oxyhydroxide, and oxides, the complexation to soil organic matter (Barber, 1984). The most common Fe minerals that can be found in soils are goethite (α-FeOOH), hematite (Fe_2O_3), lepidocrocite (γ-FeOOH) and magnetite (Fe_3O_4).
By using a simplified approach, the low solubility of Fe^{3+} in soil can be explained by the low solubility product constant (Kps) of $Fe(OH)_3$, referred to the following equation:

$$Fe(OH)_3 \leftrightarrow Fe^{3+} + 3OH^- \qquad Kps=10^{-39.4}$$

The solubility product constant is in relation with the concentrations of ions in solution in the following way:

$$Kps = 10^{-39,4} = Keq \cdot [Fe(OH)_3] = [Fe^{3+}] \cdot [OH^-]^3$$

Being $Fe(OH)_3$ in the solid phase, $[Fe(OH)_3] = 1$ and Fe^{3+} concentration can be calculated as:

$$[Fe^{3+}] = \frac{10^{-39.4}}{[OH^-]^3}$$

It is evident that Fe^{3+} solubility is a function of pH, and the increase of one pH unit decreases the solubility of Fe 1000 times, and *viceversa*.
For example, following the formula written above, at pH=5 $[Fe^{3+}]$ will be $4 \cdot 10^{-13}$ M, while at pH=8.5 it will be 10^{-23} M.

Consequently, only in aerated acidic soils there are appreciable concentrations of Fe^{3+} in solution. While in neutral aerated soils the concentration of Fe^{3+} is always below 10^{-15} M (Lemanceau et al., 2009), a value lower than the nutritional requirements of the majority of crops. Conversely, in conditions of persistent anaerobiosis, such as in submerged or waterlogged soils, there is an increase of Fe^{2+}, that is more soluble than Fe^{3+}.

1.4.3 Symptoms and responses to Fe deficiency in plants: *Strategy I* and *II*

Fe is not a mobile element in the plant, so its deficiency symptoms are visible first on young leaves, as the typical chlorosis (Figure 10), a fading of the green color caused by a reduction in chlorophyll production.

Figure 10: Ferric chlorosis on citrus leaves. (http://ucanr.edu/)

At a cellular level, Fe deficiency also causes a reduction in chloroplasts size and protein content in this organelle (Nishio et al., 1985; Spiller et al., 1987). The increase of de-epoxidized xanthophyll cycle pigments is also an effect of Fe-deficiency (Jiang et al., 2001). When plants are grown in controlled conditions, such as in nutrient solution, there is a strict positive correlation between leaf total Fe concentration and that of chlorophyll (Terry and Javier, 1986). This correlation, however, is poor or absent in plants grown in calcareous soils, where Fe concentration in chlorotic leaves may be similar or even higher than in green leaves. This phenomenon, called "chlorosis paradox", is thought to be the result of restricted leaf expansion and consequently a diminished dilution of Fe by growth (Römheld, 2000).

The central role of this nutrient and its low bioavailability promoted in plants the evolution of strategies for enhancing Fe uptake at the root level. These strategies involve both morphological and physiological changes, and mechanisms that allow the plant to modify rhizosphere chemistry. The strategies of plants for Fe

acquisition can be divided in two main categories: *Strategy I* typical of dycotiledons and non-gramineaceous monocotyiledons, and *Strategy II*, typical of graminaceous monocotiledons.

Strategy I

On chemical basis, this strategy relies on Fe solubilization through rhizosphere acidification (Zocchi and Cocucci, 1990), operated by an H^+-ATPase. This enzyme activity is induced by Fe-deficiency conditions and promotes the following reaction, called H^+-promoted dissolution (Stumm and Sulzberger, 1992):

$$Fe(OH)_3 + 3H^+ \rightarrow Fe^{3+} + 3H_2O$$

On the other hand, Fe^{3+} can also be solubilized by organic acids that chelates the cation. Fe^{3+} is then reduced by plasma membrane enzymes belonging to the ferric chelate oxidase reductase (FRO) family. This enzyme reduces the chelated Fe^{3+} to Fe^{2+}, using cytosolic NADPH as reducing power (Robinson et al., 1999). The Fe^{2+} is then absorbed by the high-affinity membrane transporter IRT1, a member of ZIP transporter family (Vert et al., 2002). The expression of both *AtFRO2* and *AtIRT1* vary diurnally and is increased under Fe deficiency conditions.

Moreover, recent evidence supports the existence of another mechanism for Fe mobilization, which relies on the secretion of Fe deficiency-induced secondary metabolites with Fe- mobilizing properties. Among these metabolites, phenolics, and in particular coumarins are believed to play an important role, acting as chelating agents and/or reductants and were demonstrated to have a role in the mobilization of Fe pools in cell walls and apoplast (Jin et al., 2007; Bashir et al., 2011; Ishimaru et al., 2011; Fourcroy et al., 2014; Tsai and Schmidt, 2017). However, several studies showed that the reduction rates of Fe^{3+} by root exudates are much lower than for enzymatic Fe^{3+} reduction through FRO2 (Romheld and Marschner, 1983; Schmidt, 1999).

The reduction of Fe^{3+} to Fe^{2+} can also be carried out by roots through the secretion of electrons, according to the reaction:

$$Fe(OH)_3 + 3H^+ + e^- \rightarrow Fe^{2+} + 3H_2O$$

The dissolved Fe^{2+} has a solubility higher than Fe^{3+}, as suggested by the solubility product constant of $Fe(OH)_2$, that is $10^{-15.1}$.

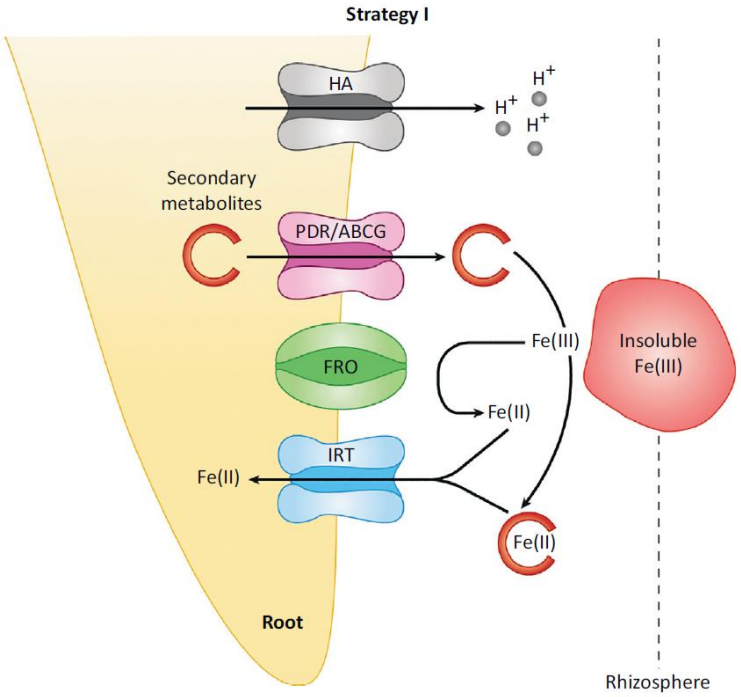

Figure 11: Model for root responses to iron deficiency in Strategy I plants: increased acidification of the rhizosphere by H^+-ATPase, secretion of secondary metabolites with iron-mobilizing properties through pleiotropic drug resistance (PDR) or ATP-binding cassette (ABCG) transporters, induction of ferric reductase activity, reduction of Fe(III)-chelates to Fe^{2+}, uptake of Fe^{2+} across the plasma membrane by high-affinity transporters. Adapted from Tsai and Schmidt (2017)**.**

On the morphological aspect, Fe deficiency is associated to the inhibition of root elongation, increase in the diameter of apical root zones and root hair formation (Marschner, 2012). These morphological changes are often linked to the formation of rhizodermal transfer cells, that are the sites of the increased proton extrusion and reducing activity (Kramer et al., 1980).

The homeostasis of Fe, together with the expression of effector genes involved in the response to Fe deficiency of *Strategy I* plants, is regulated at the transcriptional level by a rich network of bHLH (basic helix-loop-helix) transcription factors.

In *Arabidopsis thaliana*, two regulatory networks, the FER-LIKE IRON DEFICIENCY INDUCED TRANSCRIPTION FACTOR (FIT) network and the POPEYE (PYE) network, are involved into the modulation of Fe deficiency responses (Ivanov*et al*. 2012). Both FIT and PYE are members of the basic helix-loop-helix (bHLH) transcription factor family, suggesting the importance of this protein family in Fe homeostasis. FIT is known to be induced in response to Fe deficiency and it is involved in the regulation of FRO2 and IRT1 (Bauer et al. 2007). PYE is considered a positive regulator of Fe absorption and it was also reported to be upregulated in Fe deficiency conditions in root pericycle (Long et al., 2010). Another important regulator of Fe homeostasis is BRUTUS (BTS) that is considered a negative regulator of Fe absorption. *AtBTS* was shown to be upregulated in Arabidopsis in the perycycle of Fe-deficient roots. A similar transcriptional behavior was reported for *At*PYE whose expression is regulated by AtBTS through the interaction with other PYE-Like factors (Long et al., 2010).

This fine co-regulation between *AtPYE* and *AtBTS*, even if they have opposite roles in the Fe deficiency response, is explained to occur for maintaining Fe homeostasis under fluctuating growth conditions. In fact, it requires a balance of many processes, including the inhibition and the activation of Fe uptake from the rhizosphere and intercellular and intracellular Fe transport.

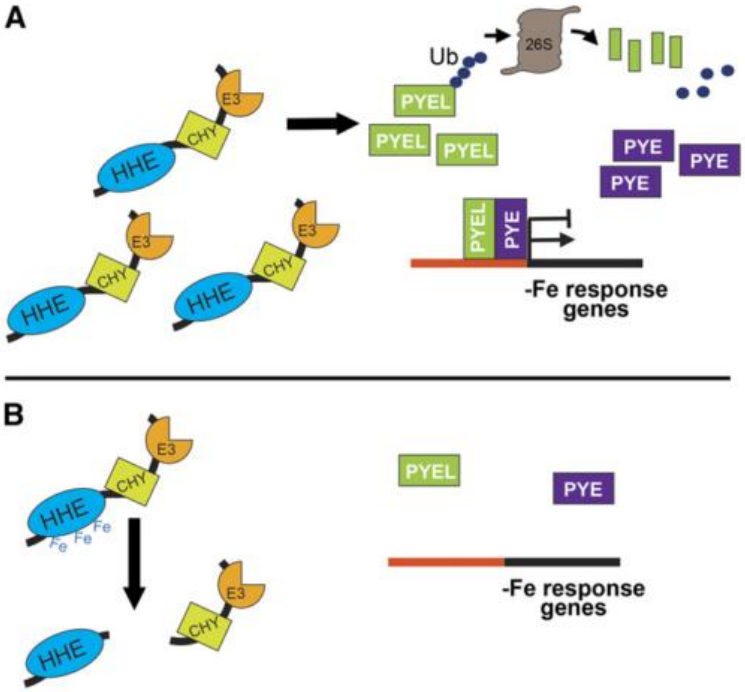

Figure 12: Model for BTS protein stability and function (Selote et al., 2015).

BTS is transcriptionally induced by Fe deficiency along with the bHLH transcription factors PYE and PYEL. Under low-Fe conditions, the BTS protein is more stable and regulates PYEL/PYE regulatory activity through its E3 ligase activity to modulate and fine-tune PYEL/PYE-mediated Fe deficiency response in plants (Figure 12A). Upon recovery of Fe, transcriptional induction of BTS, PYE, and PYEL decreases. Elevated levels of the micronutrient are sensed through the hemerythrin (HHE) cation-binding domains, altering BTS conformation and stability. This response results in the proteolysis of BTS protein, thereby further reducing the Fe responsive E3 ligase capacity of the cells (Figure 12B) (Long et al., 2010; Selote et al., 2015).

However, in calcareous soils *Strategy I* is not so effective. In fact, carbonates can react with extruded protons forming bicarbonate:

$$CaCO_3 + H^+ \rightarrow Ca^{2+} + HCO_3^-$$

And the bicarbonate anion can also buffer the acidification, according to the following reaction:

$$HCO_3^- + H^+ \rightarrow H_2CO_3 \rightarrow CO_2 + H_2O$$

Therefore, the acidification strategy is hampered by the buffering capacity of the soil. Moreover, it was demonstrated that bicarbonate could induce Fe chlorosis by inhibiting the expression of the ferric reductase, the Fe transporter and the H^+-ATPase genes in Arabidopsis, pea, tomato, and cucumber (Lucena et al., 2007).

Strategy II

This strategy is typical of graminaceous monocotiledons, also called Fe-efficient plants. These plants, release non-proteinogenic pepdides called phytosiderophores (PS) from the roots under Fe-deficiency (Takagi et al., 1984). PS belong to the mugineic acid family and are produced by three molecules of L-methionine that are polymerized to form nicotianamine (NA). NA, after deamination and hydroxylation, is converted to 2-deoxymugineic acid and then to other PS. The expression of genes encoding enzymes involved in this pathway are often upregulated in response to Fe deficiency (Bashir et al., 2006).

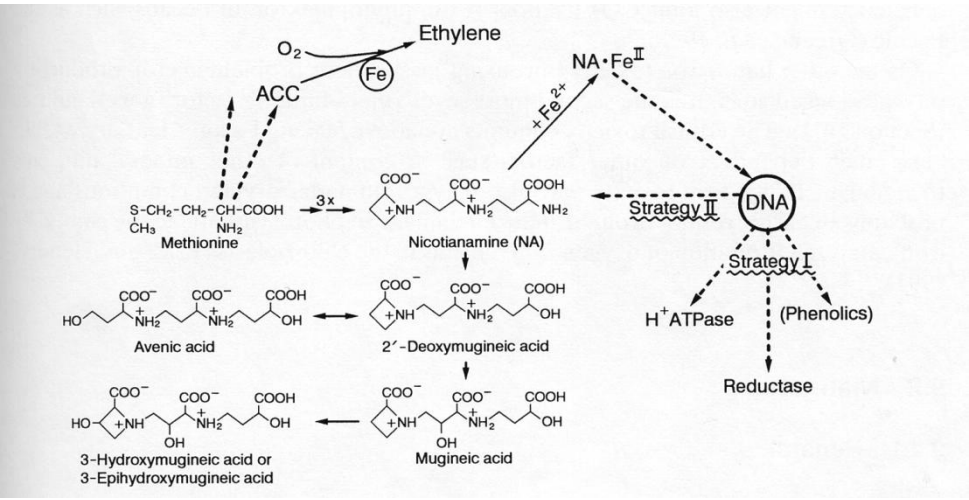

Figure 13: Model of phytosiderophore biosynthesis and other Fe-related factors in roots (Marschner, 2012).

PSs chelate Fe^{3+} in the rhizosphere and the complexes are absorbed by the plant. PSs are released by the root through a specific transporter, TOM1 (Nozoye et al., 2011) and, when the Fe(III)-PS is formed, it is absorbed by roots through another specific transporter (YS1), a proton symporter (Curie et al., 2001). The maize *yellow stripe 1* (*ys1*) mutant is deficient in the Fe^{3+}-PS uptake thus exhibiting the typical interveinal ferric chlorosis.

Figure 14: Comparison between a *ys1* mutant maize leaf (left) and a wild-type one (right) (https://www.bio.umass.edu/biology/sites/imladris.bio.umass.edu.biology/files/gbi-images/p1040707-1.jpg).

The expression of genes codifying for TOM1 and YS1 transporters is upregulated in Fe-deficiency (Curie et al., 2001; Nozoye et al., 2011) and also PS release and Fe^{3+}-PS uptake rate are enhanced in this condition (Walter et al., 1994; Schaaf et al., 2004). Moreover, PSs can also chelate Zn, Cu and other metallic cations (Schaaf et al., 2004).

All these responses are regulated at transcriptional level by various transcription factors. The best characterized transcription factor is IRON-RELATED TRANSCRIPTION FACTOR 2 (IRO2), a bHLH protein encoded in rice by *OsIRO2*. The IRO2 transcription factor that is strongly induced in Fe-deficiency conditions, positively regulates various genes related to *Strategy II* (including *NAS1*, *NAS2*, *NAAT1*, *DMAS1*, *TOM1*, and *YSL15*) and genes involved in the methionine cycle (Ogo et al., 2007). Also in maize, *ZmIRO2* (*GRMZM2G057413*) was reported to be up regulated in roots of Fe-deficient plants, confirming its role in *Strategy II* plants (Zanin et al., 2017). The presence of *Strategy I*-like mechanisms have also been hypothesized for rice. In fact this species is considered to use a combined strategy, being able to absorb both the Fe(III)-PS complex, and Fe^{2+} through an IRT transporter (Ishimaru et al., 2006). Moreover, rice plants possess an efflux transporter for phenolic compounds (phenolics efflux zero-like transporter, PEZ), which is an essential component in Fe solubilisation from apoplastic space (Bashir et al., 2011).

Zanin et al. (2017) through a transcriptomics study of the response to Fe-deficiency conditions in maize revealed the presence of *Strategy I* components usually described in dicotyledons. In fact a gene encoding a FER-Like transcription factor (*GRMZM2G107672*) was reported to be overexpressed in Fe-deficiency conditions (Zanin et al., 2017)

1.5 Fertilizers

1.5.1 Main phosphate fertilizers: production and limits

The main source of phosphate fertilizers is nowadays represented by phosphorites, or rock phosphate, a limited and non-renewable resource. Phosphate is contained in this mineral as tri-calcium phosphate ($Ca_3(PO_4)_2$), insoluble in water and so not available for plants. This salt is made soluble through a specific industrial treatment, called acid attack. Depending on the acid used for phosphorite solubilization the following products are obtained.

- Single superphosphate: is produced by the attack of phosphorite with sulfuric acid (H_2SO_4), obtaining mono-calcium phosphate ($Ca(H_2PO_4)_2$); the mixture of this salt is left in dedicated cellars for the aging, and later is milled and granulated. It has a minimum P_2O_5 content of 16% soluble in neutral ammonium citrate, (of which at least 93% soluble in water), according to UE normative.
- Concentrated superphosphate: is obtained by the addition of ortophosphoric acid (H_3PO_4) during the attack with sulfuric acid (H_2SO_4). It has a minimum P_2O_5 content of 25% soluble in neutral ammonium citrate, (of which at least 93% soluble in water), according to UE normative;
- Ortophosphoric acid (H_3PO_4): produced by the attack of phosphorite with an excess of sulfuric acid (H_2SO_4); a solution of H_3PO_4 containing $CaSO_4$ in suspension is obtained, and $CaSO_4$ is separated through filtration. The remaining solution is concentrated up to the adequate level for the final use.
- Triple superphospate: produced by the attack of phosphorite with concentrated ortophosphoric acid (H_3PO_4); it is composed almost exclusively by mono-calcium phosphate ($Ca(H_2PO_4)_2$). It has a minimum P_2O_5 content of 38% soluble in neutral ammonium citrate, (of which at least 93% soluble in water), according to UE normative; (Perelli, 2009).

The limit of phosphate fertilizers up to now available is that when applied to soils having a constitutive low P availability they are subjected to insolubilization processes, making them in short time unavailable for the plants. This problem was only partially solved through granulation, the development of modified-release fertilizers via the inclusion into bio-degradable films, and through the optimization of field application. In the end, the use efficiency of phosphate fertilizers is still very low, about 10-20%. This data, together with the non-renewable nature of phosphorite, makes it necessary to increase the use efficiency of fertilizers, making them more available and less prone to sequestration by soil.

1.5.2 Main Fe fertilizers and their limits

Fe is often a limiting nutrient in soils, especially in calcareous soils, due to its low availability. In this the application of Fe-containing fertilizers is a common

procedure, in order to restore an adequate nutritional supply and preserve crops productivity. For this purpose, the main Fe-containing fertilizers available on the market are described below.

- Ferric sulfate ($FeSO_4$): it is very cheap and generally used by foliar spaying, where it is often ineffective for its low capacity of trespassing the cuticle barrier. If applied to the soil, Fe^{2+} is rapidly oxidized to Fe^{3+} that precipitates as hydroxides, not available for plants.
- Chelates: synthetic compounds such as ferric sodium ethylenediaminetetraacetate (NaFeEDTA), ferric sodium ethylenediamine-di(o-hydroxyphenilacetate) (NaFeEDDHA), ferric sodium hydroxyethylenediaminetriacetate (NaFeHEEDTA) and ferric sodium diethylenetriaminepentaacetate (NaFeDTPA), that are characterized by a stable bond between metal cation and the chelating agent. The chelating agent stabilizes and protects the metal cation, thus preventing it from precipitation. These compounds are effective when applied through foliar spray, but are expensive and when used directly to soil they represent a temporarily solution, given that they are not retained by the soil solid fraction. Moreover, given that they are susceptible to leaching, the risk of groundwater contamination should be considered (Cesco et al., 2006).
- Complexes: in addition to chelates, also complexes of Fe with organic substances that protect the element and help the assimilation are used. These substances are mainly natural organic substances such as citrate, gluconate, lignosulfonate. The low stability of these compounds makes them unsuitable for maintaining Fe in solution, particularly when applied to calcareous soils (Lucena, 2003).

Therefore it is important to develop new Fe fertilizers with a good availability and less prone to leaching.

1.6 NPs

Nanomaterials are defined as materials with at least one dimension between 1 and 100 nanometers (nm) in size. Materials in the micrometer scale mostly exhibit physical properties that are the same as those of the bulk (ordinary scaled material) form. Conversely, materials in the nanoscale often show “novel and significantly improved physical, chemical and biological properties, phenomena and processes due to their nanoscale size”, as defined in the United States by the National Science and Technology Council (2000). On the other hand, the definition of nanomaterial in the range between 1 to 100nm is arbitrarily and the EU commission proposed another definition for nanomaterial: “material containing particles, in an unbound state or as an aggregate or as an agglomerate and where, for 50% or more of the particles in the number size distribution, one or more external dimensions is in the size range 1 to 100 nm” (Potočnik, 2011).

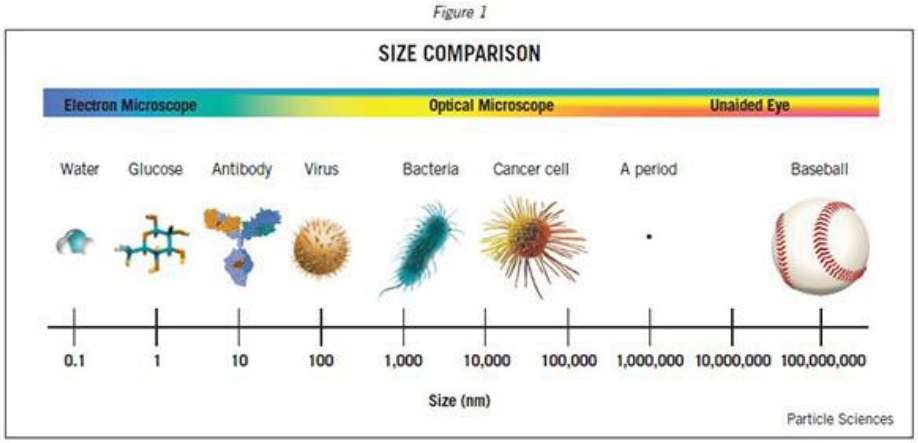

Figure 15: Comparison of the size of many objects from the nanoscale to the macroscale (http://www.particlesciences.com/services/micro-nano-technology/).

The application of nanotechnology and nanoparticles (NPs) is nowadays widespread, and spaces from nanoelectronics, catalysis, luminescence, to environmental applications such as the development of sensors for the detection of contaminants, and biological applications such as biotechnology and medicine. (Cao and Wang, 2011). In the last 10 years, particular attention was posed to the effects of NPs on plants, first on the toxicological aspect, and later on the nutritional aspect. These aspects are treated in the following paragraph.

1.6.1 Effects of NPs on plants

1.6.1.1 Toxicological aspects

Currently, a number of studies have demonstrated the toxicity of some NPs to plant species. ZnO NPs have been shown to reduce ryegrass (*Lolium perenne*) biomass significantly when grown in hydroponic conditions (Lin and Xing, 2008). The authors also reported the shrinking of root tips, the highly vacuolation or collapse of root epidermal and cortical cells. In this case, the toxicity was mainly observed in the root apparatus and shoot Zn contents under ZnO NPs treatments were much lower than that under Zn^{2+} treatments, implying that little (if any) ZnO NPs could translocate up in the ryegrass in this study.
Water-soluble fullerene caused inhibition of growth of *Arabidopsis thaliana* seedlings grown on agar medium (Liu et al., 2010) reducing the root length up to 60% and hypocotyl length up to 25%. This was caused by several factors such as the disruption of the auxin distribution in the root cap, the alteration of cell division in the meristematic zone, the interference in microtubule arrangement in the elongation zone and decreased activity of cell in the root tip. Moreover, water-soluble fullerene aggregates adhered to the normal seedling roots but internalized into the repressed roots.
Beyond root toxicity, some NPs were reported to be translocated through the vascular tissues, such as carbon-coated FeNPs (Cifuentes et al., 2010), that can easily penetrate through the root in four different crop plants (pea, sunflower, tomato and wheat), and spread through the aerial part of the plants in less than 24

hours. These particles also accumulated in wheat leaf trichomes, but did not show toxic effects on plants.
Wang et al., (2012) demonstrated also the transport through both xylem and phloem of CuO NPs in hydroponically grown maize (*Zea mays*), observing chlorotic symptoms and the reduction of fresh weight of root and shoot tissues by 60% and 34%, respectively.
On the other hand, the effects of NPs on plants seem to be conditioned also by their size and chemical composition. Larue et al., (2012) studied the effects of TiO_2 NPs with diameters ranging from 14 nm to 655 nm on wheat (*Triticum aestivum*). NPs above 140 nm were not accumulated in wheat roots, while NPs between 36-140 nm, were accumulated in root parenchyma but did not reach the stele and consequently did not translocate to the shoot. Only particles smaller than 36 nm accumulated in the shoot and this accumulation did not impact wheat seed germination, biomass and transpiration, nor induced any modification of photosynthesis and oxidative stress. A positive effect on wheat was observed for the smallest NPs that caused, during the first stages of development, an increase of root elongation. This effect, observed in comparison to the other results, seems to be more a biostimulant-like rather than toxicity effect (Yakhin et al., 2017a).

1.6.1.2 NPs as fertilizers

The first evidence that reported positive effects of a nanomaterial on plant growth (Khodakovskaya et al., 2012) revealed that carbon nanotubes (CNTs) can penetrate tomato seeds and affect their germination and growth rates. The germination was dramatically higher for seeds grown on medium containing CNTs (10-40 µg/mL) compared to control seeds. Analytical methods indicated that the CNTs are able to penetrate the thick seed coat and support water uptake inside seeds, a process which can affect seed germination and growth. Fresh weight of total biomass increased 2.5-fold for the seedlings germinated and grown on CNTs containing medium compared with seedlings developed on the standard medium. This effect was attributed by the authors as a better supply of water to the seed, given that seed germinated on CNTs containing medium had 58% of moisture, while seeds unexposed to CNTs kept only 38.9% of moisture. This result, together with the evidence that ZnO NPs were shown to enter the root tissue of ryegrass (Lin and Xing, 2008), generated a great interest and stimulated the idea of using nanotechnology in fertilizers in the scientific community: "*This suggests that new nutrient delivery systems that exploit the nanoscale porous domains on plant surfaces can be developed*" (DeRosa et al., 2010).
Although many reviews are available in the literature (Nair *et al.*, 2010; Khot *et al.*, 2012; Ghormade et al., 2011; Liu and Lal, 2015; Ditta et al. 2015; Chhipa, 2017), the directly-related research is very scarce. However, some recent research has demonstrated the promising perspective of nanofertilizer development and application. Here are reported some of the more meaningful approaches.
Alidoust and Isoda (2013) investigated the effect of Fe_2O_3 NPs (6 nm) and citrate-coated Fe_2O_3 NPs on SPAD index and growth of soybean (*Glycine max*) grown in pots. The results were compared to the effects of bulk Fe_2O_3. The Fe_2O_3 NPs produced a significant positive effect on root elongation, particularly when

compared to the bulk Fe_2O_3 suspensions, only with treatments at concentrations greater than 500 mg L^{-1}. Plants amended with citrate-coated Fe_2O_3 NPs showed significant increases in SPAD index in comparison to the non-amended plants, while Fe_2O_3 NPs without citrate coating did not show a significant increase. In the experiments no negative effects on soybeans growth were observed after application of NPs. No control versus an electrolytic Fe form or a typical fertilizer was used.

Ghafariyan et al. (2013) reported that low concentrations of magnetite (Fe_3O_4) NPs significantly increased the chlorophyll contents in sub-apical leaves of soybeans (*Glycine max*) in a greenhouse test under hydroponic conditions, suggesting that soybean could use this type of Fe_3O_4-NPs as source of. Fe. The impact of using Fe-NPs was similar to that of Fe-EDTA at concentrations of 45 mg L^{-1}.

Delfani et al. (2014) investigated the effect of FeO NPs on black-eyed pea (*Vigna sinensis*) grown in greenhouse. FeO NPs, and a regular Fe salt were applied through foliar spray. Application of FeO-NPs at 500 mg L^{-1} improved crop performance more than that by application of the regular Fe salt, increasing the number of pods per plant, weight of 1000-seeds, Fe content in leaves, and chlorophyll content. The abovementioned improvements were 28%, 4%, 45%, and 12%, respectively.

The fertilizing potential of Fe_2O_3 NPs at various concentrations (20 nm) and Fe-EDTA (only at 50 mg Fe·kg^{-1} soil) was compared by Rui et al., (2016) on peanut (*Arachis hypogaea*) grown in a calcareous sandy soil. Fe_2O_3 NPs increased root length, plant height, biomass, SPAD values and Fe concentration in roots and shoot relative to non-fertilized plants. The increases were similar to that of plants fertilized with Fe-EDTA. However, when Fe_2O_3 NPs were added in the same amount as Fe-EDTA (50 mg Fe·kg^{-1} soil), Fe concentration in tissues of Fe-EDTA-treated plants was significantly higher than in Fe_2O_3 NPs ones. Fe_2O_3 NPs adsorbed onto sandy soil instead of leaching, as chelates usually do. A control versus a bulk counterpart was not investigated.

Beyond Fe oxides, also salts can be used for NPs production. Sánchez-Alcalá et al. (2012) investigated the capacity of nanosiderite ($FeCO_3$ NPs) to alleviate chlorosis of various crops grown in pot on a calcareous soil. Two pot experiments in which a SID (normal $FeCO_3$ NPs) or SIDP ($FeCO_3$ NPs produced in the presence of phosphate) suspension was applied to a calcareous soil at a rate of 2 g Fe·kg^{-1} showed $FeCO_3$ NPs to prevent iron chlorosis in chickpea (*Cicer arietinum*). In an experiment with five successive crops, one initial application of 0.7 g Fe·kg^{-1} soil in the form of SID or SIDP was as effective as FeEDDHA in preventing Fe chlorosis. The residual effect of nanosiderite when applied to the first crop alone clearly exceeded that of FeEDDHA.

Another salt that was investigated is hydroxyapatite ($Ca_5(PO_4)_3(OH)$) (Liu and Lal, 2014). The fertilizing potential of carboxymethylcellulose-stabilized hydroxyapatite NPs (CMC-HA NPs, 16nm) was evaluated on soybean (*Glycine max*) grown in pots on a medium composed by perlite and peat moss, and amended through fertigation. The effect of synthetic fertilizer with CMC-HANPs was compared with: tap water, synthetic fertilizer without P, synthetic fertilizer with regular $P(Ca(H_2PO_4)_2)$. The treatment with CMC-HA NPs caused values of

plant height, shoot biomass, root biomass and soybean dry yield always higher, even if not significantly, than plants treated with regular P.
Beyond the nutritional supply, some nanomaterials, in particular carbon-based nanomaterials (CNMs), showed positive effects on root plant growth (Mukherjee et al., 2016). The treatments with multi-wall nanotubes (MWCNTs) increased the root length of ryegrass plants hydroponically grown (Lin and Xing, 2007) and of corn seedlings in agar medium (Lahiani et al., 2013). Similar results were observed when onion and cucumber plants in hydroponics were exposed to uncoated CNT (Cañas et al., 2008). The effects of carbon materials, that do not represent a source of nutrient for plants, seem to represent a biostimulant-like effect (Yakhin et al., 2017b).
The mechanism of nutrient delivery by NPs to the plant, has not been clarified. One of the primary mechanisms involved in an ameliorated nutrient delivery could be their dissolution in water/soil solution. In other words, NPs simply dissolve in solution and release the nutrient. Plants absorb the soluble nutrient ions indiscriminately as those from the dissolved conventional fertilizers. However, the dissolution rate and extent of NPs in water/soil solution should be higher than those of the related bulk solids because of the much smaller particle sizes and higher specific surface areas of the former (Liu and Lal, 2015). In addition, a transport of NPs by mass flow to the roots and an interaction/accumulation in the apoplast could also be envisaged. No information regarding the two above described mechanisms is at the best of our knowledge present in the literature.
Furthermore, recently it has been suggested that NUE could be improved with the use of nanoencapsulated fertilizers. The mode of action of these materials is based on the molecular recognition between root exudates and the encapsulation, with the latter that can be solubilized and/or degraded by exudates (Monreal et al., 2016; Dimkpa and Bindraban, 2017).
The brief description of the literature here presented shows that many of the research is focused on some specific materials (e.g. Fe oxides), and there is still a lack of evidence for many materials, in particular for those that can deliver more than one nutrient. At the present, there are no published studies investigating the effects of ferric phosphate NPs ($FePO_4$ NPs) on plants.

1.6.2 NPs synthesis

Many methods were developed for the synthesis and production of NPs. These methods can be divided in top-down and bottom-up approaches. Top-down approaches include milling or attrition, repeated quenching and lithography. Milling produces particles with a broad size distribution and variable geometry. Moreover, they may contain impurities from the milling medium. More generally, top-down approaches are limited to few applications, and are generally costly (Cao and Wang, 2011).
Bottom-up approaches are more popular and common in the synthesis of NPs, and many methods have been developed. Bottom-up approaches involve methods based on the homogenous nucleation such as co-precipitation methods and synthesis in confined environments such as micelles and microemulsions, and spray pyrolysis (Cao and Wang, 2011).

The synthesis of NPs inside micelles and microemulsions were used for the preparation of metallic NPs (Boutonnet et al., 1982; Naoe et al., 2008), and polymeric NPs (Eastoe et al., 2006). Spray pyrolysis involves the spraying in small droplets of a solution containing the chemical precursors that are combusted in the flame. Metal oxides are produced having final compositions determined by the precursor solution composition (Baranwal et al., 2001; Kim et al., 2008).

For formation of NPs by homogenous nucleation, a supersaturation of growth species must be created. For example, when two solutions of salts are mixed together and they contain two ions whose solubility product constant (Kps) is lower than the concentrations of the ions in the resulting solution, they precipitate as insoluble salt. The higher is the grade of supersaturation, more will be the nucleation points that will be formed, and smaller will be the particles (Haruta and Delmon, 1986).

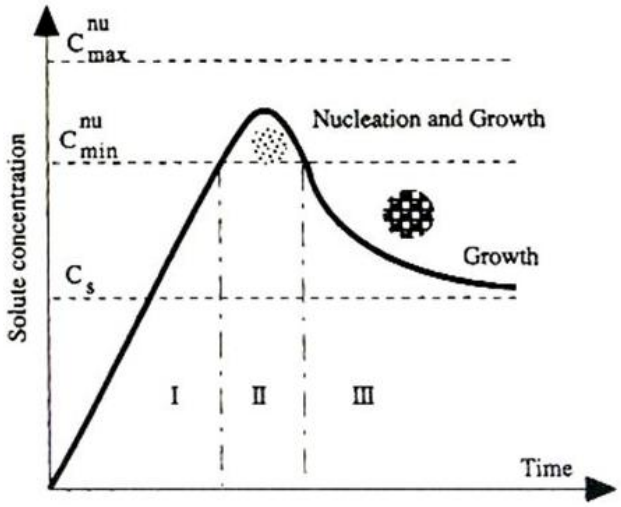

Figure 16: Schematic illustration of the process of nucleation and subsequent growth during homogeneous nucleation. From Haruta and Delmon, (1986)**.**

Among various chemical methods for synthesis of different types NPs, the co-precipitation process has several advantages including, good homogeneity, low cost, high purity of product and not requiring organic solvents and heat treatment (Nazari et al., 2014). For this reason, co-precipitation is widely used for the synthesis of metal oxides NPs (Petcharoen and Sirivat, 2012; Kandpal et al., 2014; Das and Srivasatava, 2016) but also for the synthesis of NPs made of insoluble salts such as $FeCO_3$ (Sánchez-Alcalá et al., 2012), $Ca_5(PO_4)_3(OH)$ (Liu and Lal, 2014), CaF_2 (Omolfajr et al., 2011) and $FePO_4$ (Kandori et al., 2006; Lu et al., 2012; Zhang et al., 2013; Zhang et al., 2014).
Co-precipitation methods are often carried out in batch: for example, Sánchez-Alcalá et al. (2012) produced $FeCO_3$ NPs by mixing 200 mL of 1 mol L^{-1} $FeSO_4$ with 200 mL of 1 mol L^{-1} K_2CO_3 in a beaker, and adding 200 mL of deionised H_2O. Also Liu and Lal (2014), prepared CMC-HA NPs in batch, adding dropwise 25 mL of $Ca(OH)_2$ solution to 50 mL of CMC solution under constantly mixing.

After the mixture was stirred for 12 h, 25 mL of H_3PO_4 solution was dropwise added to the mixture, also under constantly stirring.

Kandori et al. (2006) produced $FePO_4$ NPs through the aging of a solution of $FeCl_3$ and H_3PO_4 at temperatures between 40°C and 80°C, for variable time periods depending on the reagents concentrations. The data indicate that the precipitation does not occur instantly but is needed a period of reaction at controlled temperature.

However, co-precipitation can also be carried out in continuous, and continuous synthesis was demonstrated for $FePO_4$ NPs (Lu et al., 2012; Zhang et al., 2013; Zhang et al., 2014). In these works the authors optimized a method for the synthesis of high purity $FePO_4$ NPs with an average size of about 20 nm. This method is based on the extremely fine and rapid mixing of a Fe^{3+} solution with a HPO_4^{2-} solution in a mixing chamber at a low residence time in the chamber obtained through high flows and a small volume of it.

NPs have the tendency to lower their very high surface energy, which is the origin of their thermodynamic instability. Bare NPs tend to stabilize themselves by lowering the surface area through agglomeration (Aiken and Finke, 1999; Liu and Lal, 2014), and this can then cause sedimentation over time. In order to avoid it, NPs have to be stabilized (Aiken and Finke, 1999). This can be achieved by the use of stabilizing agents, also called cappants, that avoid or minimize the aggregation of NPs. This method is commonly used when NPs are used in suspension in an aqueous medium (Singh et al., 2009; Javed et al., 2016). For example, Liu and Lal (2014) stabilized hydroxyapatite ($Ca_5(PO_4)_3(OH)$) NPs adding CMC to the Ca^{2+} precursor. This method demonstrated to be effective in avoiding NPs sedimentation over time.

NPs stabilization can also be performed on purified NPs, after the reaction. Alidoust and Isoda (2013)produced 6 nm Fe_2O_3 NPs and stabilized them with citrate. Fe_2O_3 NPs were mixed with 20 mmol $\cdot L^{-1}$ citric acid and stirred for 90 min at 90 °C.

However, NPs purification methods and the possible capping are evaluated in relation to the use of obtained NPs. For example, in some applications the aggregation of NPs is not a concern, such as in the production of materials that will be used dry, such as $FePO_4$ NPs for the development of $LiFePO_4$ cathodes. In fact, in this papers (Kandori et al 2006; Lu et al., 2012; Zhang et al., 2013; Zhang et al., 2014) no stabilization of NPs is performed, and purification methods that were applied (such as filtration or centrifugation and drying), clearly caused an important NPs aggregation, as shown by TEM images reported in the papers.

2 AIM OF THE THESIS

This thesis, part of the Joint Project 2014 UniVR-FCP Cerea "Nanofert" is aimed at evaluating the effects of ferric phosphate NPs ($FePO_4$ NPs) on different crops grown in hydroponics. The idea was to study the capacity of these NPs to deliver P and Fe to plants, for understanding their potential as innovative fertilizer.

In fact, crops NUE is usually low, in particular referring to the uptake of nutrients applied through fertilizers. Phosphorous and Fe are essential mineral nutrients limiting in a wide range of conditions the agricultural productivity. Phosphate fertilizers to-date on the market have a very low use efficiency that does not exceed 10%-25%. Moreover, stocks of rock phosphates, the raw material for the production of P fertilizers, are running out. Iron, is present in the soil in high total amounts, but it is scarcely available in aerobic soils. Iron fertilizers present on market are at the moment expensive and have a limited temporal effectiveness. It is estimated that Fe deficiency occurs in about 30% of soils while P deficiency occurs in almost 65% of soils. It is therefore evident the need to develop more efficient fertilizers for these two nutrients. In this context, the use of nanotechnologies could offer an opportunity as envisaged by many authors. Nanomaterials are widely used in medical and pharmaceutical fields, but examples of application of such nanomaterials in plant nutrition are very few and no one described the use of $FePO_4$ NPs.

The first aim was the optimization of a simple, economically advantageous and industrially scalable synthesis method for producing $FePO_4$ NPs, that could provide a product with a convenient shelf-life making it potentially exploitable in the fertilizer market. Then, the effectiveness of $FePO_4$ NPs as source of P and Fe for two crop species, cucumber (*Cucumis sativus*), a *Strategy I* plant for Fe acquisition, and maize (*Zea mays*) a *Strategy II* plant was evaluated, through the study of morpho-physiological parameters and expression analysis of genes involved in the regulation of P and Fe homeostasis. The different parameters were evaluated in comparison to plants grown with non-nanometric ferric phosphate (bulk-$FePO_4$).

3 MATERIALS AND METHODS

3.1 Synthesis of $FePO_4$ NPs

In order to find a simple, economically advantageous, and industrially scalable method for the synthesis of iron (III) phosphate ($FePO_4$) NPs many synthesis methods were assayed. All used methods are based on co-precipitation: a kind ofreaction where two solutions of soluble salts are mixed together and an insoluble product is formed, typically a salt with a low solubility product. $FePO_4$, due to its low solubility product ($1.3 \cdot 10^{-22}$ for $FePO_4$ and $9.91 \cdot 10^{-16}$ for $FePO_4 \cdot 2H_2O$) is commonly synthesized with this strategy.

3.2 Batch synthesis as in Kandori et al. (2006)

The first method that was tried is a set of combinations according to the batch method published by Kandori et al. (2006). It consists in the aging of a solution of $FeCl_3$ and H_3PO_4 at temperatures between 40°C and 80°C, for variable time periods depending on the reagents concentrations. The set of conditions that were investigated is listed in Table 1.

Condition name	T (°C)	t	$[FeCl_3]$	$[H_3PO_4]$	$[KH_2PO_4]$
A	60	4h	0.1	0.1	-
B	60	15h	$3.16 \cdot 10^{-3}$	$3.16 \cdot 10^{-2}$	-
C	25	5’	0.01	-	0.1
D	60	2h	0.01	0.01	0.09
E	60	1h50’	0.01	0.09	0.01
F	40	900	$2.5 \cdot 10^{-3}$	$3.16 \cdot 10^{-2}$	
G	80	900	$2.5 \cdot 10^{-3}$	$3.16 \cdot 10^{-2}$	

Table 1: Conditions tested with the batch method.

In detail, 50 mL of $FeCl_3$ solution was mixed under stirring with a H_3PO_4/KH_2PO_4 solution, and placed in oven for the indicated reaction time. The obtained particles were purified through centrifugation at 4500 rcf for 10 minutes and resuspension in deionized water for three times.

3.3 Rapid mixing-based synthesis

A continuous synthesis method, described by Zhang et al. (2014), was investigated. This method is based on the extremely fine and rapid mixing of two solutions in a mixing chamber due to a low residence time in the chamber obtained through high flows and a small volume of it.

The effectiveness of the method was tested with a laboratory-made system, consisting of two syringes as pressure sources and a micro-irrigation tee fitting as mixing chamber for the solutions (Figure 17).
Solution "A" contained 0.1 M $FeCl_3$ and 0.02 H_3PO_4, and a solution "B" contained 0.1 M K_2HPO_4 at pH 9.10. Syringes were hand-pushed, and the flow of each solution was about 3 $mL \cdot s^{-1}$, and mixing chamber volume was about 15 mm^3 to 25 mm^3. Obtained particles were purified through centrifugation at 4500 rcf for 45 minutes and resuspension in deionized water for three times.

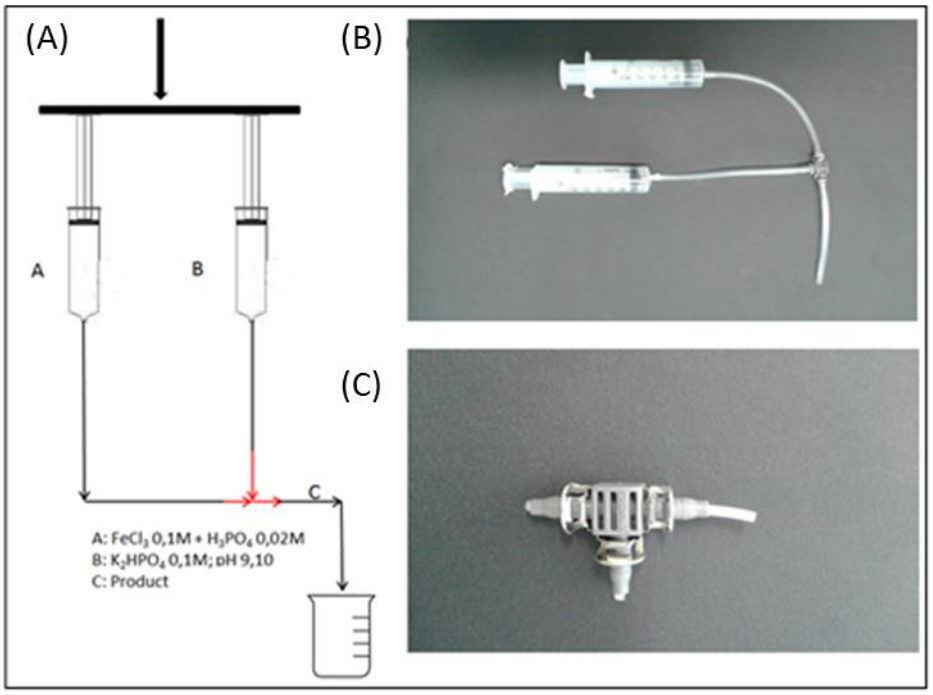

Figure 17: Schematic representation (A) and photograph (B) of the proof-of-concept system used, and detail of the tee fitting (C).

Once the effectiveness of the continuous method was determined, a pilot plant for continuous production of $FePO_4$ NPs was developed. It consisted in two dosing pumps (EMEC model AMS MF 2505V) for solutions pumping, and an HPLC mixing tee as mixing chamber (dead volume 10 µL). The system can operate with a flow of each solution of 7.5 $L \cdot h^{-1}$, with solution "A" containing 0.1 M $FeCl_3$ and 0.02 M H_3PO_4, and a solution "B" containing 0.1 M K_2HPO_4 at pH 9.10, for a potential productivity of 15 $l \cdot h^{-1}$ of raw $FePO_4$ NPs suspension. That suspension was purified through dialysis with deionized water for 24 hours. The retentate:water ratio was 1:40, and the water was changed four times at increasing time intervals. The Molecular Weight Cut-Off (MWCO) of the membrane is 14 kDa.

3.4 Laboratory-scale batch synthesis for hydroponic trials

Continuous productive processes are useful and economically advantageous for the preparation of big amounts of NPs, but are less practical and more wasteful when the plant operates for short time. For these reasons, a laboratory-scale batch synthesis method, was developed for making $FePO_4$ NPs to be used for the experiments performed at laboratory scale.
Twenty-five milliliters of a 0.6 M K_2HPO_4 solution were added drop by drop to 25 mL of a solution containing 0.6 M $Fe(NO_3)_3$ under continuous stirring at 600 rpm at room temperature (25 °C).
The resulting solution, partially precipitated, was centrifuged 20 min at 4500 rcf. The supernatant was precipitated through a treatment at 85 °C for 1h, and then let cool to room temperature under continuous stirring at 600 rpm.
The obtained suspension was then purified from by-products through dialysis with deionized water for 24 hours. The retentate:water ratio was 1:40, and the water was changed four times, at increasing time intervals. The Molecular Weight Cut-Off (MWCO) of the membrane is 14 kDa.
Fifty milliliters of the suspension were then citrate-capped through the adding of 5.55mL of 1M tribasic potassium citrate and thorough vortexing for 2 min.
The suspension was then immediately purified from the excess of citrate through dialysis.

3.5 Size distribution of NPs

Size distribution was determined through DLS (Dynamic Light Scattering) analysis with a Malvern Zetasizer ZS instrument operating with a He-Ne laser at 633 nm. Samples for DLS analysis was diluted 1:20 in deionized water and analyzed operating the instrument in size mode, measuring 173° backscatter.

3.6 Fe and P quantification in $FePO_4$ NPs suspension

The obtained suspensions were prepared for Fe and P quantification dissolving 2.5 mL of NPs suspension with 2.5mL of concentrated HCl (37%). The obtained solution was then diluted in order to fit into the range of calibration curves of the quantification methods (2.5 μM-50 μM for Fe quantification, 25μM-300 μM for P quantification. A 0.1M $FePO_4$ in 6 M HCl solution was used for the production of calibration curves and reference standards preparation. The methods used for Fe and P quantification are described in paragraph 3.6.1 and 3.6.2 respectively.

3.6.1 Iron quantification with a method optimized from Stookey (1970)

The method is based on the reduction of Fe^{3+} to Fe^{2+} with NH_2OH, and the subsequent complexation of Fe^{2+} by PDT disulfonate (3-(2-Pyridyl)-5,6-diphenyl-1,2,4-triazine-4',4''-disulfonic acid sodium salt) obtaining a colored complex with an absorption maximum at 562 nm.

Using the $FePO_4$ 0.1M stock solution the following points of the calibration curve were prepared: 2.5 µM, 5 µM, 10 µM, 15 µM,20 µM, 30 µM, 50 µM, and a 25 µM control solution that was not included in the calibration curve.
The assay was set up directly in cuvettes, by adding the solutions in the listed order:

Sample or $FePO_4$ standard	800 µL
NH_2OH (10%)	10 µL
PDT disulfonate (5 mM)	40 µL
H_2O	150 µL
Final volume	1000 µL

Absorbance values were measured after 10 minutes with an Evolution 201 spectrophotometer (Thermo Scientific) at 562 nm.

3.6.2 Phosphate quantification with a method optimized from Riley and Murphy (1962)

Using the $FePO_4$ 0.1M stock solution the following points of the calibration curve were prepared: 25 µM, 50 µM, 100 µM, 150 µM, 200 µM, 300 µM and a 175 µM control solution that was not included in the calibration curve.
First, the Murphy and Riley reagent was prepared mixing the reagents in the listed order:

H_2SO_4 (2.5 M)	50 mL
Ammoniummolybdate (4%)	15 mL
L- ascorbic acid (1.76%)	30 mL
Potassium antimony(III) tartrate hydrate (2.74 g/L)	5 mL
Final volume	100 mL

Then, the assay was set up directly in cuvettes, adding the solutions in the listed order:

Sample or $FePO_4$ standard	100 µL
Murphy and Riley reagent	160 µL
H_2O	740 µL
Final volume	1000 µL

Absorbance values were measured after 10 minutes with an Evolution 201 spectrophotometer (Thermo Scientific)at 720 nm.

3.7 Plant material and growth conditions

Cucumis sativus var. Viridis F1 hybrid seeds (Franchi Sementi S.p.A.) were germinated on paper towel moistened with 1 mM$CaSO_4$ at 24°C in the dark. After 6 days, 6 seedlings per condition were transferred to 2-L pots containing aerated

nutrient solution. Plants were grown under a 16/8 h light/dark photoperiod at 24±2 °C with a light intensity of 200-250 μmol m^{-2} s^{-1} as PAR (Photosynthetically Active Radiation). The composition of the complete nutrient solution (control) was: 0.7 mM K_2SO_4, 2mM $Ca(NO_3)_2$, 0.5mM $MgSO_4$, 0.1 mM KH_2PO_4, 0.1 mM KCl, 100 μM FeNaEDTA, 10 μM H_3BO_3, 0.5 μM $MnSO_4$, 0.5 μM $ZnSO_4$, 0.2 μM $CuSO_4$ and 0.01 μM $(NH_4)_6Mo_7O_{24}$. Ten experimental conditions were set up: plants grown in a complete nutrient solution (C), plants grown without P (-P), plants grown without Fe (-Fe), plants grown without both P and Fe (-P-Fe), plants grown with $FePO_4$ NPs as source of P (-P+NPs), plants grown with $FePO_4$ NPs as source of Fe (-Fe+NPs), plants grown with $FePO_4$ NPs as source of both P and Fe (-P-Fe+NPs), plants grown with bulk $FePO_4$ as source of P (-P+bulk $FePO_4$), plants grown with bulk $FePO_4$ as source of Fe (-Fe+bulk $FePO_4$), and plants grown with bulk $FePO_4$ as source of both P and Fe (-P-Fe+bulk $FePO_4$). Both $FePO_4$ NPs and bulk $FePO_4$ were added at a concentration equivalent to 100 μM. In the solutions without KH_2PO_4, K^+ cations were balanced using 0.2mM KCl instead of 0.1mM. The nutrient solution was changed twice a week and adjusted to pH 6 with 1N NaOH.

Zea mays L. inbred line P0423 seeds (Pioneer Hybrid Italia S.p.A.) were germinated on paper towel moistened with deionized water at 25°C in the dark. After 3 days, 6 seedlings per condition were transferred to 2-L pots containing aerated nutrient solution. Plants were grown under a 16/8 h light/dark photoperiod at 25±2°C with a light intensity was 200-250 μmol m^{-2} s^{-1} as PAR (Photosynthetically Active Radiation). The composition of the complete nutrient solution (control) was: 0.7 mM K_2SO_4, 2 mM $Ca(NO_3)_2$, 0.5 mM $MgSO_4$, 0.1 mM KH_2PO_4, 0.1 mM KCl, 100 μM FeNaEDTA, 10 μM H_3BO_3, 0.5 μM $MnSO_4$, 0.5 μM $ZnSO_4$, 0.2 μM $CuSO_4$ and 0.01 μM $(NH_4)_6Mo_7O_{24}$. Ten experimental conditions were set up: plants grown in a complete nutrient solution (C), plants grown without P (-P), plants grown without Fe (-Fe), plants grown without both P and Fe (-P-Fe), plants grown with $FePO_4$ NPs as source of P (-P+NPs), plants grown with $FePO_4$ NPs as source of Fe (-Fe+NPs), plants grown with $FePO_4$ NPs as source of both P and Fe (-P-Fe+NPs), plants grown with bulk $FePO_4$ as source of P (-P+bulk $FePO_4$), plants grown with bulk $FePO_4$ as source of Fe (-Fe+bulk $FePO_4$), and plants grown with bulk $FePO_4$ as source of both P and Fe (-P-Fe+bulk $FePO_4$). Both $FePO_4$ NPs and bulk $FePO_4$ were added at a concentration equivalent to 100 μM. In the solutions without KH_2PO_4, K^+ cations were balanced using 0.2 mM KCl instead of 0.1 mM. The nutrient solution was changed twice a week, and adjusted to pH 6 with 1N NaOH.

3.8 SPAD index measurement and plants sampling

The sampling-time points for both plant species were chosen on observational basis, looking for appreciable differences in symptoms among the different experimental conditions. Following this rationale, the plant sampling occurred after 14 and 17 days of growth for cucumber and maize, respectively. SPAD Index was determined taking five measurements per leaf using a SPAD-502 Plus Chlorophyll meter® (Konica Minolta). In the case of cucumber, at the end of the

experiment (14 days) the SPAD index was determined for the first (the youngest fully expanded) leaf of each plants while for maize (17 days) a mean SPAD index value was calculated using the SPAD values of all leaves.
The root apparatus of three plants of each pot was rinsed two times in milliRho water and three times in milliQ water and separated from the shoot. Shoots and roots of each plant were immediately weighted (fresh weight) and after drying at 60 °C for 72 hours (dry weight).
For RNA extraction, shoots and roots of one plant per pot were separately collected and frozen in liquid nitrogen, and then stored at -80 °C .

3.9 WinRHIZO^{TM} analysis

Plants root apparatuses of three plants per pot were scanned with EpsonV700 perfection, and images were analyzed with WinRHIZO^{TM} software, 2015a Pro version (Regent Instruments Inc.), using the "root morphology" mode. This software analyses the digital images acquired, estimating parameters such as total root length, mean root diameter, root surface area, and total root volume, allowing the quantification of the effects of treatments on root development.

3.10 Sample digestion for ICP-MS analysis

Dried plant tissues were milled using mortar and pestle, and then approximately 10 to 20 mg of homogenized material was mineralized with 250µLof ultra-pure 68% HNO_3 (Romil LTD) and 1 mL of 30% H_2O_2 at 180°C for 20 minutes in a StartD® microwave digestion system (Milestone Srl), following the thermal profile shown in Figure 18.

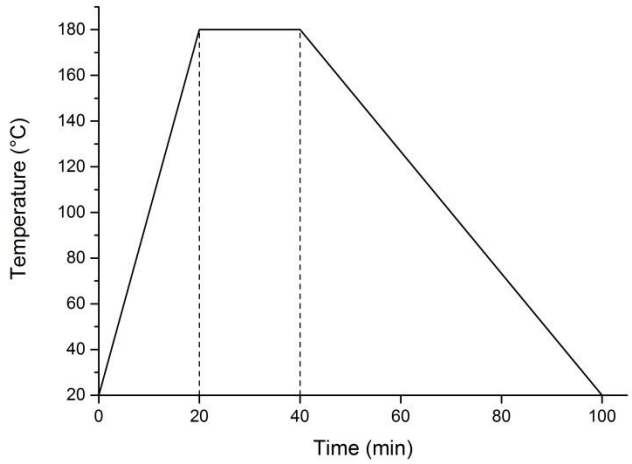

Figure 18: Representation of the thermal profile used for the samples digestion before ICP-MS analysis.

The digested samples were diluted up to 2% HNO_3 with ultra-pure grade water (18.2MΩ·cm at 25 °C), and then analyzed using an Agilent 7500ce ICP-MS detection system (Agilent technologies).

3.11 ICP-MS analysis

The ICP-MS (Inductively Coupled Plasma Mass Spectrometry) technique allows the multi-elemental quantification of samples, in a broad range of concentrations, from parts per trillion (ppt) to parts per million (ppm). This technique adopts argon (Ar) inductively coupled plasma as a source of ions and a quadrupole mass analyzer to separate the ions before detection. Ar gas is firstly ionized with a spark produced by two electrodes, and the electrons released are inductively accelerated by a radiofrequency source, to give stable, high-density plasma. Ar gas is the most common element used for plasma generation, because its first-ionization energy, is higher than first-ionization of most of elements, but lower than their second-ionization energy. This allows the generation of single charge ions, minimizing doubly charged species.
A peristaltic pump conveys the sample to the nebulizing system, where it is mixed with an Ar flux. The so-formed aerosol then reaches the plasma torch, where it is atomized and ionized. The resulting ion-beam passes through two cones (sampling cone and skimmer cone) with the purpose of reaching the required degree of vacuum, and subsequently, positively charged ions are extracted with a series of electrostatic lenses and focused to the quadrupole. Here, ions are separated according to their mass/charge ratio (m/z). The ions are then detected by an electron multiplier and the resulting signal is acquired by a computer. A general diagram of the instrument is described in Figure 19.

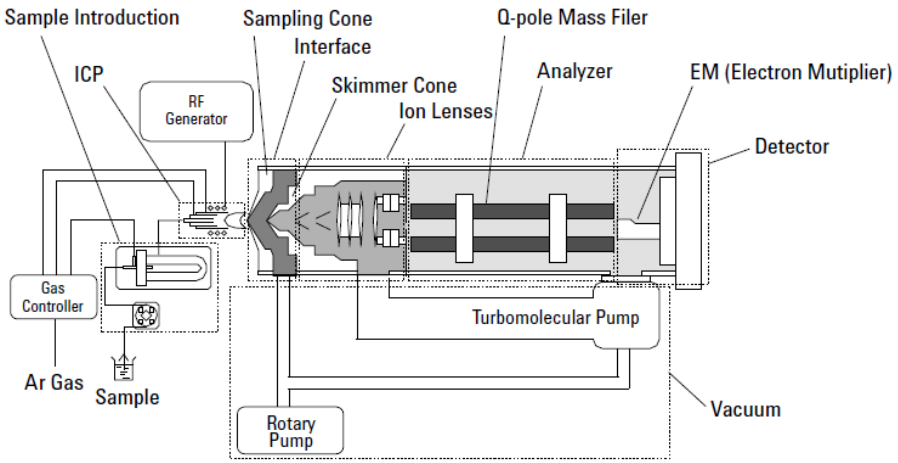

Figure 19: General diagram of the Agilent ICP-MS 7500 series.

The Agilent ICP-MS 7500ce used in this work is also provided with an octopole reaction cell upstream to the quadrupole mass analyser (Figure 20). This cell, pressurized with He, allows the elimination of most of the molecular interference, such as Ar^+ ions, polyatomic ions, doubly charged and oxidized species.

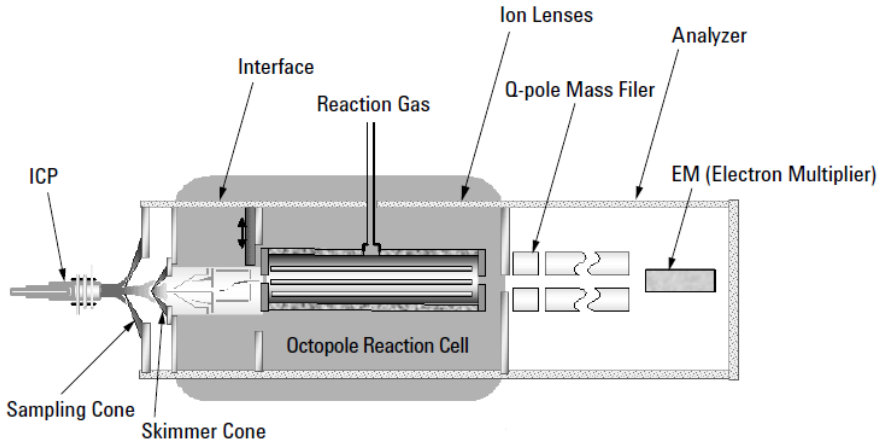

Figure 20: Octopole reaction system.

The concentration of mineral nutrients was determined by means of Agilent 7500ce ICP-MS. Calibration curves were built diluting a custom-made multielement standard (Romil LTD), with the following stock solution composition: K (20.000 ppm), Ca (10.000 ppm), Mg and P (2.000 ppm), Na (400 ppm), Fe (50 ppm) Mn (40 ppm), B and Zn (20 ppm), Cu (5 ppm), Co, Mo and Se (1 ppm). Twelve-points curves were so obtained, spanning this way the concentration more than three orders of magnitude (Supplementary Table 1). Measurement accuracy and matrix effect errors were checked using NIST standard reference material 1515 (Apple leaves), that was digested and analysed as the samples. Concentrations of elements that could not be determined in apple leaves reference within an interval of ± 10 % of the declared value were not further processed and are not reported in the result section.

3.12 TEM observation of $FePO_4$ NPs and roots

Portions of tertiary roots of cucumber plants were collected and fixed in a 1.5% glutaraldehyde solution for 24 hours at 4°C in the dark. Fixed roots were then washed three times in 0.1M, pH 6.95 cacodilate buffer and post-fixed in osmium tetroxide for 2h in dark. After the post-fixation, roots were washed other three times in 0.1M pH 6.95 cacodilate buffer, dehydrated in a graded series of ethanol, and embedded in araldite resin. Thin sections were prepared using an ultra-microtome, and placed on Cu grids for observation with a Tecnai G2 (FEI) Transmission Electronic Microscope (TEM), operating at 120 kV. 10 µL of $FePO_4$ NPs suspension were deposited on copper (Cu) grids and let dry at room temperature.

3.13 ESEM observation and EDAX analysis of cucumber roots

Portions of roots of cucumber plants grown with $FePO_4$ NPs as P source (-P+NPs) were washed three times in deionized water, dried gently with absorbing paper and observed with a Quanta 200 (FEI) Environmental Scansion Electronic

Microscope (ESEM) operating at 20 kV, looking for electron dense crusts and performing on these an Energy Dispersive X-ray Spectroscopy (EDAX) analysis. Fe and P peaks intensities were normalized on the peak of C for comparison.

3.14 RNA extraction and cDNA synthesis

RNA was extracted from roots using Spectrum^{TN} Plant Total RNA Kit (Sigma-Aldrich Co. LLC) from 80 mg of tissue previously homogenized with liquid nitrogen, following the "A" protocol of manufacturer's instructions. RNA integrity was verified through a 1% agarose gel electrophoresis with TAE buffer (0.04 Tris-acetate, 1 mM EDTA), using EuroSafe Nucleic Acid Staining Solution (Euroclone®) for bands detection. RNA was then quantified with NanoDrop One (Thermo Scientific®). One microgram of total RNA was treated with 10 U of DNAse RQ1 (Promega®), with the following mix:

Total RNA	1 µg
RQ1 DNAse 10X buffer	1 µL
RQ1 DNAse	1 µL
H_2O	to 10 µL

The reaction was incubated for 30 minutes at 37 °C, and stopped by adding 1 µL of stop solution (Promega®) and treating the mixture at 65°C for 10 minutes.
Then, 10 µL of treated RNA were added with 1 µL of oligodT_{15} (20 pmol/µL). The mixture was heated at 70 °C for 5 minutes and then immediately transferred in ice for 5 minutes. In the end, the following mix was added to the samples:

5X buffer (Promega®)	4 µL
$MgCl_2$ (25 mM)	2.4 µL
dNTPs (0.5 mM)	1 µL
RNAse inhibitor (50 u/µL, Promega®)	1 µL
ImProm-II Reverse Transcriptase (Promega®)	1 µL
Final volume	9.4 µL

The reverse transcription reaction was conducted at the following thermal profile: 5 minutes at 25°C, 1 hour at 42°C, and 15 minutes at 70°C using a Gene Pro TC-E-48D thermal cycler (BIOER). The quality of obtained cDNA was checked through PCR using couples of primers of housekeeping genes.

3.15 Target genes selection and bioinformatics analyses

Gene expression analysis for the used plant species focused on homologs of known transcription factors involved in Fe and P homeostasis in Arabidopsis or transcription factors known to be involved in Fe and P homeostasis in the model species used.
Regarding the response to P deficiency, homologs of *AtPhr1* were taken in account. PHR1 is a transcription factor known to be a key regulator of the

response to P starvation in Arabidopsis, promoting the expression of a series of effector genes, such as *AtPht1* and *AtPho1* (Briat et al., 2015). Maize homologs of *AtPhr1* were previously identified (Calderon-Vazquez et al. 2011).
On the other hand, we identified two homologs of the *Arabidopsis thaliana* and *Oryza sativa* PHR1 transcription factor gene in cucumber by comparing the corresponding amino acid sequences.
In addition, transcription factors involved in the response to Fe deficiency were studied. In maize the gene expression analysis focused on genes encoding IRO2 and FER-Like transcription factors, regulators of the response to Fe deficiency in *Strategy II* and *Strategy I* plants, respectively (Zanin et al., 2017).
In cucumber, genes encoding proteins homologous to the ZINC FINGER PROTEIN BRUTUS (*AtBTS*) and transcription factor bHLH47 (*AtPYE*) were identified through amino acid similarity with *Arabidopsis thaliana* proteins. Amino acids sequences were retrieved from UniProt (http://www.uniprot.org).

Gene name	Locus name	UniProtKB Entry
AtPHR1	At4g28610	Q94CL7
AtPHL1	At5g29000	Q8GUN5
OsPHR1	Os03g0329900	Q10LZ1
OsPHL1	Os07g0438800	Q6Z156
AtBTS	At3g18290	Q8LPQ5
AtPYE	At3g47640	Q9SN74

Table 2: Set of Arabidopsis and rice genes used for bioinformatics analysis. Gene name, locus name and entry ID (UniProt) were reported.

These protein sequences were used for a Blastp (Altschul et al., 1997) analysis against Cucumber Chinese long genome v2 (http://www.icugi.org/). The hits with the lowest e-value and identity of at least 40% were taken into account. Moreover, the predicted transcripts were blasted against EST (Expressed Sequence Tag) database in order to exclude wrong transcript predictions.

3.16 Housekeeping gene selection and primers design

Cucumber housekeeping genes were chosen from a set of constitutively expressed cucumber genes (Migocka and Papierniak 2011; Warzybok and Migocka 2013). The three most stably expressed, which are those encoding a CLATHRIN ADAPTOR COMPLEX SUBUNIT (CACS; *GW881874*), a F-BOX PROTEIN (F-BOX; *GW881870*) and a TIP41-LIKE FAMILY PROTEIN (TIP41;*GW881871*) were evaluated for the expression stability among our ten experimental conditions and independent experiments, using Normfinder algorithm (Andersen et al, 2004), a Microsoft Excel-embedding program that estimates the inter-group and intra-group variance of the expression level. Combining the two values, the algorithm produces a "*stability value*", a number inversely proportional to expression stability. In this way, the best couple of housekeeping genes for Real-time RT-PCR data normalization was chosen. Maize housekeeping genes were chosen from a set of stably expressed genes reported in (Lin et al., 2014). Even in this case, the expression stability of three of these

genes, which encode an UNKNOWNPROTEIN (UNK; *GRMZM2G047204*), a DUF1296 DOMAIN CONTAINING PROTEIN (DUF; *GRMZM2G163888*) and a CYCLIN-DEPENTENT KINASE PROTEIN (CDK;*GRMZM2G149286*) was evaluated with Normfinder algorithm, and the best couple was chosen.

Gene-specific primers for Real-time RT-PCR analysis were designed using the 3'-UTR (3'-UnTraslated Region) of each transcript, between the stop codon and the polyadenylation site, which is known to be a highly gene-specific region. The design was made in order to obtain amplification products about 100-bp long and a primer melting temperature as near as possible to 60 °C. Potential primer homodimers and heterodimers and intramolecular hairpin formation were also predicted using Oligoanalyzer software (http://eu.idtdna.com/calc/analyzer). Primers specificity was also checked through Blastn analysis against the reference genome, looking for non-specific annealing. Each primer couple was first tested through normal PCR, and then melting curves of amplicons were acquired starting from 60 °C, with increasing temperature steps of 0.3 °C every 15 seconds, up to 95 °C. Melting curves, plotted as the negative first derivative on Y axis (-dF/dT) were evaluated for the absence of multiple peaks, thus verifying the absence of non-specific products.

3.17 Real-time RT-PCR

Real-Time RT-PCR analyses were performed on StepOnePlus™ (Applied Biosistems) system using the FastSYBR® Green Master Mix. Primers concentration was 0.350 mM and 1 ul of fourfold diluted template cDNA was used. Reaction conditions were the following: 20seconds at 95°C for initial denaturation, 3 seconds at 95°C and 30 seconds at 60°C for 40 cycles. Primers used are reported in table 3:

Gene ID (Cucurbit genomics database)	Name		Forward
Csa7M071610	*TIP41*	Forward	5'-TGCAGAAGACCCAAAAGCTTA-3'
		Reverse	5'-CAGCACCAACATACACGAGA-3'
Csa5M642160	*F-box*	Forward	5'-TGCAGAAGACCCAAAAGCTTA-3'
		Reverse	5'-CAGCACCAACATACACGAGA-3
Csa3M902930	*CACS*	Forward	5'-ATTTCTTCTGGGCTGCCTGT-3'
		Reverse	5'-CACAAGCCAACATCGAAGGA-3'
Csa3M608690	*PHR1*	Forward	5'-GCTATGGTCTCTGCATTTTCT-3'
		Reverse	5'-AGCCAAAACCAAGGACTACC-3
Csa1M666970	*PHL1*	Forward	5'-GCAGAGATGTTCATTGATGGC-3'
		Reverse	5'-GTCAGTTGGCCATGACTTCC-3'
Csa1M009660	*PYE*	Forward	5'-GGTGTGAGTTCGAGAAGGCT-3'
		Reverse	5'-TTTGGCCCTTTGAGAGAGGT-3'
Csa1M024210	*BTS*	Forward	5'-CATATCCCGGGTCTATGTAGA-3'
		Reverse	5'-GTGGTAAGGCGATGATGTTCT-3'

Gene ID (Gramene database)	Name		Forward
GRMZM2G047204	*UNKN*	Forward	5'-TGCCTGTTCTGTGTGATGGA-3'
		Reverse	5'-CAAGCAAACAAGGGACGGG-3'
GRMZM2G149286	*CDK*	Forward	5'-CACGAAGAGGAAAACTGAAGA-3'
		Reverse	5'-AAGAGCCTGCCTTACGGAAT-3'
GRMZM2G163888	*DUF*	Forward	5'-CTATCAAGGGCAGAGTCATCA-3'
		Reverse	5'-GGGTTTCGGTGTTCAGGGC-3'
GRMZM2G162409	*GLK15*	Forward	5'-TCACGGTATCACTGAATCCCA-3'
		Reverse	5'-GGCAAAACAAGTCAAACCCC-3'
GRMZM2G006477	*GLK17*	Forward	5'-TGGTGAGTTGTACCGCTCTT-3'
		Reverse	5'-ATAAAGACGGCTGCCAGGAA-3'
GRMZM2G107672	*FER-Like*	Forward	5'-GCTCTTGTCAAGGAAGGCT-3'
		Reverse	5'-TAATCCAGCCGAACATGACC-3'
GRMZM2G057413	*IRO2*	Forward	5'-AGCCAACTGGTGTAAACTGTG-3'
		Reverse	5'-GCTTTCAAACGACCCTTATATC-3'

Table 3: Sequence of forward and reverse primers used in Real-time RT-PCR experiments. Gene ID and protein name are reported.

Mean Normalized Expression (MNE) (Simon, 2003) was calculated for every sample as reported below:

$$MNE = \frac{(E_{ref})^{CTref}}{(E_{target})^{CTtarget}}$$

E_{ref} is the mean amplification efficiency of the housekeeping gene; E_{target} is the mean amplification efficiency of the target gene; CT_{ref} is the cycle of threshold of housekeeping gene for the sample; CT_{target} is the cycle of threshold of target gene for the sample. The determination of each CT was carried out using StepOne™ software (Applied Biosistems). The efficiency of each reaction was calculated using LinRegPCR software (Ramakers et al., 2003) starting from fluorescence raw data.
The geometric mean of MNE values obtained in way against the housekeeping genes was calculated as below:

$$MNEmean = \sqrt{MNEa \times MNEb}$$

The mean MNE of every sample was normalized against the mean MNE of control obtaining the expression ratio as percentage of control:

$$ratio = \frac{MNE_{mean}(sample)}{MNE_{mean}(control)} \quad X100$$

3.18 Anthocyanins quantification in root tissues

Frozen tissues of maize root apparatuses were homogenized with mortar and pestle with liquid nitrogen. Anthocyanins were extracted from 300 mg of homogenate with 3 mL of a 1% HCl in methanol solution. The mix was incubated for 4 hours in the dark at 4°C, and mixed every 30 minutes. The obtained extracts were centrifuged at 12000 rcf for 1 hour. Supernatant absorbance was measured with an Evolution 201 spectrophotometer (Thermo Scientific) at 530 nm and 657 nm, and anthocyanins content was calculated with the following formula:

$$A_{530} - 0.25 \cdot A_{657}$$

and expressed as μg of cyanidine-3-glucoside· g_{FW}^{-1} using as 29600 as molar extinction coefficient ($A \cdot M^{-1} \cdot cm^{-1}$) and 449.2 $g \cdot mol^{-1}$ as formula weight (Pietrini et al., 2002).

3.19 Data analyisis

Data processing was performed with Microsof EXCEL, statistical analysis and bar graphs plotting were performed with GraphPad PRISM® 6.01. To compare the means among treatments one-way ANOVA with post-hoc Turkey's test was used, and differences were considered significant with $p<0.05$. Size distribution graphs were plotted with Origin Pro 9.0 (OriginLab).

4 RESULTS

4.1 $FePO_4$ NPs synthesis

In order to assess the effect of $FePO_4$ NPs on plant nutrition – even in lab conditions – is necessary to set up a method for $FePO_4$ NPs synthesis. The optimization of the method focused on the optimization of a simple, economically advantageous and industrially scalable synthesis method for producing $FePO_4$ NPs, that could provide a stable and easily to distribute product. Co-precipitation is the cheapest among the known techniques for NPs synthesis, so the work focused on methods based on this principle.

4.1.1 $FePO_4$ NPs synthesis according to Kandori et al. (2006)

This NPs synthesis is based on the method reported by Kandori et al.(2006), that involves the aging of a solution of $FeCl_3$ and H_3PO_4 at temperatures between 40°C and 80°C, for variable time periods, depending on the reagents concentrations. Table 1 shows an overview of the size of NPs obtained in different condition as estimated by DLS (Dynamic Light Scattering) analysis. Reaction conditions B, F and G are the same described by Kandori et al. (2006), while the other consist in the *de novo* experiments.

Reaction conditions	T (°C)	T (min)	$FeCl_3$ (M)	H_3PO_4 (M)	KH_2PO_4 (M)	Size (nm)	St.dev (nm)
A	60	240	0.1	0.1	-	460	130
B	60	900	$3.16 \cdot 10^{-3}$	$3.16 \cdot 10^{-2}$	-	400	183
C	25	5	0.01	-	0.1	162/620	132
D	60	120	0.01	0.01	0.09	2000	306
E	60	110	0.01	0.09	0.01	350	114
F	40	900	$2.5 \cdot 10^{-3}$	$3.16 \cdot 10^{-2}$		NM	
G	80	900	$2.5 \cdot 10^{-3}$	$3.16 \cdot 10^{-2}$		NM	

Table 4: Size of NPs obtained by the batch reactions synthesis using the method described by Kandori et al. (2006). NM: not measured due to fast sedimentation.

As reported in Table 4, all conditions investigated, except for condition C, did not allow to obtain particles of size near to 100 nm. Particle size plots for conditions A, B, D and E are shown in Supplementary Figure S1.

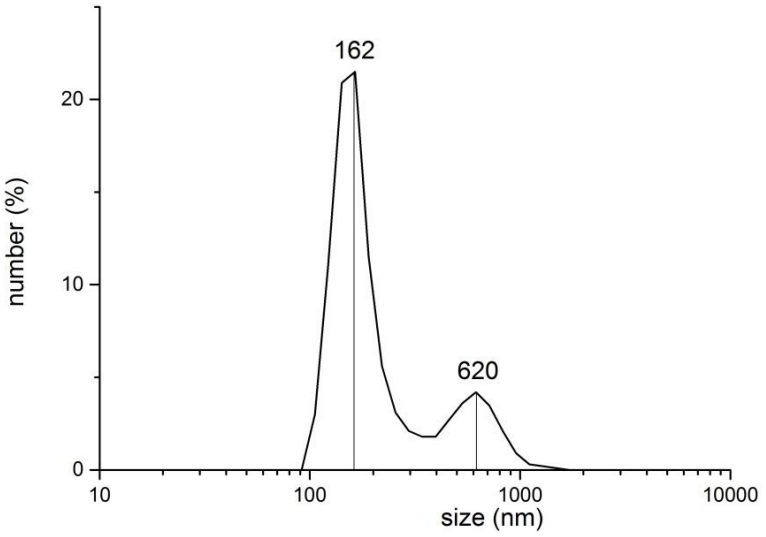

Figure 21: Particle size distribution obtained for the conditions C. Analysis was performed through DLS technique.

Conditions C, the only one that led to a peak near to 100 nm, shows an additional peak at 620 nm (Figure 21). Considering Table 4 it can be noticed that this reaction condition is the only that had KH_2PO_4 as phosphate (PO_4^{3-}) source and that reacted for short time (5 minutes) at room temperature. The elemental analysis of the obtained NPs in the conditions C, showed a Fe/P molar ratio of 0.822±0.04, suggesting the hypothetical formula $Fe(PO_4)_{0.89}(H_2PO_4)_{0.32}$.
Due to the short time of reaction and the presence of two different peaks of particles, it was speculated that some different reactions, involving more dissociated salts of PO_4^{3-} such as the monobasic or the dibasic could exist.

4.1.2 Proof-of-concept of continuous synthesis

Several methods of $FePO_4$ NPs synthesis using monobasic phosphate or dibasic phosphate as PO_4^{3-} source solution were reported (Lu et al., 2012; Zhang et al., 2013; Zhang et al., 2014) describing a continuous method of $FePO_4$ NPs synthesis based on the extremely fine and rapid mixing of two solutions in a mixing chamber. The effectiveness of this method was so tested with a laboratory-made system, consisting of two 30 mL syringes as pressure sources and a micro-irrigation tee fitting as mixing chamber for the solutions. Figure 22 shows the particles size distribution obtained with this method, after purificationthrough centrifugation and resuspension in deionized water for three times.

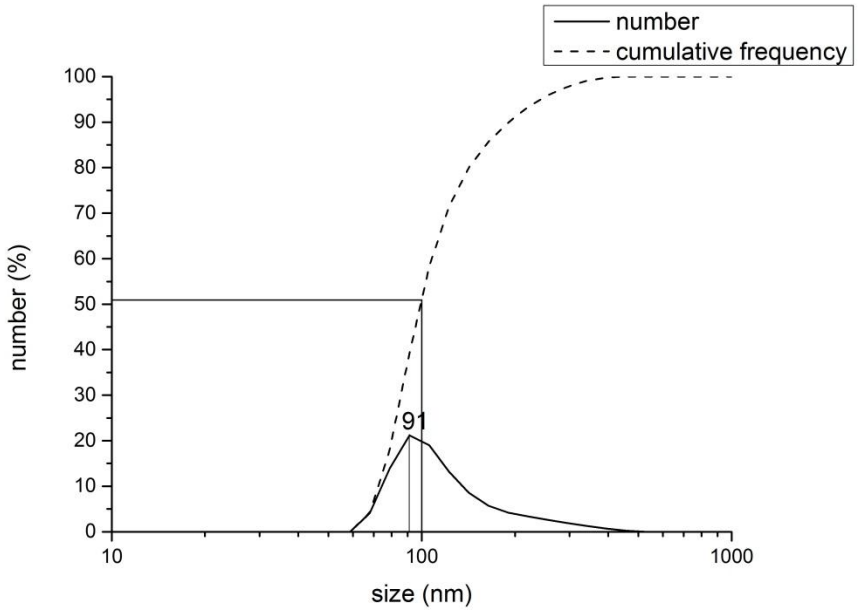

Figure 22: Size distribution of particles obtained with the syringes proof-of-concept method. The analysis was performed through DLS technique.

Figure 23 shows the size distribution of a sub-fraction of particles shown in Figure 22 obtained using the supernatant taken after 25 minutes of centrifugation at 4500 rcf.

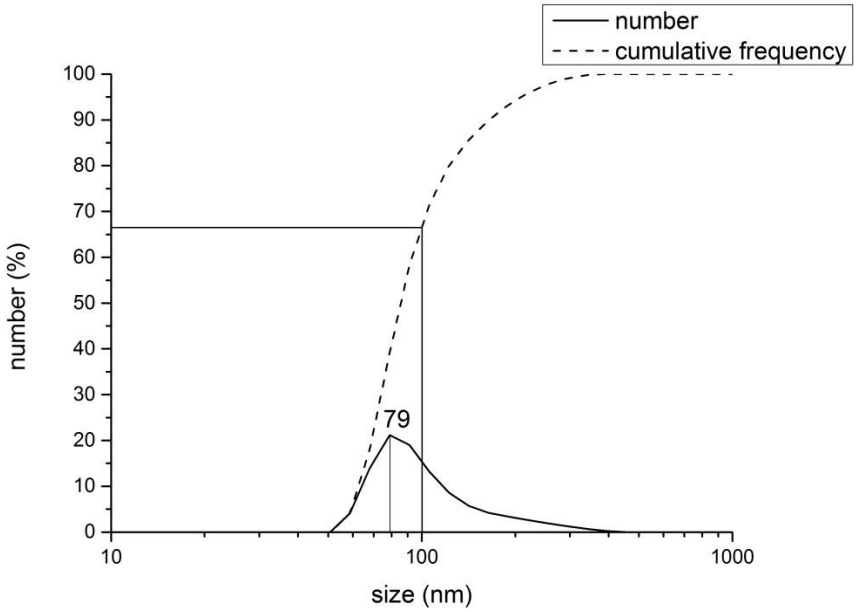

Figure 23: Particle size distribution of particles obtained with the syringes proof-of-concept method. Supernatant obtained with centrifugation at 4500 rcf for 25 minutes. Analysis was performed through DLS technique.

It is evident that the continuous method is more effective in the production of particles smaller than 100 nm, allowing to reach the threshold of 50% of particles smaller of 100 nm. This value is recommended by the European Union for the definition of nanomateriali (Potočnik, 2011).

4.1.3 Continuous synthesis with a pilot plant

Once the effectiveness of the continuous method was verified, a pilot plant for the continuous $FePO_4$ NPs synthesis was set up, using two dosing pumps for solutions pumping, and an HPLC mixing tee as mixing chamber (Figure 24).

Figure 24: Pilot plant for continuous $FePO_4$ NPs synthesis.

The system could produce 15 $L \cdot h^{-1}$ of raw $FePO_4$ NPs suspension, that were purified through dialysis.
Figure 25 shows the results of the DLS analysis of the NPs produced by the device, with a peak of particles at 78 nm. About 64% of particles are smaller than 100 nm.

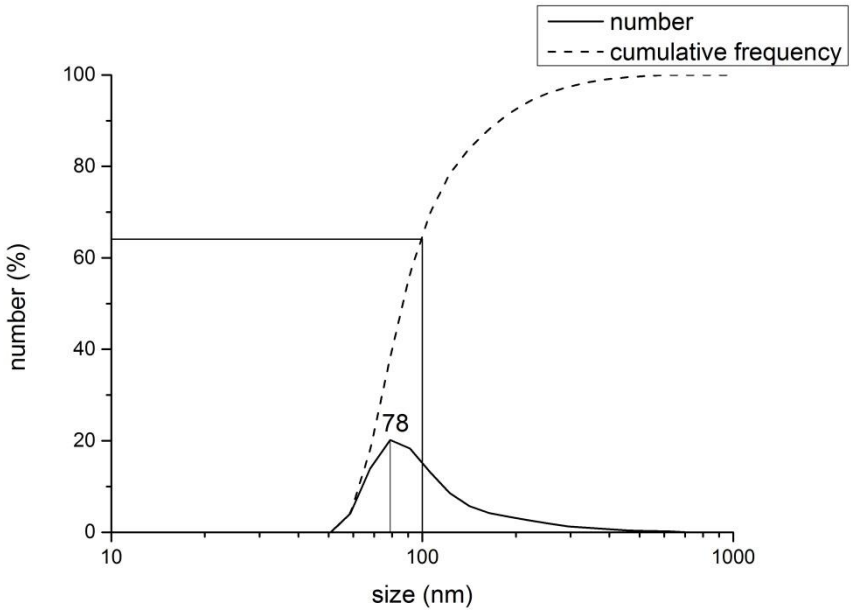

Figure 25: Size distribution of $FePO_4$ particles obtained with the continuous pilot plant. The analysis was performed through DLS technique.

Figure 26 shows TEM (Transmission Electron Microscopy) visualizations of the obtained $FePO_4$ NPs. It is evident that single NPs are much smaller than 100 nm, being about 20-25 nm in diameter. In addition, the NPs can aggregate together, thus explaining the broad range of size distribution measured with DLS analysis, given that this last technique cannot discriminate single particles from aggregates.

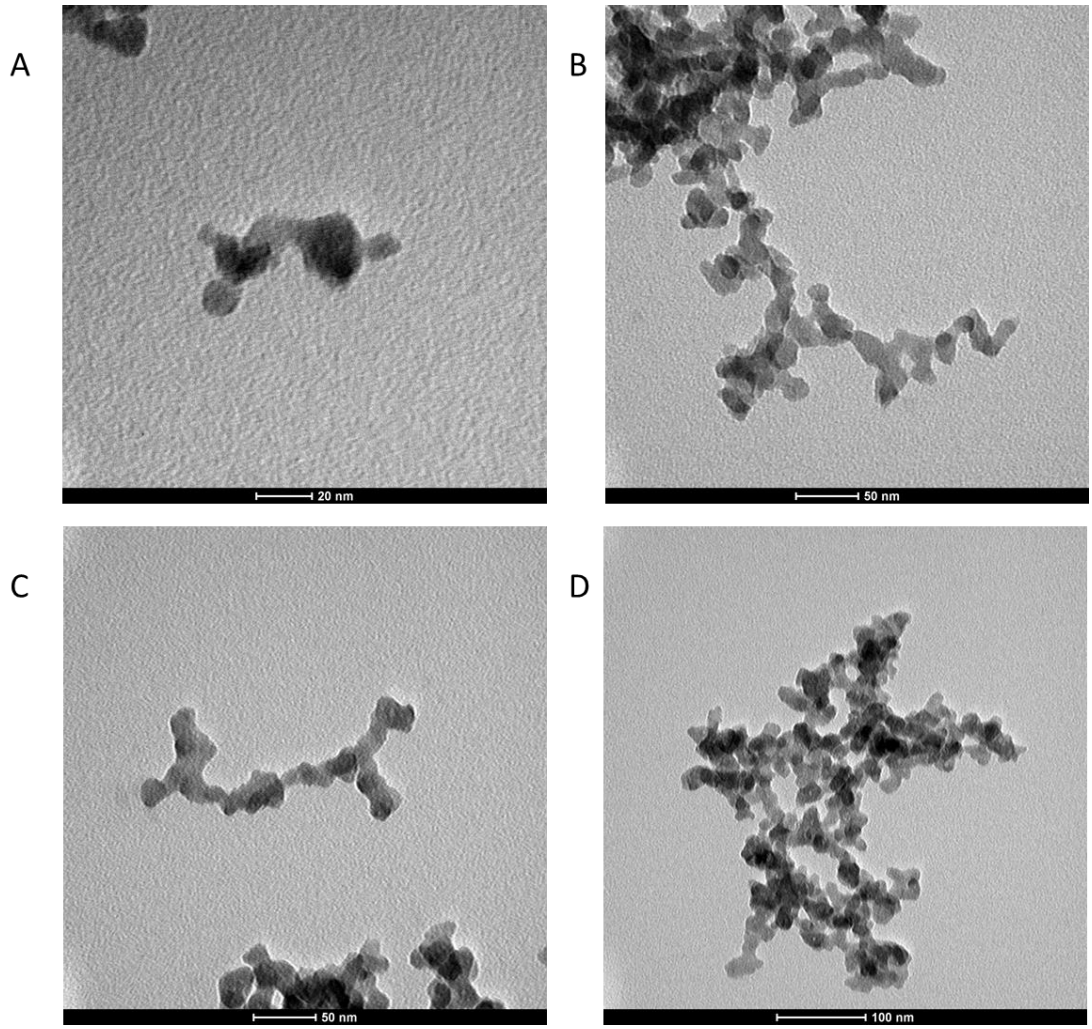

Figure 26: TEM visualization of $FePO_4$ NPs obtained with the continuous pilot plant.

4.1.4 $FePO_4$ NPs stability on long time periods and citrate capping effectiveness

$FePO_4$ NPs suspensions obtained with the pilot plant, even if small and with more than 50% of the aggregates smaller than 100 nm, showed to be not stable for long period, aggregating and then sedimenting.
In fact, comparing the DLS analysis of $FePO_4$ NPs suspension after 1 hour to the synthesis (Figure 25) with the DLS analysis of the same $FePO_4$ NPs suspension after 8 months of storage at room temperature (Figure 27), it is possible to see that the peak size shifted from 78 nm to 140 nm, and the portion of aggregates smaller than 100 nm dramatically was reduced from 64% to 8%.
To solve this problem, NPs were citrate capped through the addition of tribasic potassium citrate and thorough vortexing in order to reduce aggregation on long time periods.

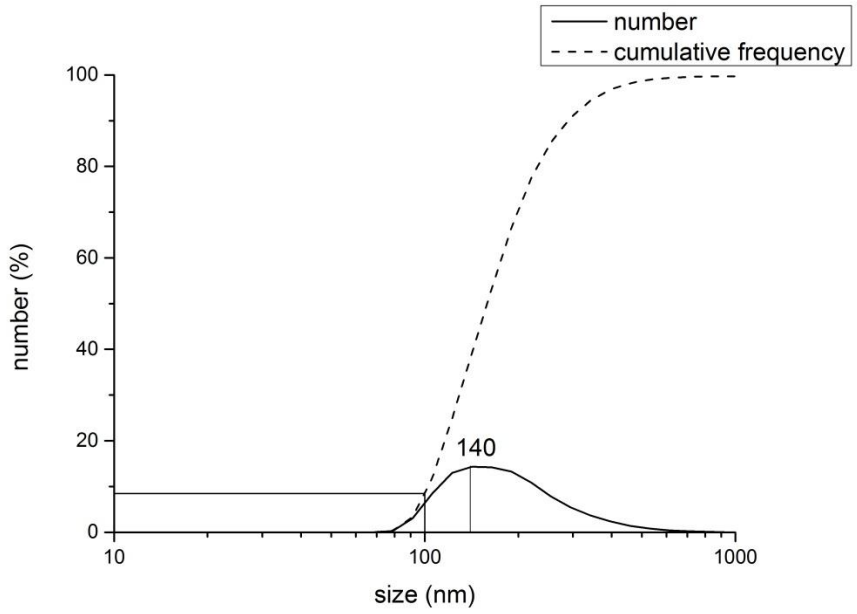

Figure 27: Size distribution of $FePO_4$ particles obtained with the continuous pilot plant after 8 months of storage. The analysis was performed through DLS technique.

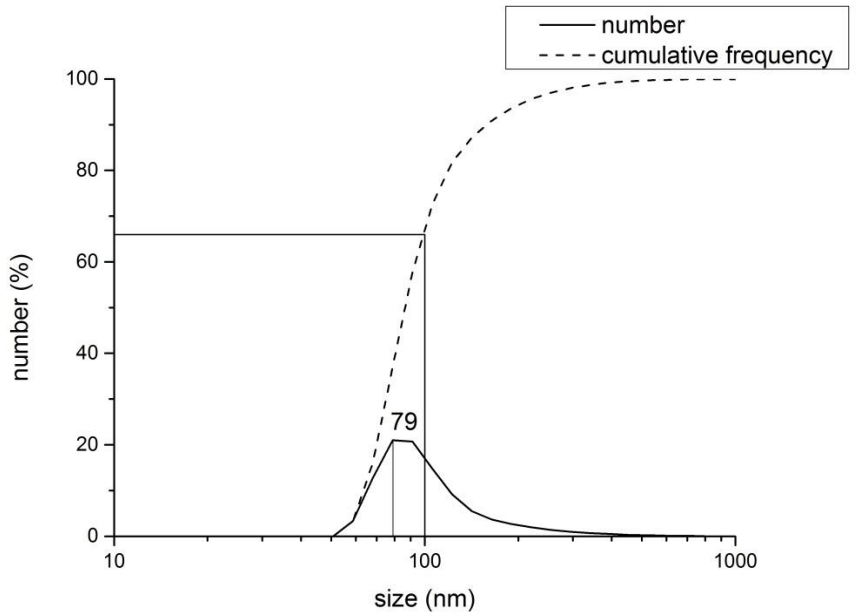

Figure 28: Size distribution of citrate-capped $FePO_4$ particles obtained with the continuous pilot plant after 8 months of storage. Analysis was performed through DLS technique.

The citrate-capping of $FePO_4$ NPs is effective (Figure 28) in stabilizing the suspension, preventing it from aggregation and sedimentation for at least 8 months.

4.1.5 Laboratory-scale batch synthesis

As already explained in material and methods section continuous productive process are useful and economically advantageous for making large amounts of NPs, but they are less practical and more wasteful when the plant operates for short time. For these reasons, a laboratory-scale batch synthesis method, was developed for the production of citrate-capped $FePO_4$ NPs to be used in our experiments.

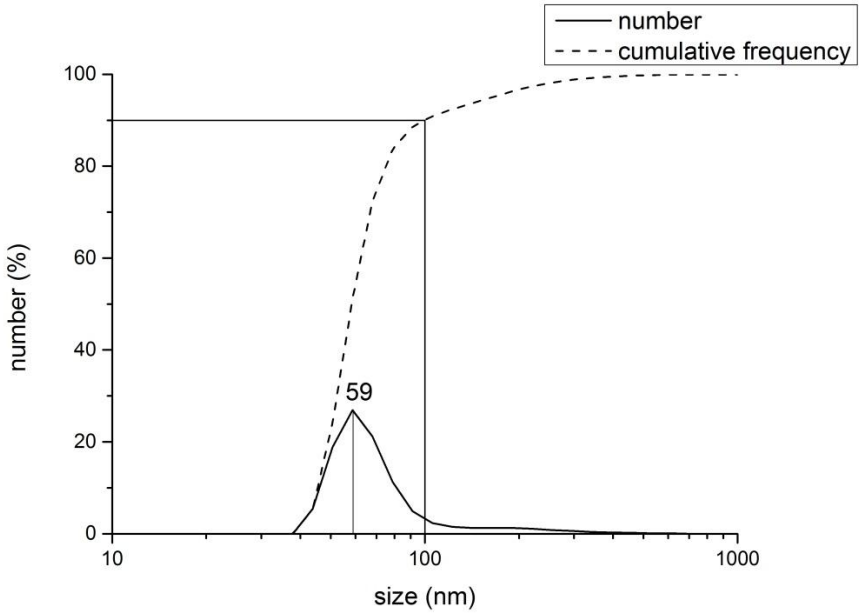

Figure 29: DLS analysis of citrate-capped NPs produced with the batch method optimized for laboratory scale. Analysis was performed through DLS technique.

Figures 29 and 30 show the results of DLS analysis and TEM visualization, respectively, of $FePO_4$ NPs synthesized at lab-scale. NPs were smaller than 20 nm, but could aggregate together, with a size peak of aggregates of 59 nm. About 90% of them are smaller than 100 nm.

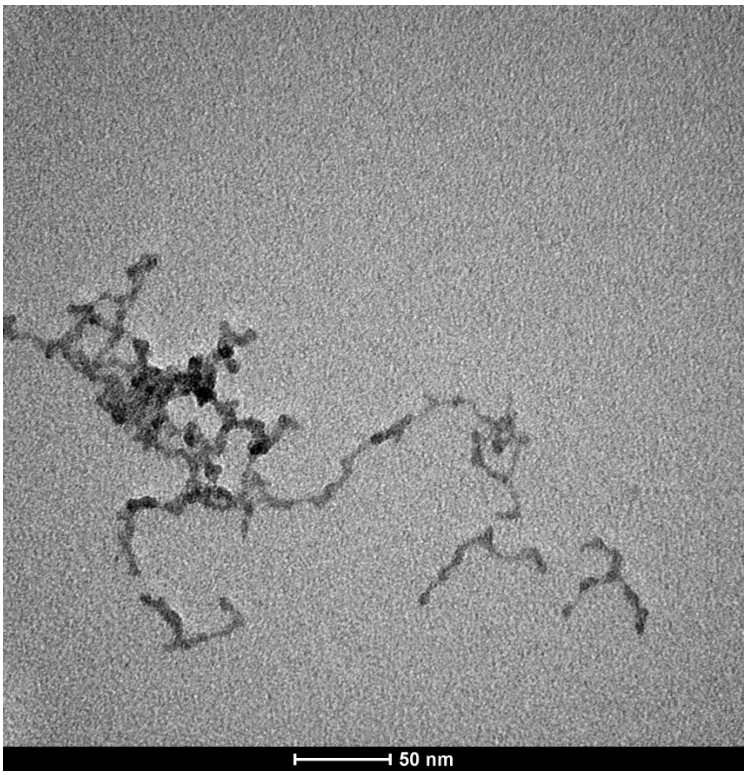

Figure 30: TEM visualization of $FePO_4$ NPs produced with the batch method optimized for laboratory scale

Fe/P molar ratio was 1.055 calculated using the quantification of both elements in the suspension (0.141M for Fe and 0.133 for P), suggesting the hypothetical formula $Fe(PO_4)_{0.95}(OH)_{0.15}$.

These NPs were tested for their effectiveness as nutrient source through growth experiments in hydroponics using cucumber (*Cucumis sativus*) and maize (*Zea mays*) seedlings.

4.2 Effects of $FePO_4$ NPs on plants

4.2.1 Experimental design

The obtained $FePO_4$ NPs were tested for their effectiveness as P and Fe sources on two crop species: cucumber (*Cucumis sativus*), a *Strategy I* plant for Fe acquisition, and maize (*Zea mays*) a *Strategy II* plant. The experiments were carried out in hydroponics. Three growth and treatment experiments (biological replicates) were independently set up. The experiments were designed in order to evaluate the effect of $FePO_4$ NPs as source of both nutrients, or source of sole P and Fe. For this reason, as negative controls plants grown without P (-P), without Fe (-Fe), or without both nutrients (-P-Fe) were used. In addition, in order to analyze if the size of $FePO_4$ particles could cause different effects on plants, we included a treatment with non-nanometric $FePO_4$ (bulk $FePO_4$) in the experiment. Both $FePO_4$ NPs and bulk $FePO_4$ were added at the same concentration used for P and Fe in the complete nutrient solution (100 µM).

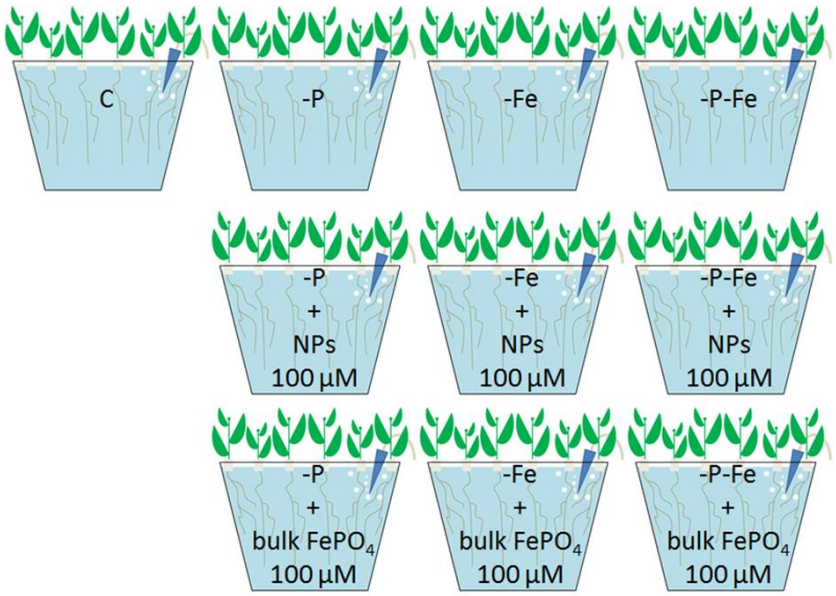

Figure 31: Schematic representation of the experimental condition set up.

4.2.2 Effects of $FePO_4$ NPs on cucumber (*Cucumis sativus*)

4.2.2.1 Morpho-physiological parameters

Morpho-physiological parameters were evaluated at the end of the experiments (after 14 days of hydroponically growth) in order to evaluate the effect of the different forms of $FePO_4$ applied (NPs or bulk material) on plants growth.
At first glance, a better growth of plants treated with $FePO_4$ NPs in comparison with the ones grown with the non-nano (bulk) $FePO_4$ can be noticed (Figure 32).

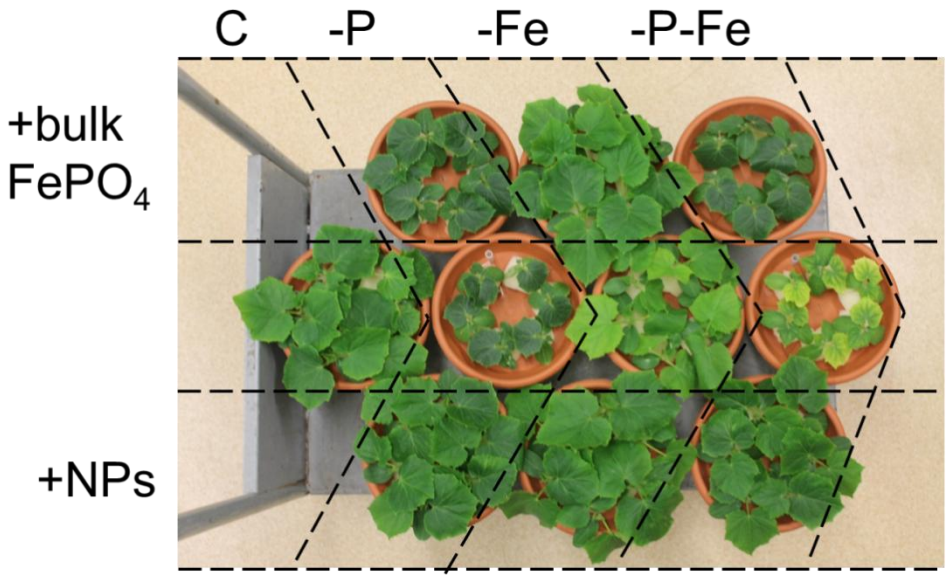

Figure 32: Cucumber plants after 14 days of growth in hydroponics.

SPAD index, a parameter that correlates to chlorophyll content in the leaf tissue, was measured. The first leaf exhibited more differences in SPAD index, so this parameter was chosen to be shown instead of the mean SPAD index of all leaves. Plants grown without P^-(-P) and with bulk $FePO_4$ (-P+bulk $FePO_4$) as source of P showed higher SPAD index values than the positive control (Figure 13A). This effect is a known P deficiency symptom (Hecht-Buchholz, 1967), due to a reduced leaf growth, and it is appreciable even at the phenotypic level (Figure 10). On the other hand, plants grown with $FePO_4$ NPs as P source (-P+NPs) did not present differences from the positive control.

As expected, in plants grown without Fe (-Fe), SPAD index was significantly reduced when compared to the positive control (Figure 33B). On the contrary, for plants grown with $FePO_4$ NPs (-Fe+NPs) and bulk $FePO_4$ (-Fe+bulk $FePO_4$) as Fe source differences from the positive control were not recorded.

A reduction in SPAD Index was recorded in plants grown under double deficiency (-P-Fe) when compared to the positive control, while plants grown with $FePO_4$ NPs as source of both nutrients (-P-Fe+NPs) were not different from the positive control (Figure 33C). On the other hand, plants grown with bulk $FePO_4$ as source of both Fe and P (-P-Fe+bulk $FePO_4$) had higher SPAD values than other conditions, suggesting a P-deficiency condition.

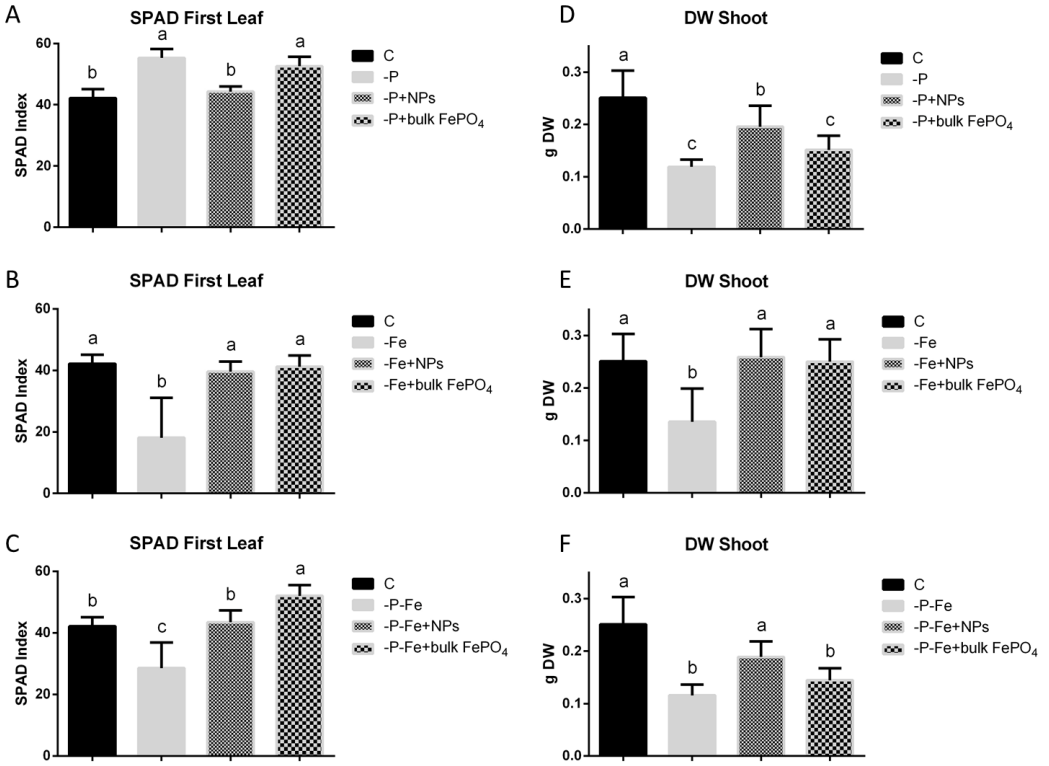

Figure 33: SPAD index of the first leaf (A, B and C) and dry weight of shoot (D, E and F) of cucumber plants treated with different nutrient sources. A and D: Control plants (C), plants grown without P (-P), plants grown with $FePO_4$ NPs as P source (-P+NPs), plants grown with bulk $FePO_4$ as P source (-P+bulk $FePO_4$); B and E: Control plants (C), plants grown without Fe (-Fe), plants grown with $FePO_4$ NPs as P source (-Fe+NPs), plants grown with bulk $FePO_4$ as Fe source (-Fe+bulk $FePO_4$); C and F: Control plants (C), plants grown without both P and Fe (-P-Fe), plants grown with $FePO_4$ NPs as source of both P and Fe (-P-Fe+NPs), plants grown with bulk $FePO_4$ as source of both P and Fe (-P-Fe+bulk $FePO_4$). Data are means ± SD of three independent experiments with three plants (technical replicates) each for dry weight, and six plants (technical replicates) for SPAD index (One-way ANOVA with Turkey's post hoc test, $p<0.05$).

Regarding shoot biomass, it is evident that all deficiency conditions led to a reduction of the dry weight of the aerial part, in comparison to the positive control (Figure 33D, E and F). Plants grown with $FePO_4$ NPs as source of P (-P+NPs) produced less shoot biomass than the positive control. Anyway, these values are higher than those recorded for plants grown with bulk $FePO_4$ (-P+bulk $FePO_4$), that showed similar values of P-deficient plants (Figure 33D). $FePO_4$ NPs and bulk $FePO_4$ as Fe sources did not cause differences in the dry biomass relative to the positive control.

On the other hand, considering the double deficiency (Figure 33F), similar values of shoot dry weight were recorded for plants grown with $FePO_4$ NPs (-P-Fe+NPs) and bulk $FePO_4$ (-P-Fe+bulk $FePO_4$).

Regarding the effects of the treatments on root parameters, dry weight was slightly affected although these differences were not statistically significant (Figure 34A, B and C). However, a decreasing trend in biomass was observed for plants grown without Fe (-Fe) and both nutrients (-P-Fe) when compared to the positive control. On the contrary, an increasing trend was recorded for all plants grown with $FePO_4$ NPs.

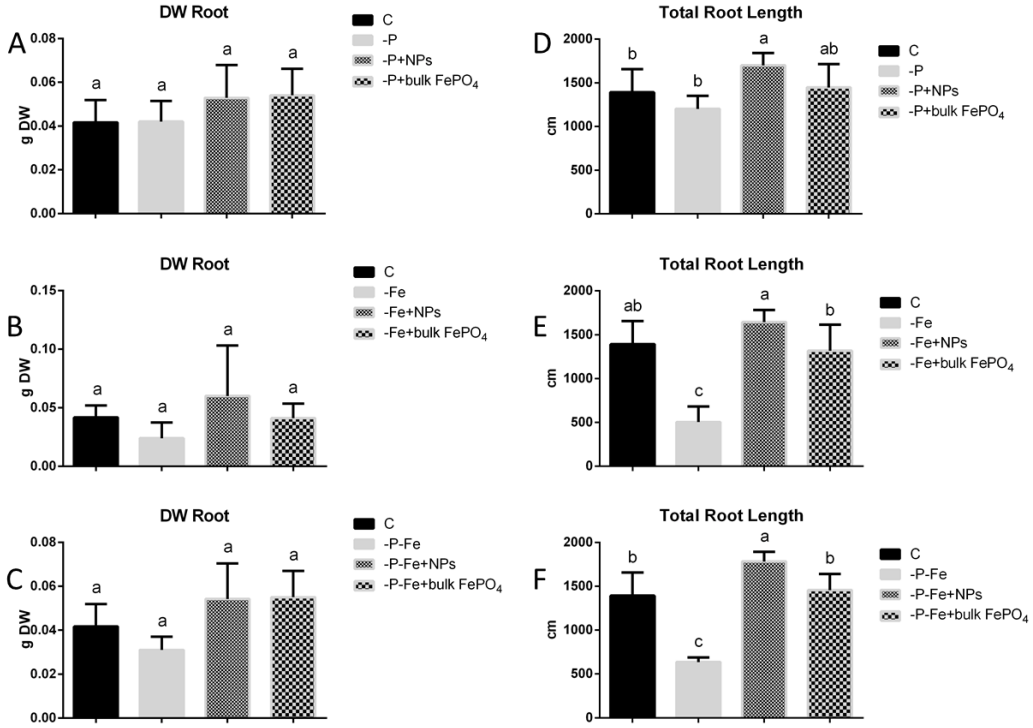

Figure 34: Root dry weight (A, B and C) and total root length (D, E and F) of cucumber plants treated with different nutrient sources. A and D: Control plants (C), plants grown without P (-P), plants grown with $FePO_4$ NPs as P source (-P+NPs), plants grown with bulk $FePO_4$ as P source (-P+bulk $FePO_4$); B and E: Control plants (C), plants grown without Fe (-Fe), plants grown with $FePO_4$ NPs as P source (-Fe+NPs), plants grown with bulk $FePO_4$ as Fe source (-Fe+bulk $FePO_4$); C and F: Control plants (C), plants grown without both P and Fe (-P-Fe), plants grown with $FePO_4$ NPs as source of both P and Fe (-P-Fe+NPs), plants grown with bulk $FePO_4$ as source of both P and Fe (-P-Fe+bulk $FePO_4$). Data are means ± SD of three independent experiments with three plants (technical replicates) each (One-way ANOVA with Turkey's post hoc test, $p<0.05$).

The effects of treatments on the root apparatus were more evident on total root length (Figure 34D, E and F). This parameter was estimated analyzing roots images with WinRHIZO^{TM} software. Plants grown with $FePO_4$ NPs displayed the higher root length, with significant differences from the control for plants grown with NPs as sources of P (-P+NPs). Considering Fe, the well-known inhibition of root growth due to Fe-deficiency can be observed both in single deficiency (Figure 14E) and in double deficiency (Figure 34F). This symptom is not present for plants grown with both forms of $FePO_4$ (bulk and NPs). Furthermore, plants grown with $FePO_4$ NPs as source of both P and Fe (-P-Fe+NPs) had total root length values even higher than the control (Figure 34F).

Also for root surface area plants grown with $FePO_4$ NPs displayed the higher root length among treatments (Figure 35A, B and C). However this behavior was significant only considering the differences between the plants treated with NPs and those grown without P and Fe at the same time. Considering Fe, both plants grown in single deficiency (Figure 35B) and double deficiency (Figure 35C) showed a root growth inhibition. This symptom was not observed for plants grown with both forms of $FePO_4$ (bulk and NPs).

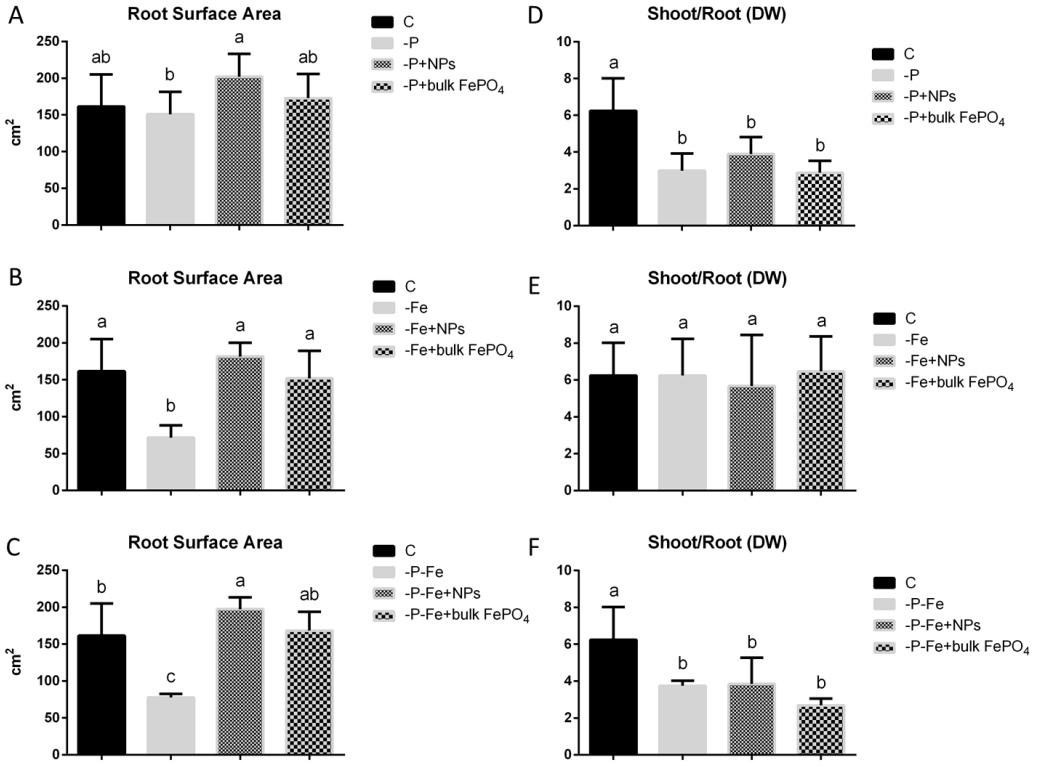

Figure 35: Root surface area (A, B and C) and Shoot/Root ratio calculated using dry weight values (D, E and F) of cucumber plants treated with different nutrient sources. A and D: Control plants (C), plants grown without P (-P), plants grown with $FePO_4$ NPs as P source (-P+NPs), plants grown with bulk $FePO_4$ as P source (-P+bulk $FePO_4$); B and E: Control plants (C), plants grown without Fe (-Fe), plants grown with $FePO_4$ NPs as P source (-Fe+NPs), plants grown with bulk $FePO_4$ as Fe source (-Fe+bulk $FePO_4$); C and F: Control plants (C), plants grown without both P and Fe (-P-Fe), plants grown with $FePO_4$ NPs as source of both P and Fe (-P-Fe+NPs), plants grown with bulk $FePO_4$ as source of both P and Fe (-P-Fe+bulk $FePO_4$). Data are means ± SD of three independent experiments with three plants (technical replicates) each (One-way ANOVA with Turkey's post hoc test, $p<0.05$).

Given that a typical response of plants to P deficiency is the alteration of the shoot/root ratio in favor to larger roots growth, this parameter was also evaluated. This parameter was significantly lower than the positive control for plants grown with both forms of $FePO_4$ (NPs and bulk), when applied as sources of P (Figures 35D and F).

4.2.2.2 Macro- and micronutrient content in plant tissues

The concentration of P, Fe and other mineral nutrients (Mg, K, Ca, Mn, Cu, Zn) in shoot and root tissues was evaluated by multi-elemental analysis through ICP-MS. In the following paragraphs the main results showing the significant differences between the treatments are described, with particular attention to the single deficiencies (-P and -Fe). All the results were reported in Supplemental Tables S2-S7.

P contents

Considering the shoot P contents, we observed a marked reduction in all conditions relative to their positive control (Figure 36A). However, P contents of plants grown with $FePO_4$ NPs, are significantly higher than in plants grown with bulk $FePO_4$ as P source and of those grown without the macronutrient. At root level, P concentrations of plants grown with the two forms of $FePO_4$ were higher than in plants grown without the macronutrient but not significantly different among them (Figure 36 B).

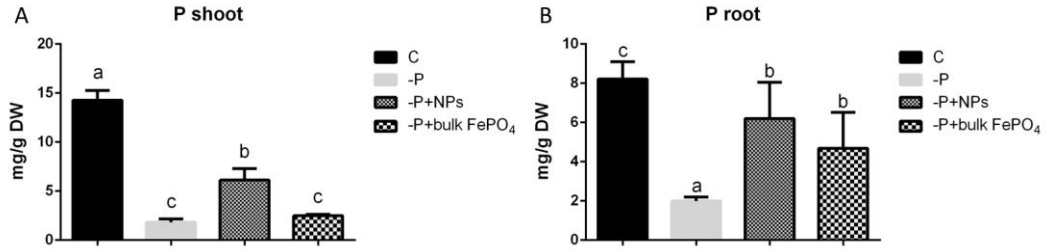

Figure 36: P concentrations (mg/gDW) in shoots (A) and roots (B) of cucumber plants treated with different nutrient sources; control plants (C), plants grown without P (-P), plants grown with $FePO_4$ NPs as P source (-P+NPs), plants grown with bulk $FePO_4$ as P source (-P+bulk $FePO_4$). Data are means ± SD of three independent experiments with three plants (technical replicates) each (One-way ANOVA with Turkey's post hoc test, $p<0.05$).

Fe contents

Shoot Fe concentrations of plants grown with both forms of $FePO_4$ as a source of Fe was not significantly different from the positive control (Figure 37A). However, Fe concentrations for plants grown with bulk $FePO_4$ were slightly lower. As expected, the shoot Fe content of plants grown without the micronutrient showed the lowest values. Concerning root Fe contents, our results underlined a higher amount of this element in plants grown with $FePO_4$ NPs, with levels two times higher than the plants grown with bulk $FePO_4$ and four times higher than the positive control (Figure 37B).

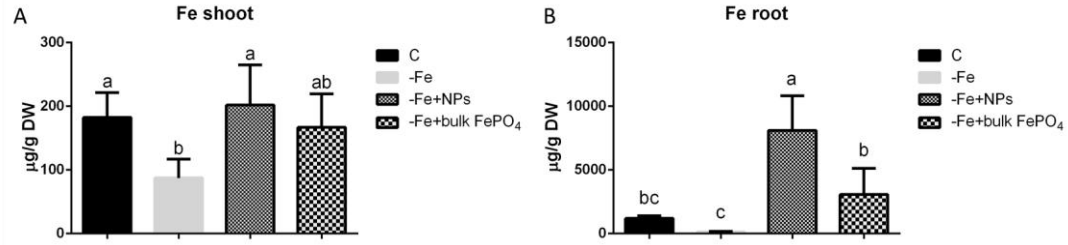

Figure 37: Fe concentrations (µg/gDW) in shoots (A) and roots (B) of cucumber plants treated with different nutrient sources; control plants (C), plants grown without Fe (-Fe), plants grown with $FePO_4$ NPs as Fe source (-Fe+NPs), plants grown with bulk $FePO_4$ as Fe source (-Fe+bulk $FePO_4$). Data are means ± SD of three independent experiments with three plants (technical replicates) each (One-way ANOVA with Turkey's post hoc test, $p<0.05$).

Mg contents

Iron-deficient plants showed an amount of Mg in shoots about two times higher than that measured for the positive control (Figure 38A). A significant increase in Mg concentration was also observed for plants grown with bulk $FePO_4$, but not for plants grown with NPs. On the other hand, no significant differences could be recorded in roots for this nutrient (Figure 38B).

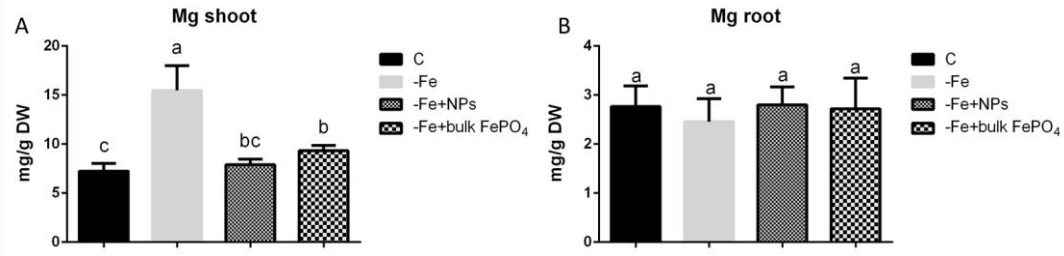

Figure 38: Mg concentrations (mg/gDW) in shoots (A) and roots (B) of cucumber plants treated with different nutrient sources; control plants (C), plants grown without Fe (-Fe), plants grown with $FePO_4$ NPs as Fe source (-Fe+NPs), plants grown with bulk $FePO_4$ as Fe source (-Fe+bulk $FePO_4$). Data are means ± SD of three independent experiments with three plants (technical replicates) each (One-way ANOVA with Turkey's post hoc test, $p<0.05$).

Zn contents

Plants grown without Fe displayed an increase in Zn concentrations in both shoots and roots, if compared to the positive control (Figure 39). This behavior could also be reported in roots of plants grown with bulk $FePO_4$ as Fe source (Figure 39B), while plants grown with $FePO_4$ NPs had similar Zn levels of the positive control in both tissues.

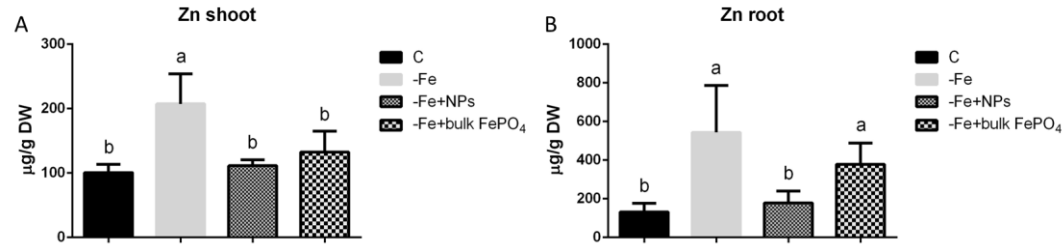

Figure 39: Zn concentrations (µg/gDW) in shoots (A) and roots (B) of cucumber plants treated with different nutrient sources; control plants (C), plants grown without Fe (-Fe), plants grown with $FePO_4$ NPs as Fe source (-Fe+NPs), plants grown with bulk $FePO_4$ as Fe source (-Fe+bulk $FePO_4$). Data are means ± SD of three independent experiments with three plants (technical replicates) each (One-way ANOVA with Turkey's post hoc test, $p<0.05$).

Mn contents

Plants grown without Fe showed an increase in Mn concentration in both shoot and root relative to the positive control. A similar result was observed for plants grown with bulk $FePO_4$, with an increase particularly evident in root tissues (Figure 40B). On the other hand, plants grown with $FePO_4$ NPs displayed values

of Mn concentration similar to the positive control in both tissues (Figure 40A and B).

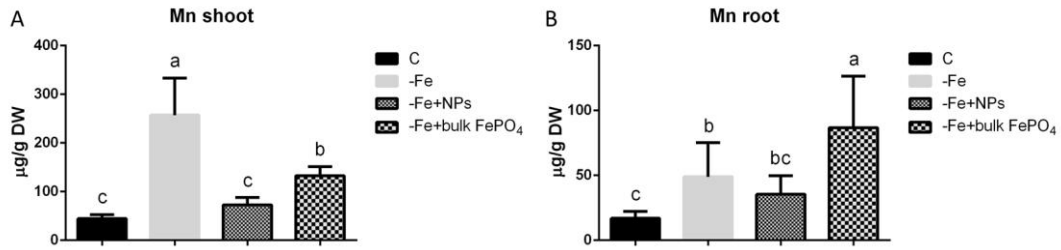

Figure 40: Mn concentrations (µg/gDW) in shoots (A) and roots (B) of cucumber plants treated with different nutrient sources; control plants (C), plants grown without Fe (-Fe), plants grown with $FePO_4$ NPs as Fe source (-Fe+NPs), plants grown with bulk $FePO_4$ as Fe source (-Fe+bulk $FePO_4$). Data are means ± SD of three independent experiments with three plants (technical replicates) each (One-way ANOVA with Turkey's post hoc test, $p<0.05$).

Cu contents

Also in the case of Cu shoot and root tissues of Fe-deficient plants showed concentrations higher than the positive control. Furthermore as for Mn and Zn, an increase of the micronutrient concentration in plants grown with bulk $FePO_4$ can be seen together with similar levels between positive control and plants grown with $FePO_4$ NPs (Figure 21).

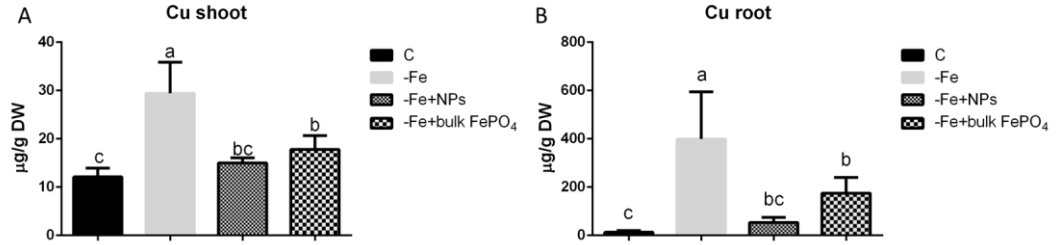

Figure 41: Cu concentrations (µg/gDW) in shoots (A) and roots (B) of cucumber plants treated with different nutrient sources; control plants (C), plants grown without Fe (-Fe), plants grown with $FePO_4$ NPs as Fe source (-Fe+NPs), plants grown with bulk $FePO_4$ as Fe source (-Fe+bulk $FePO_4$). Data are means ± SD of three independent experiments with three plants (technical replicates) each (One-way ANOVA with Turkey's post hoc test, $p<0.05$).

4.2.2.3 TEM observation of cucumber tertiary roots

Plants grown in hydroponics in the presence of $FePO_4$ NPs as phosphorous source showed a visible marked orange coloration of roots (Figure 42). On the basis of this observation, tertiary roots of plants grown with $FePO_4$ NPs were analyzed at TEM (Transmission Electron Microscope) in order to understand if $FePO_4$ NPs can enter into roots, tre-passing cell wall and plasma membranes without being dissolved.

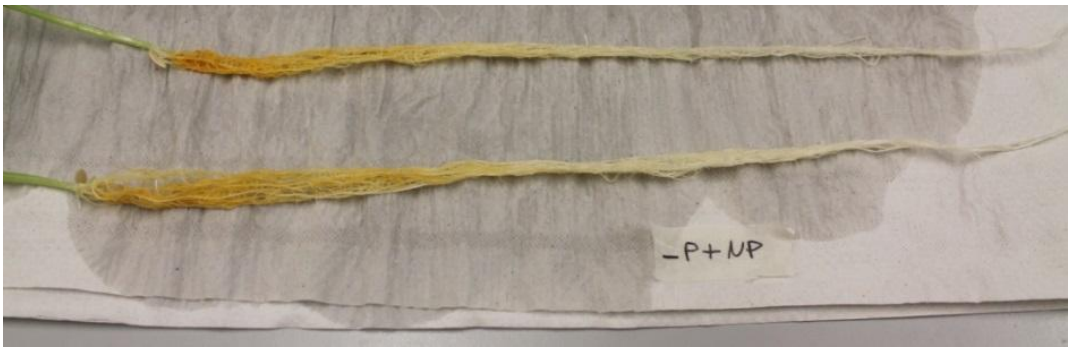

Figure 42: Orange roots coloration of a cucumber plant grown with $FePO_4$ NPs as P source.

Figure 23A shows that $FePO_4$ NPs could not be observed within roots, but only outside in aggregated form (Figure 23B). On the other hand, outside the cell wall some lath-shaped, electron dense nanometric objects were observed mixed together with NPs. Other images are reported in Supplementary figure S2.

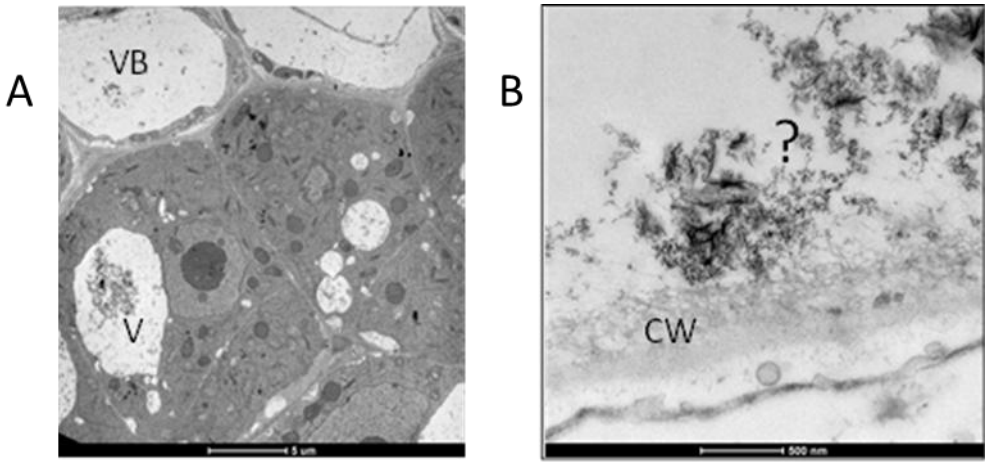

Figure 43: TEM observation of a cross section of a tertiary root of a cucumber plant grown with $FePO_4$ NPs as P source. In A: VB: Vascular Bundle; V: Vacuole; In B: CW: Cell Wall; ?: unexpected and unknown nano sized black laths.

4.2.2.4 ESEM observation and ESEM-EDAX analysis of cucumber roots

In order to investigate the chemical nature of the orange coloration of roots and of the lath-shaped, electron dense nanometric objects that were observed mixed together with NPs outside cell wall, portions of roots of cucumber plants grown with $FePO_4$ NPs as P source (-P+NPs) were observed using a SEM (Scansion Electronic Microscope). During the observation, some electron dense crusts were noticed on roots surface (Figure 24), and were analysed though EDAX (Energy Dispersive X-ray Spectroscopy).

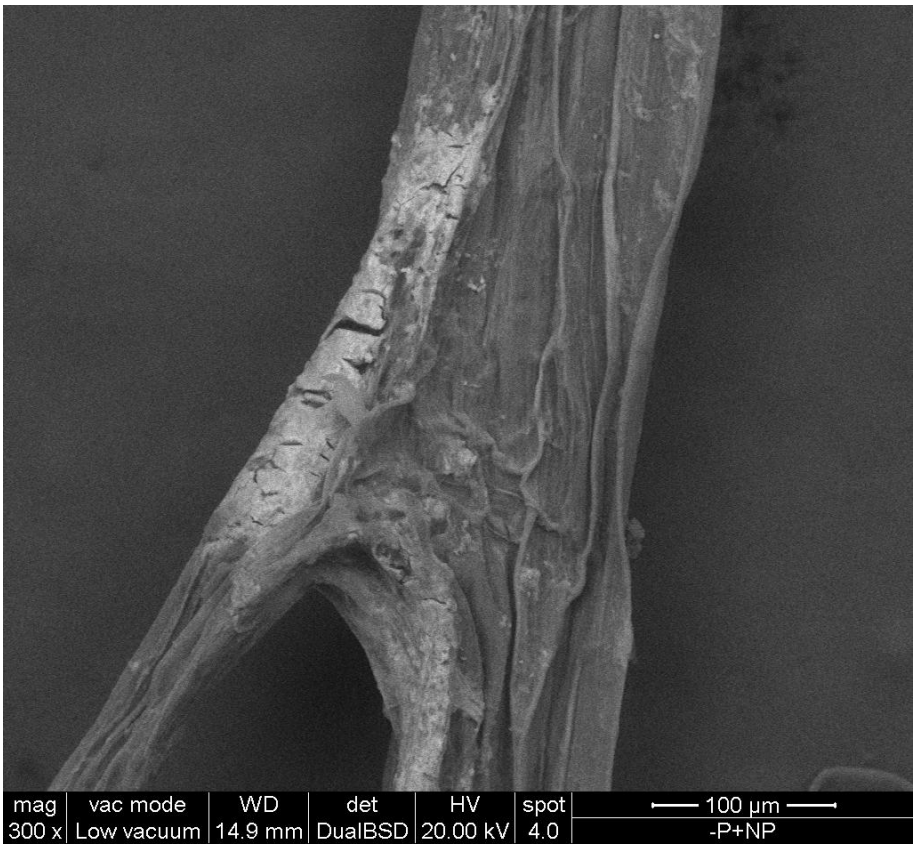

Figure 44: ESEM observation of roots of cucumber plants grown with $FePO_4$ NPs as P source (-P+NPs); notice the electron dense crusts (bright color on the left).

The analysis revealed that these electron dense crusts had a Fe/P atomic ratio between 2.49 and 3.84, indicating a clear excess of Fe if compared to the stoichiometry of $FePO_4$. Complete EDAX analysis results are reported in supplementary tables and figures (Report S1).

4.2.2.5 Gene expression analysis

Cucumber homologs of transcription factors known to be regulators of PO_4^{3-} (PHR1 and PHL1) and Fe (PYE and BTS) homeostasis were identified through their amino acid similarity, using Blastp analysis against Cucumber Chinese long genome v2 (Table 5).

Locus name	Arabidopsis homolog	Putative protein length
Csa3M608690	PHR1(51.6%)/PHL1(45.1%)	482 aa
Csa1M666970	PHR1(45.8%)/PHL1(49.1%)	444 aa
Csa1M009660	PYE (47.5%)	260 aa
Csa1M024210	BTS (67.6%)	1256 aa

Table 5: Locus names, and protein lengths of the putative cucumber transcription factors. The aminoacidic identity with the homolog is indicated in parenthesis.

Real-Time RT-PCR analysis was performed on cucumber roots for these genes. As housekeeping genes for data normalization CACS (Csa3M902930) and F-BOX (Csa5M642160) were chosen, being the best couple of genes for our samples according to Normfinder analysis.
Figure 45 shows the expression levels of *Csa3M608690* (45A) and *Csa1M666970* (45B) genes, encoding proteins homologous to AtPHR1 and AtPHL1 transcription factors, respectively. AtPHR1 and AtPHL1 are well-known key regulators of plant adaptation to Pi deficiency (Briat et al., 2015).
The *Csa3M608690* gene in plants grown without P appears to be downregulated in comparison to the positive control (-28%). The same trend, even if less pronounced is could be noticed in plants grown with bulk $FePO_4$ as source of phosphorous (-10%). On the other hand, this gene is upregulated in plants grown with $FePO_4$ NPs as phosphorous source.
For the gene *Csa1M666970* no significant differences could be observed, even though it was slightly upregulated in plants grown with $FePO_4$ NPs as phosphorous source.

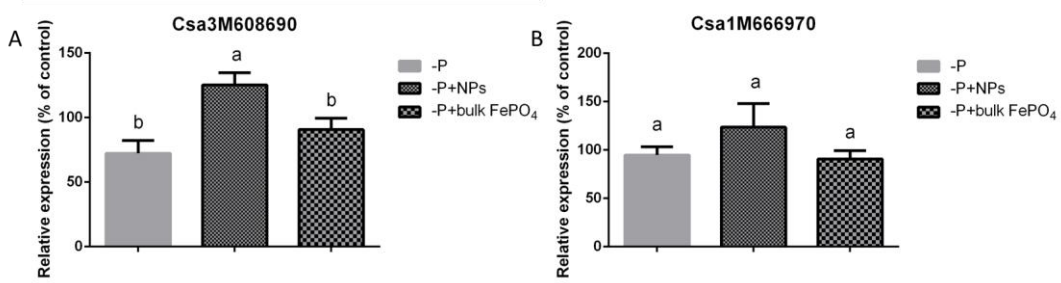

Figure 45: Relative expression expressed as percentage of the level of positive control of *Csa3M608690* (A) and *Csa1M666970* (B) genes in roots of maize plants treated with different nutrient sources; plants grown without P (-P), plants grown with $FePO_4$ NPs as P source (-P+NPs), plants grown with bulk $FePO_4$ as P source (-P+bulk $FePO_4$). Data are means ± SD of three indipendent experiments with three technical replicates each (One-way ANOVA with Turkey's post hoc test, $p<0.05$).

Figure 46 shows the expression levels of *Csa1M009660* (46A) and *Csa1M024210* (46B), homologs of *AtPYE* and *AtBTS* transcription factors respectively, known to be key regulators of iron deficiency response network (Zhang et al. 2015).
Csa1M009660 exhibited an upregulation in all conditions, although the differences were not significant (Figure 46A). Anyway, it can be observed that the overexpression is less pronounced for plants grown with $FePO_4$ NPs as Fe source.
Regarding *Csa1M024210*, a significant upregulation in plants grown without the micronutrient is evident (+200%), but did not occur in plants grown with the two forms of $FePO_4$ (bulk and NPs), as suggested by expression levels similar to the positive control.

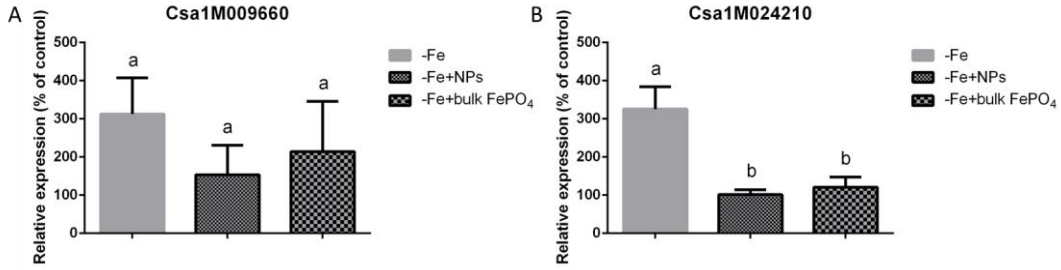

Figure 46: : Relative expression expressed as percentage of the level of positive control of *Csa1M009660* (A) and *Csa1M024210* (B genes in roots of maize plants treated with different nutrient sources; plants grown without Fe (-Fe), plants grown with $FePO_4$ NPs as Fe source (-Fe+NPs), plants grown with bulk $FePO_4$ as Fe source (-Fe+bulk $FePO_4$). Data are means ± SD of three independent experiments with three technical replicates each (One-way ANOVA with Turkey's post hoc test, $p<0.05$).

4.2.3 Effects of $FePO_4$ NPs on maize (*Zea mays*)

4.2.3.1 Morpho-physiological parameters

For maize, morpho-physiological parameters were evaluated after 17 days of growth in hydroponics. Chlorophyll content in leaves were evaluated by the measurement of SPAD index (Figure 47).

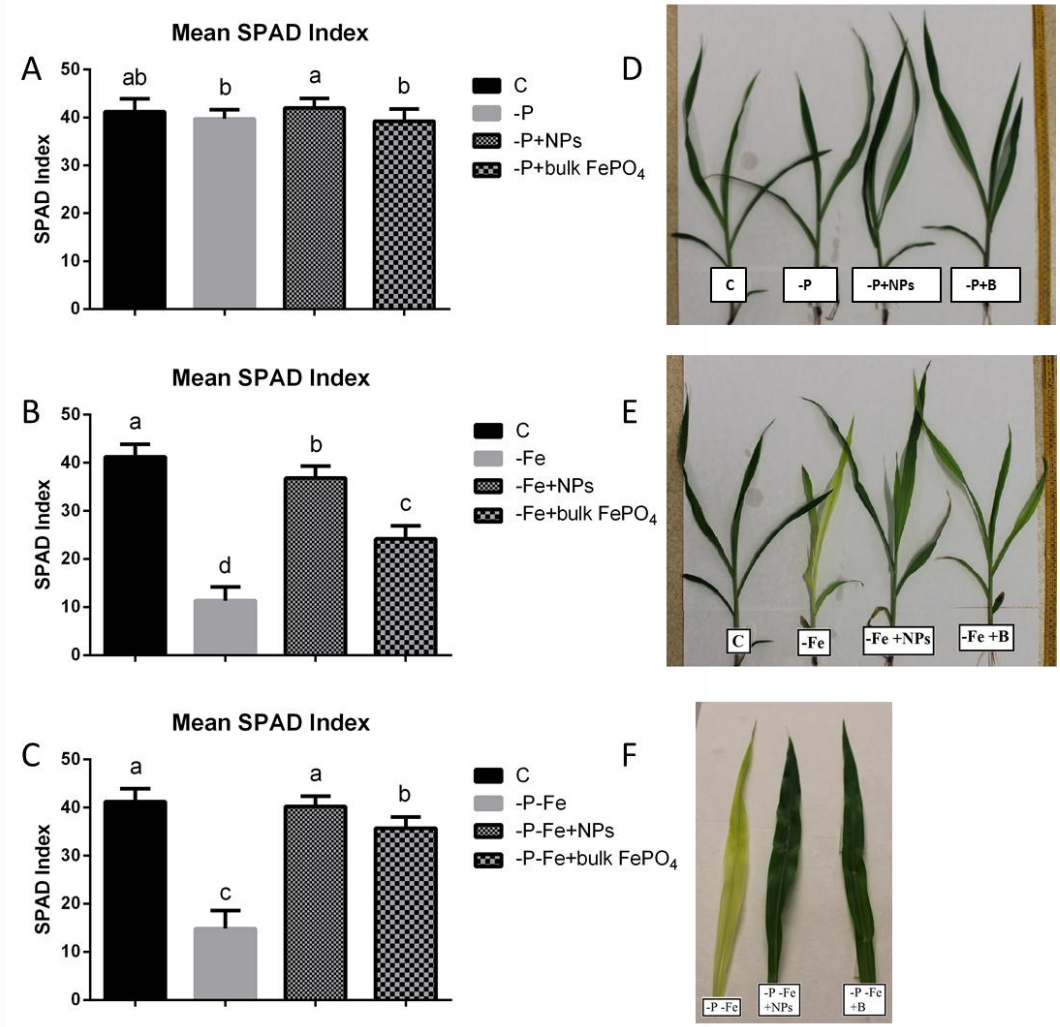

Figure 47: Mean SPAD Index (Figure A, B e C) and leaf details (Figure 24D, E and F) of maize plants treated with different nutrient sources; A and D: Control plants (C), plants grown without P (-P), plants grown with $FePO_4$ NPs as P source (-P+NPs), plants grown with bulk $FePO_4$ as P source (-P+bulk $FePO_4$); B and E: Control plants (C), plants grown without Fe (-Fe), plants grown with FePO4 NPs as P source (-Fe+NPs), plants grown with bulk $FePO_4$ as Fe source (-Fe+bulk $FePO_4$); C and F: Control plants (C), plants grown without both P and Fe (-P-Fe), plants grown with $FePO_4$ NPs as source of both P and Fe (-P-Fe+NPs), plants grown with bulk $FePO_4$ as source of both P and Fe (-P-Fe+bulk $FePO_4$). Data are means ± SD of three independent experiments with six plants (technical replicates) each (One-way ANOVA with Turkey's post hoc test, $p<0.05$).

Plants grown in conditions that affected only P composition of the nutrient solution (-P) did not show particular differences in chlorophyll content (Figure 47A). As expected, the SPAD index of Fe-deficient plants (-Fe) was dramatically lower than in control plants (Figure 47B). Conversely, plants grown with $FePO_4$ NPs as Fe source (-Fe+NPs) show SPAD values close to that of positive control, and higher than that of plants grown with bulk $FePO_4$ as source of Fe (-Fe+bulk $FePO_4$). In the same way, doubly-deficient plants (-P-Fe) exhibited a strong reduction in chlorophyll content, a behavior that was not recorded for plants grown with $FePO_4$ NPs as source of both nutrients (-P-Fe+NPs) (Figure 47C). These differences can also be observed visually by pictures of leaf details (Figures 47E and 47F).

Regarding dry biomass production, P nutritional status of plants did not particularly affect the dry weight of shoots, except for a slight decrease for plants grown without the macronutrient (Figure 48A).

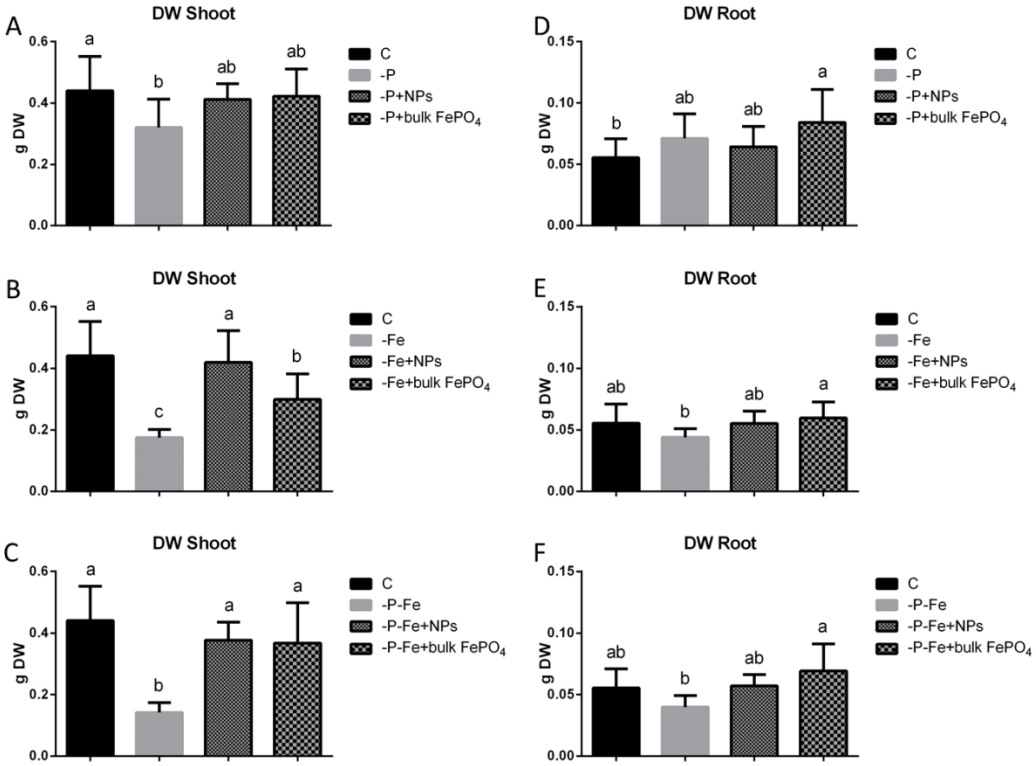

Figure 48: Dry weights of shoot (A-C) and root (D-F) of maize plants treated with different nutrient sources. A and D: Control plants (C), plants grown without P (-P), plants grown with $FePO_4$ NPs as P source (-P+NPs), plants grown with bulk $FePO_4$ as P source (-P+bulk $FePO_4$); B and E: Control plants (C), plants grown without Fe (-Fe), plants grown with $FePO_4$ NPs as P source (-Fe+NPs), plants grown with bulk $FePO_4$ as Fe source (-Fe+bulk $FePO_4$); C and F: Control plants (C), plants grown without both P and Fe (-P-Fe), plants grown with FePO4 NPs as source of both P and Fe (-P-Fe+NPs), plants grown with bulk $FePO_4$ as source of both P and Fe (-P-Fe+bulk $FePO_4$). Data are means ± SD of three independent experiments with three plants (technical replicates) each (One-way ANOVA with Turkey's post hoc test, $p<0.05$).

On the other hand, Fe shortage greatly affected shoot biomass production, and an appreciable reduction also occurred for plants grown with bulk $FePO_4$ as Fe source (-Fe+bulk $FePO_4$) (Figure 48B). On the contrary plants grown with NPs as

Fe source (-Fe+NPs) had similar values as the positive control. When the two forms of $FePO_4$ (NPs and bulk $FePO_4$) were applied as source of P and Fe a shoot biomass production comparable to the positive control was achieved (Figure 48C).
Conversely, root dry weight was not affected by nutrient deficiencies, and only some slight increases in the values of plants treated with bulk $FePO_4$ are observable. In fact, plants grown with bulk $FePO_4$ as P source (-P+bulk $FePO_4$) have higher root biomass than contol plants, while plants grown with bulk $FePO_4$ as source of Fe or both P and Fe (-Fe+bulk $FePO_4$; -P-Fe+bulk $FePO_4$) show significant differences to the corresponding nutrient deficient plants (-Fe; -P-Fe) (Figure 48D, E and F).

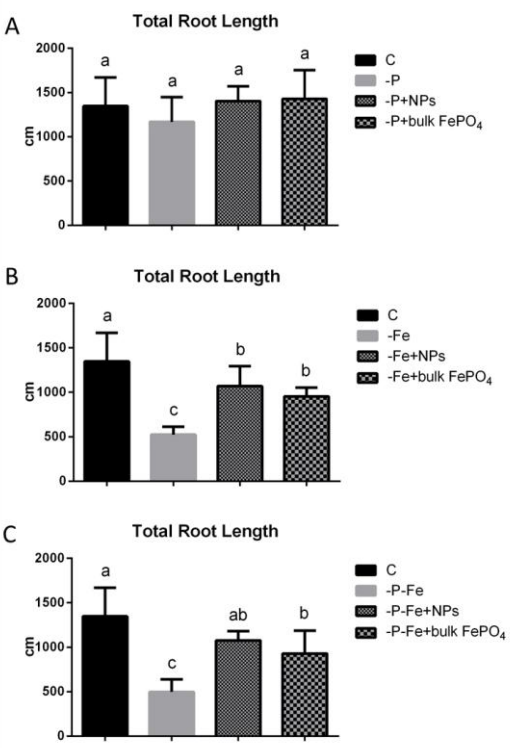

Figure 49: Total root lengths (A-C) in maize plants treated with different nutrient sources. A and D: Control plants (C), plants grown without P (-P), plants grown with $FePO_4$ NPs as P source (-P+NPs), plants grown with bulk $FePO_4$ as P source (-P+bulk $FePO_4$); B and E: Control plants (C), plants grown without Fe (-Fe), plants grown with FePO4 NPs as P source (-Fe+NPs), plants grown with bulk $FePO_4$ as Fe source (-Fe+bulk $FePO_4$); C and F: Control plants (C), plants grown without both P and Fe (-P-Fe), plants grown with $FePO_4$ NPs as source of both P and Fe (-P-Fe+NPs), plants grown with bulk $FePO_4$ as source of both P and Fe (-P-Fe+bulk $FePO_4$). Data are means ± SD of three independent experiments with three plants (technical replicates) each (One-way ANOVA with Turkey's post hoc test, $p<0.05$).

As shown in Figure 49A the effects of P shortage and different P forms on total root length were negligible. On the other hand, when Fe deficiency was applied, alone or together with P deficiency, a reduction in the root surface area was evident (Figures 49B and 49C). This decrease was less pronounced in plants grown with the two forms of $FePO_4$ (NPs and bulk $FePO_4$) as source of Fe (Figure 49B), and not significantly different from the control in plants grown with $FePO_4$ NPs as source of both nutrients (Figure 49C).

The effects of P shortage and different P forms are negligible also in respect to the surface area, as shown in Figure 50A. On the other hand, when Fe deficiency is applied, alone or together with P deficiency, a reduction in the root surface area is evident (Figures 50B and 50C). This decrease was not observed in plants grown with the two forms of $FePO_4$ (NPs and bulk $FePO_4$).

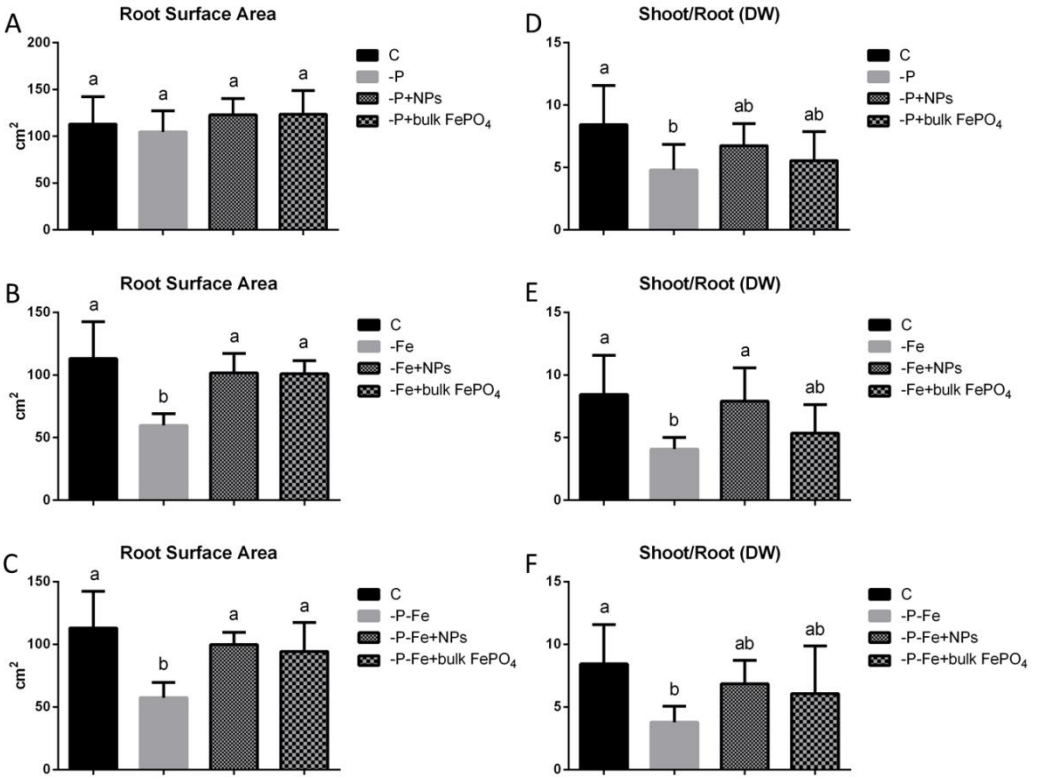

Figure 50: Root surface areas (A-C) and Shoot/Root ratio derived from dry weights (D-F) in maize plants treated with different nutrient sources. A and D: Control plants (C), plants grown without P (-P), plants grown with $FePO_4$ NPs as P source (-P+NPs), plants grown with bulk $FePO_4$ as P source (-P+bulk $FePO_4$); B and E: Control plants (C), plants grown without Fe (-Fe), plants grown with $FePO_4$ NPs as P source (-Fe+NPs), plants grown with bulk $FePO_4$ as Fe source (-Fe+bulk $FePO_4$); C and F: Control plants (C), plants grown without both P and Fe (-P-Fe), plants grown with $FePO_4$ NPs as source of both P and Fe (-P-Fe+NPs), plants grown with bulk $FePO_4$ as source of both P and Fe (-P-Fe+bulk $FePO_4$). Data are means ± SD of three independent experiments with three plants (technical replicates) each (One-way ANOVA with Turkey's post hoc test, $p<0.05$).

4.2.3.2 Anthocyanins accumulation in root tissues

Given that anthocyanins accumulation in root tissues is a known symptom of P deficiency in maize (Calderon-Vazquez, et al., 2011), these molecules were spectrophotometrically quantified in root tissues of plants grown without P (-P), with $FePO_4$ NPs (-P+NPs) and with bulk $FePO_4$ (-P+bulk $FePO_4$) as source of the macronutrient and in the positive control.

The results showed that the roots of plants grown without P had a higher anthocyanins content compared to the positive control (Figure 51). This behavior could not be observed for plants grown with $FePO_4$ NPs (-P+NPs). Moreover,

bulk $FePO_4$ caused an anthocyanins accumulation with intermediate values between positive control and plants grown without P (Figure 51).

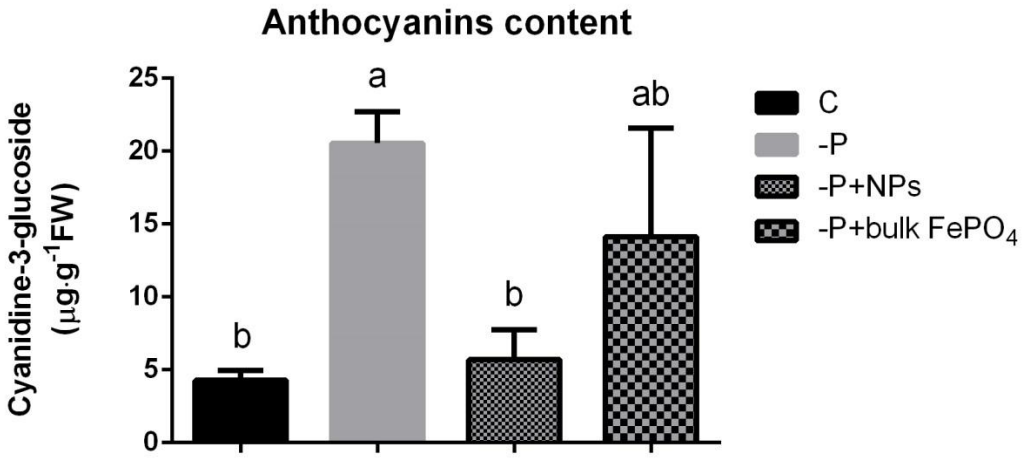

Figure 51: Anthocyanins contents (μg g^{-1} FW) in roots of maize plants treated with different nutrient sources, expressed as Cyanidine-3-glucoside; control plants (C), plants grown without P (-P), plants grown with $FePO_4$ NPs as P source (-P+NPs), plants grown with bulk $FePO_4$ as P source (-P+bulk $FePO_4$). Data are means ± SD of three independent experiments with three technical replicates (three extractions from one plant) each (One-way ANOVA with Turkey's post hoc test, $p<0.05$).

4.2.3.3 Macro- and micronutrient contents in plant tissues

The concentration of P, Fe and other mineral nutrients (Mg, K, Ca, Mn, Cu, Zn) in shoot and root tissues was evaluated by multi-elemental analysis through ICP-MS also in the experiments carried out with maize. In the following paragraphs the main results showing significant differences between the different treatments are described. Particular attention is given to the single deficiencies (-P and -Fe). All the results were reported in Supplemental Tables S8-S13.

P contents

Phosphorous content was markedly reduced in shoots of plants grown in all treatment conditions in comparison to the positive control (Figure 52A). However, at the root level (Figure 52B) plants grown with $FePO_4$ NPs as P source (-P+NPs), exhibited higher P values than plants grown with bulk $FePO_4$ as source of this macronutrient (-P+bulk $FePO_4$).

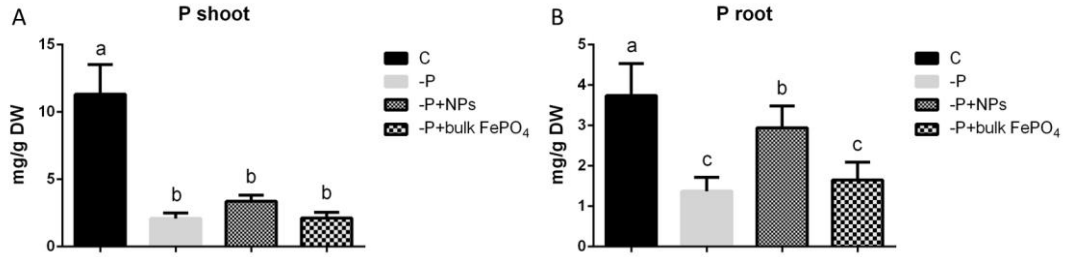

Figure 52: P concentrations (mg/gDW) in shoots and roots of maize plants treated with different nutrient sources; control plants (C), plants grown without P (-P), plants grown with $FePO_4$ NPs as P source (-P+NPs), plants grown with bulk $FePO_4$ as P source (-P+bulk $FePO_4$). Data are means ± SD of three independent experiments with three plants (technical replicates) each (One-way ANOVA with Turkey's post hoc test, $p<0.05$).

Fe contents

Shoot Fe levels of plants grown without the micronutrient and with bulk $FePO_4$ (-Fe+bulk $FePO_4$) were respectively 60% and 50% lower than the positive control (Figure 53). This reduction is less pronounced when plants were grown with $FePO_4$ NPs as Fe source (-Fe+NPs), with a reduction of 35% (Figure 53A). Looking at the concentrations of this micronutrient in roots, it appeared remarkable such a high level of this nutrient for plants grown with $FePO_4$ NPs (-Fe+NPs), with values even higher than that of the positive control. On the contrary, plants grown with bulk $FePO_4$ (-Fe+bulk $FePO_4$) showed values similar to those of plants grown without Fe (-Fe) (Figure 53B).

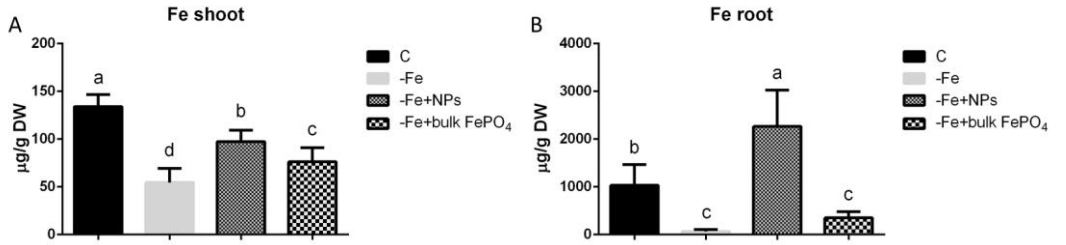

Figure 53: Fe concentrations (µg/gDW) in shoots and roots of maize plants treated with different nutrient sources; control plants (C), plants grown without Fe (-Fe), plants grown with $FePO_4$ NPs as Fe source (-Fe+NPs), plants grown with bulk $FePO_4$ as Fe source (-Fe+bulk $FePO_4$). Data are means ± SD of three independent experiments with three plants (technical replicates) each (One-way ANOVA with Turkey's post hoc test, $p<0.05$).

Mg contents

Shoot Mg concentration was not particularly modulated by the nutritional conditions, except for a slight increase in plants grown without Fe (Figure 54A). Conversely, in roots an increase of this nutrient could be observed for all the conditions, if compared to the positive control, with major increases for Fe-deficient plants (-Fe) and plants grown with bulk $FePO_4$ (-Fe+bulk $FePO_4$). Plants grown with $FePO_4$ NPs as Fe source (-Fe+NPs) showed a limited increase with intermediate values (Figure 54B).

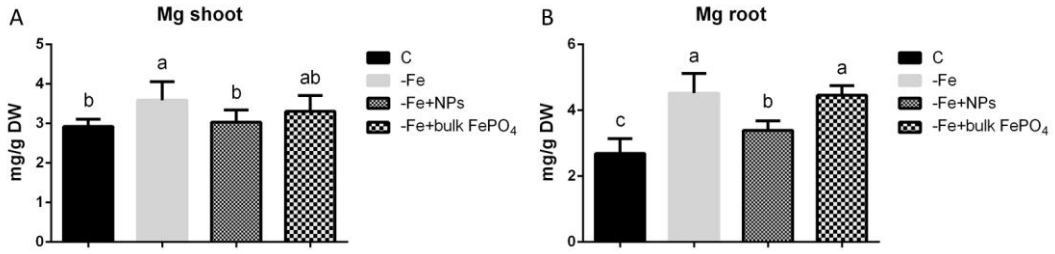

Figure 54: Mg concentrations (mg/gDW) in shoots and roots of maize plants treated with different nutrient sources; control plants (C), plants grown without Fe (-Fe), plants grown with $FePO_4$ NPs as Fe source (-Fe+NPs), plants grown with bulk $FePO_4$ as Fe source (-Fe+bulk $FePO_4$). Data are means ± SD of three independent experiments with three plants (technical replicates) each (One-way ANOVA with Turkey's post hoc test, $p<0.05$).

Zn contents

Zinc concentrations in Fe-deficient plants was significantly higher than that of control plants for both shoots and roots (Figure 55A and B). This trend also occurred in the shoots of plants grown with bulk $FePO_4$ as Fe source (-Fe+bulk $FePO_4$) (Figure 55 A), but not in roots. Zinc concentrations in shoot and root tissues of plants grown with $FePO_4$ NPs (-Fe+NPs) is comparable to control conditions.

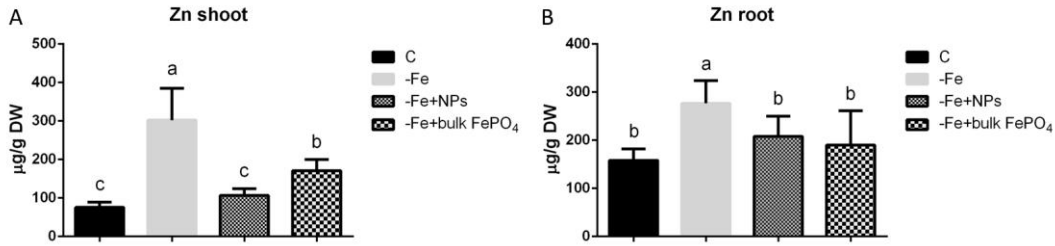

Figure 55: Zn concentrations (µg/gDW) in shoots and roots of maize plants treated with different nutrient sources; control plants (C), plants grown without Fe (-Fe), plants grown with $FePO_4$ NPs as Fe source (-Fe+NPs), plants grown with bulk $FePO_4$ as Fe source (-Fe+bulk $FePO_4$). Data are means ± SD of three independent experiments with three plants (technical replicates) each (One-way ANOVA with Turkey's post hoc test, $p<0.05$).

Mn contents

Figure 56A shows that shoot Mn tissue concentrations of plants grown without iron (-Fe) was more than double than those measured for the positive control. An increased level of this micronutrient was also recorded in plants grown with bulk $FePO_4$ as source of Fe (-Fe+bulk $FePO_4$), but not in plants grown with $FePO_4$ NPs (-Fe+NPs). This last treatment displayed Mn concentrations comparable to those of the positive control (Figure 56A). Differently from the shoot, root concentrations of this element was lower to that of the positive control in all the other growth conditions (Figure 56B).

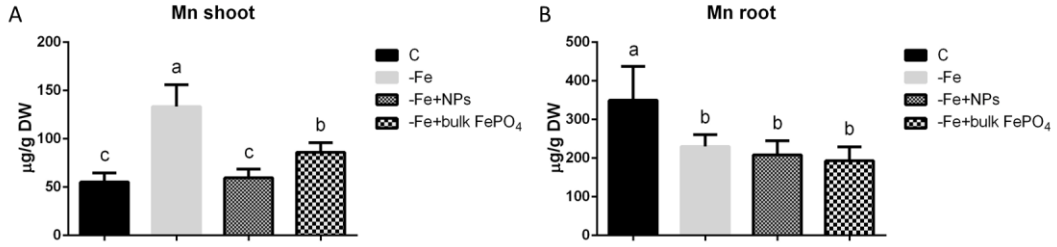

Figure 56: Mn concentrations (µg/gDW) in shoots and roots of maize plants treated with different nutrient sources; control plants (C), plants grown without Fe (-Fe), plants grown with $FePO_4$ NPs as Fe source (-Fe+NPs), plants grown with bulk $FePO_4$ as Fe source (-Fe+bulk $FePO_4$). Data are means ± SD of three independent experiments with three plants (technical replicates) each (One-way ANOVA with Turkey's post hoc test, $p<0.05$).

Cu contents

Cu concentrations showed the same pattern in both shoots and roots, with higher values in Fe-deficient plants, followed by plants grown with bulk $FePO_4$ as source of Fe (-Fe+bulk $FePO_4$) and plants grown with $FePO_4$ NPs as Fe source (-Fe+NPs). The lower values were observed in control plants (Figure 57). In shoots the difference in concentration between positive control and NPs-treated plants was not statistically significant (Figure 57A).

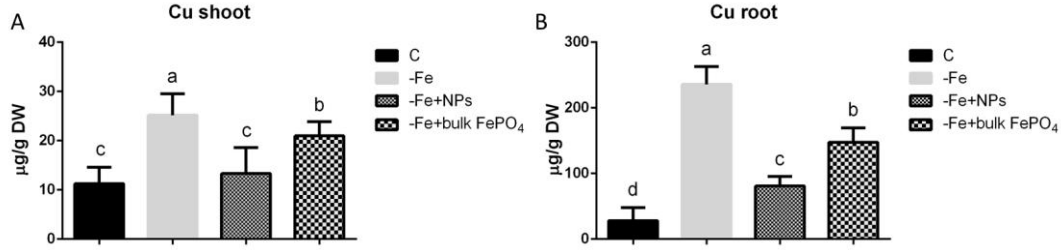

Figure 57: Cu concentrations (µg/gDW) in shoots and roots of maize plants treated with different nutrient sources; control plants (C), plants grown without Fe (-Fe), plants grown with $FePO_4$ NPs as Fe source (-Fe+NPs), plants grown with bulk $FePO_4$ as Fe source (-Fe+bulk $FePO_4$). Data are means ± SD of three independent experiments with three plants (technical replicates) each (One-way ANOVA with Turkey's post hoc test, $p<0.05$).

4.2.3.4 Gene expression analysis

Maize homologs of the *AtPHR1* transcription factor gene (*GLK15* and *GLK17*), known to be a regulator of phosporous homeostasis in Arabidopsis and genes known to be involved in the regulation of the response to iron deficiency in maize (*FER-Like* and *IRO2*) were evaluated for their expression in roots of treated plants (Table 6).

Locus name	Gene name	Protein length
GRMZM2G162409	*GLK15*	441 aa
GRMZM2G006477	*GLK17*	450 aa
GRMZM2G107672	*FER-Like*	358 aa
GRMZM2G057413	*IRO2*	222 aa

Table 6: Locus names, gene names and protein lengths of the maize transctiption factors studied.

As housekeeping genes for data normalization *GRMZM2G047204 (UKN)* and *GRMZM2G149286 (CDK*) were chosen, being the best couple of genes for our samples according to Normfinder analysis.
GLK15 expression for plants grown without phosphorous (-P) is 35% lower than in the positive control. This reduction in gene expression is only 15% and 25% for plants grown with $FePO_4$ NPs (-P+NPs) and with bulk $FePO_4$ respectively (Figure 58A). On the other hand, *GLK17* expression does not seem to be clearly influenced by the treatments applied (Figure 58B).

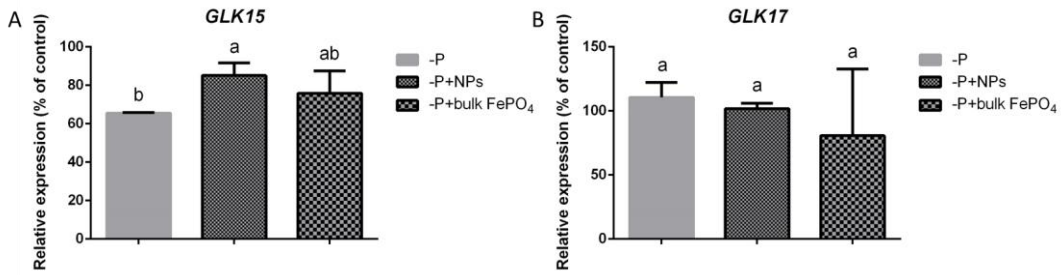

Figure 58: Relative expression expressed as percentage of the level of positive control of *GLK15* (A) and *GLK17* (B) genes in roots of maize plants treated with different nutrient sources; plants grown without P (-P), plants grown with $FePO_4$ NPs as P source (-P+NPs), plants grown with bulk $FePO_4$ as P source (-P+bulk $FePO_4$). Data are means ± SD of three independent experiments with three technical replicates each (One-way ANOVA with Turkey's post hoc test, $p<0.05$).

The *FER-Like* gene was downregulated in all treatments considered. This behavior was more pronounced for plants grown with $FePO_4$ NPs as iron source (-Fe+NPs), exhibiting values significantly lower than those of other two conditions (Figure 59A).
On the other hand, the *IRO2* gene exhibited an extremely high upregulation for all treatments, with higher values for plants grown without iron (-Fe), which are significantly different from the ones of the other two conditions (Figure 59B).

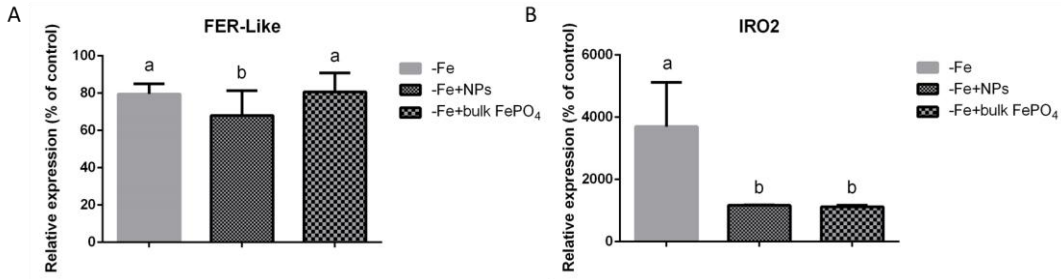

Figure 59: Relative expression expressed as percentage of the level of positive control of *Fer-Like* (A) and *IRO2* (B) genes in roots of treated maize plants; plants grown without Fe (-Fe), plants grown with $FePO_4$ NPs as Fe source (-Fe+NPs), plants grown with bulk $FePO_4$ as Fe source (-Fe+bulk $FePO_4$). Data are means ± SD of three independent experiments with three technical replicates each (One-way ANOVA with Turkey's post hoc test, $p<0.05$).

4.3 Summary of results

Here below, Table 7 and 8 summarize the more meaningful results, evidencing where the most pronounced differences and similarities can be observed among the experimental conditions.

	P				Fe			
	+	-	NPs	bulk	+	-	NPs	bulk
Morphology	xxx	x	xxx	x	xxx	x	xxx	xxx
Nutrient content	xxx	x	xx	x	xxx	x	xxx	xxx
Divalent cations balance					xxx	x	xxx	xx
Gene expression	xxx	x	xxxx[a]	xxx	xxx	x	xxx	xx

Table 7: Summary of the main results on cucumber plants. Crosses represent arbitrary scores based on the statistical significance of the differences described in the results. xxx: optimal values and/or condition; xx: sub-optimal values and/or condition; x: low values and/or deficiency condition; [a]: values unexpectedly higher than positive control.

	P				Fe			
	+	-	NPs	bulk	+	-	NPs	bulk
Morphology	xxxx	xx	xxx	xx	xxxx	x	xxx	xx
Nutrient content	xxxx	x	x	x	xxxx	x	xxx	xx
Divalent cations balance					xxxx	x	xxx	xx
Gene expression	xxxx	x	xxx	xx	xxxx	x	xxx	xxx

Table 8: Summary of the main results on maize plants. Crosses represent arbitrary scores based on the statistical significance of the differences described in the results. xxxx: optimal values and/or condition; xxx: high sub-optimal values and/or condition; xx: low sub-optimal values/and or moderate deficiency condition; low values and/or deficiency condition.

5 DISCUSSION

Phosphorous and Fe are essential mineral nutrients limiting in a wide range of conditions the agricultural productivity. Phosphorous, in particular, is an important macronutrient for its pivotal role in cellular metabolism. Phosphate fertilizers to-date on the market have a very low use efficiency that does not exceed 10%-25% (Syers et al., 2008). Moreover, stocks of rock phosphates, the raw material for the production of P fertilizers, are running out (Rosemarin et al., 2009). Iron, needed by plants in higher quantities among micronutrients, is present in the soil in high total amounts, but it is scarcely available in aerobic soils. Iron fertilizers present on market are at the moment expensive and have a limited temporal effectiveness. It is estimated that Fe deficiency occurs in about 30% of soils (Mori, 1999b) while P deficiency occurs in almost 65% of arable lands (Mori, 1999b; Kochian et al., 2004b). The need to develop more efficient fertilizers for these two nutrients is therefore evident. In this context, the use of nanotechnologies could offer an opportunity as envisaged by many authors (Nair *et al.*, 2010; Khot *et al.*, 2012; Ghormade et al., 2011; Liu and Lal, 2015; Ditta etal., 2015; Chhipa, 2017).
On the other hand, examples of application of such nanomaterials in plant nutrition are very few (Sánchez-Alcalá et al., 2012; Alidoust and Isoda, 2013; Ghafariyan et al., 2013; Delfani et al., 2014; Liu and Lal, 2014; Rui et al., 2016) and no one described the use of $FePO_4$ NPs.

The first part of this work was focused on the optimization of a simple, economically advantageous and industrially scalable synthesis method for producing $FePO_4$ NPs, that could provide a product with a convenient shelf-life making it potentially exploitable in the fertilizer market. Several techniques have been proposed for synthesis (Cao and Wang, 2011). Among them, co-precipitation appears to be a cheap and easy to use methods for NPs synthesis (Nazari et al., 2014) and the present work focused on this principle.
The first attempt for obtaining $FePO_4$ NPs based on the batch method described by Kandori et al. (2006), did not give satisfying results. In fact, the majority of tested conditions produced particles much bigger than 100 nm (Table 4). Particles obtained by us with this method were not visualized at TEM. However, it is probable that the broad and high size distribution observed at DLS (Figure 21 and Supplementary Figure S1) is due to the aggregation of smaller particles, as deducible by data reported by Kandori et al. (2006). This method was not considered satisfactory, not only for the size of the particles (mostly exceeding 100 nm) but also for the low stability over the time. Another disadvantage of that method is the low concentration of reagents solutions causing a consequent low concentration of the product. This feature, together with the discontinuous nature of the batch method, limits its productivity and industrial scalability.
A continuous method for $FePO_4$ NPs synthesis using dibasic phosphate as PO_4^{3-} source solution that was reported in several papers (Lu et al. 2012; Zhang et al. 2013; Zhang et al. 2014), was tested for its effectiveness with a laboratory-made system (Figure 17). The system produced smaller particles than the batch method,

with at least 50% of the particles smaller than 100 nm (Figure 22). This system allowed to test the continuous co-precipitation method at lab scale.
According to the encouraging results obtained with the proof-of-concept system, a pilot plant for the continuous $FePO_4$ NPs synthesis was set up, using two dosing pumps for the pumping of solutions, and an HPLC mixing tee as mixing chamber (Figure 24). The system produced particles with a size peak of 78 nm, and about 64 % of the particles smaller than 100 nm (Figure 25). Considering these results, the method can be defined simple, economically advantageous and industrially scalable. On the other hand, the particles were not stable, aggregating and sedimenting over time (Figure 27). This behavior, that represents a disadvantage for an industrial application, was solved by introducing a citrate capping treatment that stabilized the suspension for at least 8 months (Figure 28). This stabilization is of electrostatic nature, due to the repulsion of negative charges of citrate's carboxylic groups (Aiken and Finke, 1999).
A batch method for the synthesis of citrate-capped $FePO_4$ NPs was also optimized. This method allows the synthesis of $FePO_4$ NPs in small amounts without the need of setting up a plant, and is more suitable for scientific research. Comparing TEM images of particles obtained with this method (Figure 30) with particles obtained with the pilot plant (Figure 26) it is noticeable that particles produced with this method are similar or even smaller (Figure 28).
The purpose of developing a stable product drove the optimization of particles purification with dialysis, that demonstrated to be a mild purification technique, limiting NPs aggregation. This need also promoted the development of the stabilization with citrate. Comparing the purification method used by us, with other methods used in other papers, it is evident that the method for purification here adopted is related to the use of obtained NPs. For example, in the production of $FePO_4$ NPs for the production of more efficient $LiFePO_4$ cathodes for lithium batteries (Kandori et al., 2006; Lu et al., 2012; Zhang et al., 2013; Zhang et al., 2014) no stabilization of NPs was performed. Furthermore purification methods that were applied (such as filtration and washing with deionized water followed by drying), clearly caused a strong NPs aggregation, as shown by TEM images reported in the papers. However, in these applications the aggregation of NPs is not a concern. On the other hand, the capping of NPs in order to avoid, reduce, or delay aggregation is a practice that is commonly used when NPs are used in suspension in an aqueous medium (Singh et al. 2009; Javed et al., 2016). In the work published by Liu and Lal (2014), HA NPs ($Ca_5(PO_4)_3OH$) were capped with CMC, which was added directly in the Ca^{2+} source solution, and it was effective in preventing NPs sedimentation. NPs stabilization can also be performed on purified NPs, after the reaction, as we did. Kotsmar et al., (2010), for example, stabilized Fe_2O_3 NPs with citrate. Fe_2O_3 NPs were mixed with 20 mmol $\cdot L^{-1}$ citric acid and stirred for 90 min at 90 °C. An advantage of our method of citrate capping is the short time that was needed for the capping treatment (2 minutes), and the execution at room temperature, probably due to the high concentration of citrate (100 mmol $\cdot L^{-1}$). Furthermore, the citrate-capped NPs were stable even after a 8-month storage at room temperature (24±6°C).

In the second part of the work, $FePO_4$ NPs were tested for the effectiveness as source of P and Fe on cucumber and maize plants, grown in hydroponics. To the

best of our knowledge experiments aimed at assessing the effect of $FePO_4$ NPs on plant growth are not present in the literature. Liu and Lal (2014) demonstrated that HA NPs ($Ca_5(PO_4)_3OH$) increased by 30% the growth of soybean cultivated in pot on a solid substrate (peat and perlite) compared to the plants treated with a conventional fertilizer. Our data showed that in cucumber, $FePO_4$ NPs caused a higher accumulation of shoot dry biomass (Figure 33D, E and F) than in deficient plants (-P, -Fe, -P-Fe). On the other hand, $FePO_4$ NPs caused a significantly higher shoot growth relatively to bulk $FePO_4$ only when used as source of P or both P and Fe (-P+NPs, -P-Fe+NPs). Conversely, in maize, $FePO_4$ NPs induced a better growth of shoot than bulk $FePO_4$ only when applied as source of Fe (Figure 48A, B and C). Chlorophyll content in leaves is an indicator of the nutritional status of plants. P-deficiency generally causes a purpling of leaves, due to anthocyanins accumulation, and also a darker color, due to reduced leaf growth, with the consequent higher chlorophyll concentration (Hecht-Buchholz, 1967). On the contrary in leaves of Fe-deficient plants it is known that a drastic decrease in chlorophyll occurs (Marschner's, 2012). SPAD index values, that correlate to chlorophyll contents, evidenced in cucumber (Figure 33A) a darkening of leaves in plants treated with bulk $FePO_4$ as P source (-P+bulk $FePO_4$) comparable to those of plants grown without P (-P), while plants treated with $FePO_4$ NPs (-P+NPs) had SPAD values similar of those measured in control plants. The difference in the response between plants treated with the two forms of $FePO_4$ as P source was not recorded in maize (Figure 47A), where the P-deficiency symptom was not appreciable in P-deficient plants (-P). The reason for this different behavior is not easily explainable. We can hypothesize that, at least at this developmental stage, in maize, the P reservoir in seeds could satisfy plant P needs thus masking the response of the plants at the shoot level. These results can be explained on the basis of P concentration in shoot tissues. $FePO_4$ NPs determined a P concentration in cucumber significantly higher than bulk $FePO_4$ (Figure 36A), while in maize, not significant differences were observed between the two treatments (Figure 52A).

Plants grown without Fe showed evident symptoms of deficiency irrespective of the species (Figure 33B and Figure 57B). However, in the case of cucumber Fe supplied by both forms (NPs and bulk) appeared to be available to the same extent of Fe-EDTA (33B). These data were in agreement with the Fe concentrations determined in shoot in both plant species (Figure 37 and Figure 53).

An effective similar to Fe-chelates in preventing Fe chlorosis was reported also in chickpea plants treated with $FeCO_3$ NPs (Sánchez-Alcalá et al., 2012), and peanut plants treated with Fe_2O_3 NPs (Rui et al., 2016). Moreover, no differences in SPAD index values between plants grown with Fe_2O_3 NPs and bulk Fe_2O_3 were observed in soybean (Alidoust and Isoda, 2013). Differently, in maize, $FePO_4$ NPs-treated plants (-$FePO_4$+NPs) showed SPAD index values higher than plants treated with bulk $FePO_4$ (-Fe+bulk $FePO_4$) (Figure 57B). Considering the application of NPs as a source of both nutrients (-P-Fe+NPs) in both species the NP-treated plants showed SPAD index values similar to that of C (Figure 57C). On the other hand, cucumber plants grown with bulk $FePO_4$ as source of both P and Fe (-P-Fe+bulk $FePO_4$) showed an increase in SPAD (Figure 33C) suggesting the prevalence of P deficiency (Figure 33A). This hypothesis can be confirmed by analyzing P and Fe levels in shoot tissues (Table S4 and Table S7). In fact,

comparing P concentration in cucumber plants, it is possible to see that P levels were significantly different between NPs- and bulk-treated plants with values of the latter not different to P-deficient plants.
The effect of the treatments on the root apparatus was not particularly evident on dry weight of both plant species (Figure 34A, B and C and Figure 48D, E and F). No significant differences on root dry weight were observed in pot experiments when Fe_2O_3 NPs were applied to soybean (Alidoust and Isoda 2013) and peanuts (Rui et al. 2016) plants. On the other hand, Figures 34D, E and F show interesting effects on total root length, and Figures 35A, B and C on root surface area of cucumber. In fact, irrespective to the nutritional conditions, NPs exerted a positive effect on these parameters that can be tentatively explained as a biostimulant-like effect. Positive effects of nanomaterials, in particular CNMs, on root plant growth are reported (Mukherjee et al. 2016). The treatments with MWCNTs increased the root length of ryegrass plants hydroponically grown (Lin and Xing 2007) and of corn seedlings in agar medium (Lahiani et al. 2013). Similar results were observed when onion and cucumber plants grown in hydroponics were exposed to uncoated CNT (Cannas et al. 2008). In the case of maize the major effect on roots was that related to the content of anthocyanins whose synthesis is a typical P-deficiency response (Calderon-Vazquez et al., 2011). Roots of plants grown with bulk $FePO_4$, accumulated anthocyanins at a level similar to deficient plants. Conversely, plants treated with NPs showed an anthocyanins concentration similar to that of C plants (Figure 51). This result agrees well with that of P concentrations in roots (Figure 52B) and suggests that even if at the shoot level no significant symptoms of P deficiency were recordable, at the root level NPs could counteract a beginning condition of P shortage.
Considering Fe concentration in cucumber roots, it can be noticed that this element accumulates in amounts three times higher than in positive control when supplied as bulk $FePO_4$, and even seven times higher when supplied as $FePO_4$ NPs (Figure 37B). Reported values are relative to total Fe, and we cannot discriminate between symplastic and apoplastic Fe. However on the bases of these results we can assume that NPs suspended in nutrient solution can be adsorbed on the root surface and Fe somehow utilized by plants. Regarding Fe concentration in maize roots, plants grown with bulk $FePO_4$ don't differ significantly from Fe-deficient plants with levels about 7 time lower than control plants. Interestingly the treatment with $FePO_4$ NPs determined values that are double than the control (Figure 52B) thus confirming the NPs ability to improve the nutrient delivery. This result is also coherent with what observed with SPAD index (Figure 47). Moreover, Kulikova et al. (2017), studied the availability of nano-sized Fe hydroxides stabilized with humic substances on wheat seedlings, and showed, similarly to us, that plants grown with this form of Fe hydroxides accumulated in roots from 4 to 10 times more Fe than control plants, and even if in shoots the concentrations were comparable.
It is known that in plants Fe deficiency causes an increase in divalent cations concentration (Zn, Mn, Cu), both in leaves and roots (Korshunova et al., 1999; Rogers et al., 2000; Vert et al., 2002). Such accumulations were confirmed also in the present work for Fe-deficient plants, in both maize and cucumber. Moreover our data showed also an increase in Mg concentration in both shoot and root for maize, and in shoot for cucumber. It is interesting to observe that the growth of

plants with $FePO_4$ NPs as source of Fe generally determined a decrease in divalent cations concentrations making them more similar to the positive control. This suggests that plants grown with $FePO_4$ NPs are in a nutritional status more similar to the control, and confirms the idea of a better availability Fe when $FePO_4$ is in form of NPs. In a recent work, Sánchez-Alcalá et al. (2012) showed the effectiveness of $FeCO_3$ NPs in preventing chlorosis in plants grown on a calcareous soil. Our data support the idea present in literature that nanomaterials containing Fe could be an alternative to chelates for chlorosis prevention.
The question about the mode of interaction between NPs and roots is still unsolved. Some evidences showed the entrance and translocation into the plants of NPs such as CuO NPs (Wang et al., 2012), Au NPs (Zhai et al., 2014), TiO_2 (Larue et al., 2012) and Fe_3O_4 (Ghafariyan et al., 2013). However, the capacity of direct NPs uptake seems to be dependent from plant physiology, NPs composition and size (Liu and Lal, 2015). On the other hand, other authors suggest the dissolution of NPs outside the root (Wang et al., 2016).
Our TEM observations of cucumber tertiary roots grown with $FePO_4$ NPs as P source (-P+NPs), showed that $FePO_4$ NPs were not present into roots (Figure 43A), but only accumulated outside the cell wall in aggregated form (Figure 43B). This result is coherent with the idea that every particle bigger than 5 nm in diameter has a negligible passage through the plant cell wall (Baron-Epel et al., 1988), and suggests that in this case the mechanism of delivery of nutrients could be the dissolution in the apoplast, and the uptake of ions mediated by transmembrane transporters.

Moreover, together with $FePO_4$ NPs, also some lath-shaped, electron-dense nanometric objects could be clearly observed (Figure 43B). These deposits could be iron hydoxides. In fact, feroxyhyte (δ'-FeOOH) NPs stabilized with humic substances showed a similar shape as reported by Kulikova et al. (2017). However, according to Vodyanitskii, (2010), these putative hydroxide deposits could also be lepidocrocite (γ-FeOOH), a mineral that predominates near plant roots where plasma membrane reductase activities and root exudates (mainly citrate and phenolics) can reduce Fe(III) to Fe(II) in (hydr)oxides. Further Fe(II) oxidation and hydrolysis results in lepidocrocite formation (Vodyanitskii, 2010). We could speculate that the same mechanism would act on $FePO_4$ NPs during the acquisition of PO_4^-, and the consequent precipitation of Fe(III) as hydroxide. In addition, ESEM-EDAX analysis (Figure 44 and Supplemental Report S1) performed using root of cucumber plants treated with NPs as P source (Figure 42) revealed a higher amount of Fe in the electron-dense deposits as suggested by Fe/P ratio ranging between 2.49 and 3.84. These results are line with the hypothesis that NPs, in this nutritional condition, is more effective as source of P relative to Fe justifying the accumulation of Fe in electron-dense deposits on root surface. In this nutritional condition, NPs are the only source of P while Fe was available not only as NPs but also as Fe-EDTA.

In the tentative to ascertain root molecular responses to the availability of P and Fe supplied in the different forms we analyzed the expression of key regulator genes. Regarding the response to P nutrition, homologs of *AtPHR1* were taken in account. AtPHR1 is a transcription factor known to regulate the responses to P

starvation in promoting the expression of a series of effector genes, such as *AtPHT1* and *AtPHO1* (Briat et al. 2015). Maize homologs of *AtPHR1*, named *GLK15* and *GLK17*, were previously identified (Calderon-Vazquez et al. 2011). However, information regarding their expressional behavior in relation to the nutritional condition is not present in the literature. On the other hand, two cucumber homologs of genes encoding PHR1 transcription factor were identified (*Csa3M608690* and *Csa1M666970)* on the basis of amino acid sequence similarity with *Arabidopsis thaliana* and *Oryza sativa* proteins.

Expression of the maize gene *GLK17* did not show significant differences among the nutritional conditions (-P; -P+bulk, -P+NPs; Figure 58B). On the contrary *GLK15* (Figure 58A), the other *AtPHR1* homolog, showed to be downregulated in P-deficiency condition, while expression levels in plants grown with $FePO_4$ NPs are similar to control condition. Considering cucumber, the only gene significantly modulated by P nutritional conditions was *Csa3M608690* (Figure 45A) encoding the protein with the highest amino acid similarity with AtPHR1. As described for maize this putative regulator gene was repressed under P-shortage. However, in this case an overexpression of the gene was recorded in NPs-treated plants. The transcriptional behavior of genes encoding this transcription factor in plants in relation to P nutritional condition is not so clear. Rubio et al. (2001) reported an upregulation in response to P starvation of *AtPHR1*. The rice gene, *OsPHR2* –the ortholog of *AtPHR1*- was not modulated by P starvation both in shoots and roots (Zhou et al. 2008). In addition, Wang et al. (2014) reported the conservation between mono- and dicotyledonous plants of Pi sensing mechanisms. Both *AtPHR1* and *OsPHR2* were not modulated in response to P starvation (Wang et al., 2014). Anyway, under low P condition, AtPHR1 positively regulates genes involved in P uptake by roots (*AtPHT1* and *AtPHO1*) after its post-transcriptional activation though SUMOylation (Briat et al. 2015). Our data, particularly considering cucumber, suggest that NPs could also affect the transcriptional level of *AtPHR1* homolog (*Csa3M60869*) in response to the different condition of P availability.

As far as Fe nutrition is concerned, cucumber and maize genes encoding proteins homologous to *AtPYE* and *AtBTS* were considered. *AtPYE* and *AtBTS* are reported to be involved in the regulation of iron deficiency response in Arabidopsis (Zhang et al., 2015). The expression levels of the two identified cucumber genes, *Csa1M009660* and *Csa1M024210*, homologous to *AtPYE* and *AtBTS*, respectively, was characterized in relation to the different treatments (Figure 46). *Csa1M009660* was not significantly modulated by the nutritional treatments. However its expression was constantly higher relatively to control conditions in particular in Fe-deficient plants (Figure 46A). *AtBTS* is considered in Arabidopsis a negative regulator of Fe absorption, and it was shown to be upregulated in Arabidopsis Fe-deficient roots (Long et al., 2010; Zhang et al., 2015). Our data of Fe- deficient roots are in line with these observations. However, the expression profile of the plants treated with NPs show suggest a nutritional condition similar to the positive control.

Transcriptional analysis carried out in maize roots with the aim to characterize the expression of genes involved in the regulation of response to Fe availability (*ZmFER*-like and *ZmIRO2*) underlined a modulation dependent on the treatment (Figure 59). *ZmFER-Like* gene (Figure 59A) was downregulated in response to all

treatments relatively to the control, in particular for NPs-treated plants. Although FER-like proteins are mainly involved in the responses to Fe deficiency in *Strategy I* species (Kobayashi and Nishizawa, 2012), an up-regulation of *ZmFER-Like* gene in maize was observed under the shortage of the micronutrient (Zanin et al., 2017). Our transcriptional data suggest that the treatment with NPs could reduce more the expression of the genes involved in Fe uptake normally activated by Fe deficiency condition through the action of *ZmFER-Like*. Considering *ZmIRO2*, homolog of *OsIRO2* that positively regulates the genes involved into *Strategy II* in rice (Kobayashi and Nishizawa, 2012), we recorded an upregulation in response of all treatments relatively to the control with higher expression under Fe deficiency (Figure 59B). This results partially fits with the lower Fe concentration in roots observed in maize plants grown without Fe or with $FePO_4$ bulk. The same correlation was observed for NPs-treated plants in consideration of their higher level of Fe root concentration. In addition, it has to be considered that the activity of the transcription factor codified by this gene needs the interaction with other regulators (Kobayashi and Nishizawa, 2012).

In conclusion, $FePO_4$ NPs showed to be an effective source of P and Fe, particularly if compared to the non-nano counterpart. However, the treatment with NPs caused differential responses in cucumber and maize (Tables 7 and 8). This could be explained not only in term of physiological differences between the two species but also on the bases of the difference in the timing of the response to the deficiencies that the plants displayed in our experimental conditions. TEM observations revealed that these particles did not enter into the plant, suggesting a mechanism of delivery of nutrients at least in part based on the accumulation of NPs in the apoplast and their successive dissolution. Figure 60 represents a speculative model on how our results could be transferred on an agricultural plant-soil system.

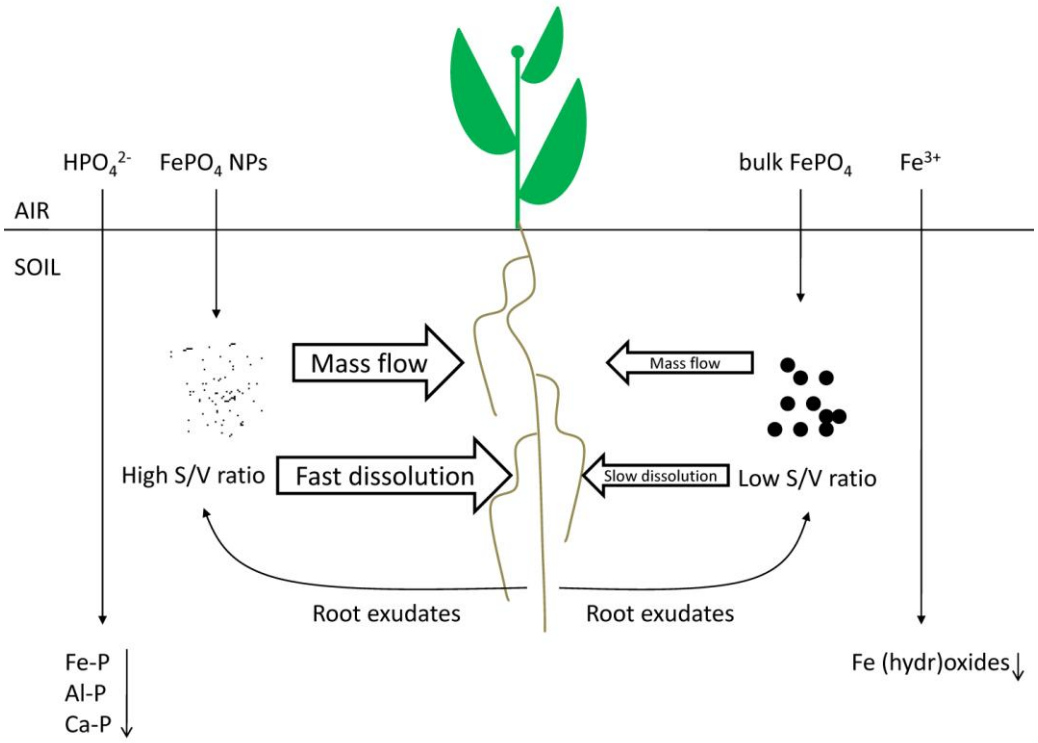

Figure 60: Speculative model representing the mechanism of nutrients delivery by $FePO_4$ NPs: the solid nature of NPs and bulk $FePO_4$ protects them from precipitation/immobilization when applied to soil (a fate to which soluble phosphates and Fe^{3+} sources are subjected); NPs, due to their small size could reach roots better through soil pores than bulk FePO4, when transported by mass flow. Moreover, the high surface/volume ratio of NPs could make their dissolution - operated by exudates - faster than for bulk $FePO_4$.

Further research for understanding plant molecular responses to $FePO_4$ NPs and the mechanisms of perception of NPs should be of interest, together with the testing in field of the fertilizing potential of $FePO_4$ NPs. In this context, the persistence of NPs in soil solution could be a key factor in nutrients delivery. To this respect, the role of soil factors such as pH and iron idroxides content, should be investigated, as potential regulators of NPs behavior. For this purpose, calcareous and/or acidic soils would be adequate substrates.
Moreover, the role of the possible interaction of NPs with substances such as root exudates and humic substances, together with the interaction with rhizosphere microorganisms should be deepened.

6 BIBLIOGRAPHY

Aiken JD, Finke RG (1999) A review of modern transition-metal nanoclusters: their synthesis, characterization, and applications in catalysis. J Mol Catal A Chem **145**: 1–44

Alidoust D, Isoda A (2013) Effect of γFe_2O_3 nanoparticles on photosynthetic characteristic of soybean (*Glycine max* (L.) Merr.): foliar spray versus soil amendment. Acta Physiol Plant **35**: 3365–3375

Altschul SF, Madden TL, Schäffer AA, Zhang J, Zhang Z, Miller W, Lipman DJ (1997) Gapped BLAST and PSI-BLAST: a new generation of protein database search programs. Nucleic Acids Res **25**: 3389–3402

Arnon D, Stout P (1939) The essentiality of certain elements in minute quantity for plants with special reference to copper. Plant Physiol **14**: 371–375

Baldi BG, Franceschi VR, Loewus FA (1987) Localization of phosphorus and cation reserves in *Lilium longiflorum* pollen. Plant Physiol **83**: 1018–1021

Baligar VC, Fageria NK, He ZL (2001) Nutrient use efficiency in plants. Commun Soil Sci Plant Anal **32**: 921–950

Baranwal R, Villar MP, Garcia R, Laine RM (2001) Flame spray pyrolysis of precursors as a route to nano-mullite powder: powder characterization and sintering behavior. J Am Ceram Soc **84**: 951–961

Baron-Epel O, Gharyal PK, Schindler M (1988) Pectins as mediators of wall porosity in soybean cells. Planta **175**: 389–395

Bashir K, Inoue H, Nagasaka S, Takahashi M, Nakanishi H, Mori S, Nishizawa NK (2006) Cloning and characterization of deoxymugineic acid synthase genes from graminaceous plants. J Biol Chem **281**: 32395–32402

Bashir K, Ishimaru Y, Shimo H, Kakei Y, Senoura T, Takahashi R, Sato Y, Sato Y, Uozumi N, Nakanishi H, Nishizawa NK (2011) Rice phenolics efflux transporter 2 (PEZ2) plays an important role in solubilizing apoplasmic iron. Soil Sci Plant Nutr **57**: 803–8011

Bauer P, Ling HQ, Guerinot M Lou (2007) FIT, the FER-LIKE IRON DEFICIENCY INDUCED TRANSCRIPTION FACTOR in *Arabidopsis*. Plant Physiol Biochem **45**: 260–261

Boutonnet M, Kizling J, Stenius P, Maire G (1982) The preparation of monodisperse colloidal metal particles from microemulsions. Colloids and Surfaces **5**: 209–225

Briat J-F, Rouached H, Tissot N, Gaymard F, Dubos C (2015) Integration of P, S, Fe, and Zn nutrition signals in *Arabidopsis thaliana*: potential involvement of PHOSPHATE STARVATION RESPONSE 1 (PHR1). Front Plant Sci **6**: 1–16

Calderon-Vazquez C, Sawers RJH, Herrera-Estrella L (2011) Phosphate deprivation in maize: genetics and genomics. Plant Physiol **156**: 1067–1077

Cañas JE, Long M, Nations S, Vadan R, Dai L, Luo M, Ambikapathi R, Lee EH, Olszyk D (2008) Effects of functionalized and nonfunctionalized single-walled carbon nanotubes on root elongation of select crop species. Environ Toxicol Chem **27**: 1922–1931

Cao G, Wang Y (2011) Nanostructures and nanomaterials: synthesis, properties and applications. World Scientific Publishing Co. Pte. Ltd., Singapore

Cesco S, Rombolà AD, Tagliavini M, Varanini Z, Pinton R (2006) Phytosiderophores released by graminaceous species promote ^{59}Fe-uptake in citrus. Plant Soil **287**: 223–233

Chhipa H (2017) Nanofertilizers and nanopesticides for agriculture. Environ Chem Lett **15**: 15–22

Cifuentes Z, Custardoy L, De la Fuente JM, Marquina C, Ibarra MR, Rubiales D, Perez-de-Luque A (2010) Absorption and translocation to the aerial part of magnetic carbon-coated nanoparticles through the root of different crop plants. J Nanobiotechnology **8**: 1–8

Cordell D, Drangert JO, White S (2009) The story of phosphorus: global food security and food for thought. Glob Environ Chang **19**: 292–305

Curie C, Panaviene Z, Loulergue C, Dellaporta SL, Briat J-F, Walker EL (2001) Maize *yellow stripe 1* encodes a membrane protein directly involved in Fe(III) uptake. Nature **409**: 346–349

Das S, Srivasatava VC (2016) Synthesis and characterization of ZnO–MgO nanocomposite by co-precipitation method. Smart Sci **4**: 190–195

Delfani M, Baradarn Firouzabadi M, Farrokhi N, Makarian H (2014) Some physiological responses of black-eyed pea to iron and magnesium nanofertilizers. Commun Soil Sci Plant Anal **45**: 530–540

DeRosa MC, Monreal C, Schnitzer M, Walsh R, Sultan Y (2010) Nanotechnology in fertilizers. Nat Nanotechnol **5**: 91

Dimkpa CO, Bindraban PS (2017) Nanofertilizers: New Products for the Industry? J Agric Food Chem acs.jafc.7b02150

Ditta A, Arshad M, Ibrahim M (2015) Nanoparticles in Sustainable Agricultural Crop

Production: Applications and Perspectives. Nanotechnol. Plant Sci. Nanoparticles Their Impact Plants. pp 1–303

Eastoe J, Hollamby MJ, Hudson L (2006) Recent advances in nanoparticle synthesis with reversed micelles. Adv Colloid Interface Sci **128–130**: 5–15

FAO (2017) The future of food and agriculture: trends and challenges.

Fourcroy P, Sisó-Terraza P, Sudre D, Savirón M, Reyt G, Gaymard F, Abadía A, Abadia J, Álvarez-Fernández A, Briat JF (2014) Involvement of the ABCG37 transporter in secretion of scopoletin and derivatives by *Arabidopsis* roots in response to iron deficiency. New Phytol **201**: 155–167

Fridovich I (1983) Superoxide radical: an endogenous toxicant. Annu Rev Pharmacol Toxicol **23**: 239–257

Ghafariyan MH, Malakouti MJ, Dadpour MR, Stroeve P, Mahmoudi M (2013) Effects of magnetite nanoparticles on soybean chlorophyll. Environ Sci Technol **47**: 10645–10652

Ghormade V, Deshpande M V., Paknikar KM (2011) Perspectives for nano-biotechnology enabled protection and nutrition of plants. Biotechnol Adv **29**: 792–803

Hamburger D, Rezzonico E, MacDonald-Comber Petétot J, Somerville C, Poirier Y (2002) Identification and characterization of the Arabidopsis *PHO1* gene involved in phosphate loading to the xylem. Plant Cell **14**: 889–902

Haruta M, Delmon B (1986) Preparation of homodisperse solids. J Chem Phys **83**: 859–868

Heber U, Viil J, Neimanis S, Mimura T, Dietz KJ (1989) Photoinhibitory damage to chloroplasts under phosphate deficiency and alleviation of deficiency and damage by photorespiratory reactions. Zeitschrift fur Naturforsch - Sect C J Biosci **44**: 524–536

Heldt HW, Flügge UI, Borchert S (1991) Diversity of specificity and function of phosphate translocators in various plastids. Plant Physiol **95**: 341–343

Hinsinger P (2001) Bioavailibility of soil inorganic P in the rhizosphere as effected by root-induced chemical changes: a review. Plant Soil **237**: 173–195

Ishimaru Y, Kakei Y, Shimo H, Bashir K, Sato Y, Sato Y, Uozumi N, Nakanishi H, Nishizawa NK (2011) A rice phenolic efflux transporter is essential for solubilizing precipitated apoplasmic iron in the plant stele. J Biol Chem **286**: 24649–24655

Ishimaru Y, Suzuki M, Tsukamoto T, Suzuki K, Nakazono M, Kobayashi T, Wada Y, Watanabe S, Matsuhashi S, Takahashi M, Nakanishi H, Mori S, Nishizawa

NK (2006) Rice plants take up iron as an Fe^{3+}-phytosiderophore and as Fe^{2+}. Plant J **45**: 335–346

Ivanov R, Brumbarova T, Bauer P (2012) Fitting into the harsh reality: regulation of iron-deficiency responses in dicotyledonous plants. Mol Plant **5**: 27–42

Javed R, Usman M, Tabassum S, Zia M (2016) Effect of capping agents: structural, optical and biological properties of ZnO nanoparticles. Appl Surf Sci **386**: 319–326

Jiang C-D, Gao H-Y, Zou Q (2001) Enhanced thermal energy dissipation depending on xanthophyll cycle and D1 protein turnover in iron-deficient maize leaves under high irradiance. Photosynthetica **39**: 269–274

Jin CW, You GY, He YF, Tang C, Wu P, Zheng SJ (2007) Iron Deficiency-Induced Secretion of Phenolics Facilitates the Reutilization of Root Apoplastic Iron in Red Clover. Plant Physiol **144**: 278–285

Kandori K, Kuwae T, Ishikawa T (2006) Control on size and adsorptive properties of spherical ferric phosphate particles. J Colloid Interface Sci **300**: 225–231

Kandpal ND, Sah N, Loshali R, Joshi R, Prasad J (2014) Co-precipitation method of synthesis and characterization of iron oxide nanoparticles. J Sci Ind Res **73**: 87–90

Khodakovskaya M, Dervishi E, Mahmood M, Xu Y, Li Z, Watanabe F, Biris AS (2012) Carbon nanotubes are able to penetrate plant seed coat and dramatically affect seed germination and plant growth. ACS Nano **3**: 3221–3227

Khot LR, Sankaran S, Maja JM, Ehsani R, Schuster EW (2012) Applications of nanomaterials in agricultural production and crop protection: a review. Crop Prot **35**: 64–70

Kim M, Hinklin TR, Laine RM (2008) Core-shell nanostructured nanopowders along $(CeO_x)_x(Al_2O_3)_{1-x}$ tie-line by liquid-feed flame spray pyrolysis (LF-FSP). Chem Mater **20**: 5154–5162

Kobayashi T, Nishizawa NK (2012) Iron uptake, translocation, and regulation in higher plants. Annu Rev Plant Biol **63**: 131–152

Kochian L V., Hoekenga OA, Piñeros MA (2004a) How Do Crop Plants Tolerate Acid Soils? Mechanisms of Aluminum Tolerance and Phosphorous Efficiency. Annu Rev Plant Biol **55**: 459–493

Kochian L V., Hoekenga OA, Piñeros MA (2004b) How do crop plants tolerate acid soils? Mechanisms of aluminum tolerance and phosphorous efficiency. Annu Rev Plant Biol **55**: 459–493

Korshunova YO, Eide D, Clark WG, Guerinot ML, Pakrasi HB (1999) The IRT1 protein from *Arabidopsis thaliana* is a metal transporter with a broad substrate

range. Plant Mol Biol **40**: 37–44

Kotsmar C, Yoon KY, Yu H, Ryoo SY, Barth J, Shao S, Prodanović M, Milner TE, Bryant SL, Huh C, Johnston KP (2010) Stable citrate-coated iron oxide superparamagnetic nanoclusters at high salinity. Ind Eng Chem Res **49**: 12435–12443

Kramer D, Römheld V, Landsberg E, Marschner H (1980) Induction of transfer-cell formation by iron deficiency in the root epidermis of *Helianthus annuus* L. Planta **147**: 335–339

Kulikova NA, Polyakov AY, Lebedev VA, Abroskin DP, Volkov DS, Pankratov DA, Klein OI, Senik S V., Sorkina TA, Garshev AV, Veligzhanin AA, Garcia Mina JM, Perminova IV (2017) Key roles of size and crystallinity of nanosized iron hydr(oxides) stabilized by humic substances in iron bioavailability to plants. J Agric Food Chem **65**: 11157–11169

Lahiani MH, Dervishi E, Chen J, Nima Z, Gaume A, Biris AS, Khodakovskaya MV (2013) Impact of carbon nanotube exposure to seeds of valuable crops. ACS Appl Mater Interfaces **5**: 7965–7973

Larue C, Laurette J, Herlin-Boime N, Khodja H, Fayard B, Flank AM, Brisset F, Carriere M (2012) Accumulation, translocation and impact of TiO*2* nanoparticles in wheat (*Triticum aestivum* spp.): influence of diameter and crystal phase. Sci Total Environ **431**: 197–208

Lauer MJ, Blevins DG, Sierzputowska-Gracz H (1989) ^{31}P-nuclear magnetic resonance determination of phosphate compartmentation in leaves of reproductive soybeans (*Glycine max* L.) as affected by phosphate nutrition. Plant Physiol **89**: 1331–1336

Lemanceau P, Bauer P, Kraemer S, Briat J-F (2009) Iron dynamics in the rhizosphere as a case study for analyzing interactions between soils, plants and microbes. Plant Soil **321**: 513–535

Lin D, Xing B (2008) Root uptake and phytotoxicity of ZnO nanoparticles. Environ Sci Technol **42**: 5580–5585

Lin D, Xing B (2007) Phytotoxicity of nanoparticles: inhibition of seed germination and root growth. Environ Pollut **150**: 243–250

Lin F, Jiang L, Liu Y, Lv Y, Dai H, Zhao H (2014) Genome-wide identification of housekeeping genes in maize. Plant Mol Biol **86**: 543–554

Liu Q, Zhao Y, Wan Y, Zheng J, Zhang X, Wang C, Fang X, Lin J (2010) Study of the inhibitory effect of water-soluble fullerenes on plant growth at the cellular level.

ACS Nano **4**: 5743–5748

Liu R, Lal R (2015) Potentials of engineered nanoparticles as fertilizers for increasing agronomic productions. Sci Total Environ **514**: 131–139

Liu R, Lal R (2014) Synthetic apatite nanoparticles as a phosphorus fertilizer for soybean (*Glycine max*). Sci Rep **4**: 5686

Long TA, Tsukagoshi H, Busch W, Lahner B, Salt DE, Benfey PN (2010) The bHLH transcription factor POPEYE regulates response to iron deficiency in *Arabidopsis* roots. Plant Cell **22**: 2219–2236

Lott JNA, Vollmer CM (1973) Changes in the cotyledons of *Cucurbita maxima* during germination. Protoplasma **78**: 255–271

Lu Y, Zhang T, Liu Y, Luo G (2012) Preparation of $FePO_4$ nano-particles by coupling fast precipitation in membrane dispersion microcontactor and hydrothermal treatment. Chem Eng J **210**: 18–25

Lucena C, Romera FJ, Rojas CL, Garcia MJ, Alcantara E, Perez-Vicente R (2007) Bicarbonate blocks the expression of several genes involved in the physiological responses to Fe deficiency of Strategy I plants. Funct Plant Biol **34**: 1002–1009

Lucena JJ (2003) Fe chelates for remediation of Fe chlorosis in strategy I plants. J Plant Nutr **26**: 1969–1984

Maathuis FJ (2009) Physiological functions of mineral macronutrients. Curr Opin Plant Biol **12**: 250–258

Marschner P (2012) Marschner's Mineral Nutrition of Higher Plants - Third Edition. Elsevier, London

Matsui K, Togami J, Mason JG, Chandler SF, Tanaka Y (2013) Enhancement of phosphate absorption by garden plants by genetic engineering: a new tool for phytoremediation. Biomed Res Int **2013**: 1–7

Monreal CM, Derosa M, Mallubhotla SC, Bindraban PS, Dimkpa C (2016) Nanotechnologies for increasing the crop use efficiency of fertilizer-micronutrients. Biol Fertil Soils **52**: 423–437

Mori S (1999) Iron acquisition by plants. Curr Opin Plant Biol **2**: 250–253

Mukherjee A, Majumdar S, Servin AD, Pagano L, Dhankher OP, White JC (2016) Carbon nanomaterials in agriculture: a critical review. Front Plant Sci **7**: 1–16

Nair R, Varghese SH, Nair BG, Maekawa T, Yoshida Y, Kumar DS (2010) Nanoparticulate material delivery to plants. Plant Sci **179**: 154–163

Naoe K, Petit C, Pileni MP (2008) Use of reverse micelles to make either spherical or worm-like palladium nanocrystals: Influence of stabilizing agent on nanocrystal

shape. Langmuir **24**: 2792–2798

National Science and Technology Council (2000) National nanotechnology initiative - leading to the next industrial revolution. Microscale Thermophys Eng **4**: 205–212

Nazari M, Ghasemi N, Maddah H, Motlagh MM (2014) Synthesis and characterization of maghemite nanopowders by chemical precipitation method. J Nanostructure Chem **4**: 99

Neumann G, Martinoia E (2002) Cluster roots - an underground adaptation for survival in extreme environments. Trends Plant Sci **7**: 162–167

Nielsen FH (1984) Ultratrace elements in nutrition. Annu Rev Nutr **4**: 21–41

Nilsson L, Lundmark M, Jensen PE, Nielsen TH (2012) The *Arabidopsis* transcription factor PHR1 is essential for adaptation to high light and retaining functional photosynthesis during phosphate starvation. Physiol Plant **144**: 35–47

Nilsson L, Müller R, Nielsen TH (2007) Increased expression of the MYB-related transcription factor, PHR1, leads to enhanced phosphate uptake in *Arabidopsis thaliana*. Plant, Cell Environ **30**: 1499–1512

Nishio JN, Abadía J, Terry N (1985) Chlorophyll-proteins and electron transport during iron nutrition-mediated chloroplast development. Plant Physiol **78**: 296–299

Nozoye T, Nagasaka S, Kobayashi T, Takahashi M, Sato Y, Sato Y, Uozumi N, Nakanishi H, Nishizawa NK (2011) Phytosiderophore efflux transporters are crucial for iron acquisition in graminaceous plants. J Biol Chem **286**: 5446–5454

Ockenden I, Dorsch JA, Reid MM, Lin L, Grant LK, Raboy V, Lott JNA (2004) Characterization of the storage of phosphorus, inositol phosphate and cations in grain tissues of four barley (*Hordeum vulgare* L.) low phytic acid genotypes. Plant Sci **167**: 1131–1142

Ogo Y, Nakanishi Itai R, Nakanishi H, Kobayashi T, Takahashi M, Mori S, Nishizawa NK (2007) The rice bHLH protein OsIRO2 is an essential regulator of the genes involved in Fe uptake under Fe-deficient conditions. Plant J **51**: 366–377

Omolfajr N, Nasser S, Mahmood R (2011) Synthesis and characterization of CaF_2 NPs with co-precipitation and hydrothermal method. J Nanomed Nanotechnol **2**: 1–12

Pant BD, Burgos A, Pant P, Cuadros-Inostroza A, Willmitzer L, Scheible WR (2015a) The transcription factor PHR1 regulates lipid remodeling and triacylglycerol accumulation in *Arabidopsis thaliana* during phosphorus starvation. J Exp Bot **66**: 1907–1918

Pant BD, Pant P, Erban A, Huhman D, Kopka J, Scheible WR (2015b) Identification of primary and secondary metabolites with phosphorus status-dependent abundance

in *Arabidopsis*, and of the transcription factor PHR1 as a major regulator of metabolic changes during phosphorus limitation. Plant Cell Environ **38**: 172–187

Petcharoen K, Sirivat A (2012) Synthesis and characterization of magnetite nanoparticles via the chemical co-precipitation method. Mater Sci Eng B **177**: 421–427

Pietrini F, Iannelli MA, Massacci A (2002) Anthocyanin accumulation in the illuminated surface of maize leaves enhances protection from photo-inhibitory risks at low temperature, without further limitation to photosynthesis. Plant, Cell Environ **25**: 1251–1259

Portis AR (1982) Effects of the relative extrachloroplastic concentrations of inorganic phosphate, 3-phosphoglycerate, and dihydroxyacetone phosphate on the rate of starch synthesis in isolated spinach chloroplasts. Plant Physiol **70**: 393–396

Potočnik J (2011) Commission recommendation of 18 October 2011 on the definition of nanomaterial (2011/696/EU). Off J Eur Union **L275**: 38–40

Ramakers C, Ruijter JM, Lekanne Deprez RH, Moorman AFM (2003) Assumption-free analysis of quantitative real-time polymerase chain reaction (PCR) data. Neurosci Lett **339**: 62–66

Ray DK, Mueller ND, West PC, Foley JA (2013) Yield trends are insufficient to double global crop production by 2050. PLoS One. doi: 10.1371/journal.pone.0066428

Riley J, Murphy J (1962) A modified single solution method for the determination of phosphate in natural waters. Anal Chim Acta **27**: 31–36

Robinson NJ, Procter CM, Connolly EL, Guerinot M Lou (1999) A ferric-chelate reductase for iron uptake from soils. Nature **397**: 694–697

Robinson SP, Giersch C (1987) Inorganic phosphate concentration in the stroma of isolated chloroplasts and its influence on photosynthesis. Aust J Plant Physiol **14**: 451–462

Rogers EE, Eide DJ, Guerinot ML (2000) Altered selectivity in an Arabidopsis metal transporter. Proc Natl Acad Sci **97**: 12356–12360

Römheld V (2000) The chlorosis paradox: Fe inactivation as a secondary event in chlorotic leaves of grapevine. J Plant Nutr **23**: 1629–1643

Romheld V, Marschner H (1983) Mechanism of iron uptake by plants. I. Fe III reduction, chelate splitting, and release of phenolics. Plant Physiol **71**: 949–954

Rui M, Ma C, Hao Y, Guo J, Rui Y, Tang X, Zhao Q, Fan X, Zhang Z, Hou T, et al (2016) Iron oxide nanoparticles as a potential iron fertilizer for peanut (*Arachis hypogaea*). Front Plant Sci **7**: 1–10

Sánchez-Alcalá I, del Campillo MC, Barrón V, Torrent J (2012) Pot evaluation of synthetic nanosiderite for the prevention of iron chlorosis. J Sci Food Agric **92**: 1964–1973

Schaaf G, Ludewig U, Erenoglu BE, Mori S, Kitahara T, Von Wirén N (2004) ZmYS1 functions as a proton-coupled symporter for phytosiderophore- and nicotianamine-chelated metals. J Biol Chem **279**: 9091–9096

Schachtman DP, Reid RJ, Ayling SM (1998) Update on phosphorus uptake phosphorus uptake by plants: from soil to cell. Mol Gen Genet **116**: 447–453

Schmidt W (1999) Mechanisms and regulation of reduction-based iron uptake in plants. New Phytol **141**: 1–26

Schuler MA (1996) Plant Cytochrome P450 Monooxygenases. CRC Crit Rev Plant Sci **15**: 135–284

Scott JJ, Loewus FA (1986) A calcium-activated phytase from pollen of *Lilium longiflorum*. Plant Physiol **82**: 333–335

Selote D, Samira R, Matthiadis A, Gillikin JW, Long TA (2015) Iron-binding E3 ligase mediates iron response in plants by targeting basic helix-loop-helix transcription factors. Plant Physiol **167**: 273–286

Sevilla A, Del Río LA, Hellín E (1984) Superoxide dismutases from a citrus plant: presence of two iron-containing isoenzymes in leaves of lemon trees (*Citrus limonum* L.). J Plant Physiol **116**: 381–387

Simon P (2003) Q-Gene: processing quantitative real-time RT-PCR data. Bioinformatics **19**: 1439–1440

Singh AK, Viswanath V, Janu VC (2009) Synthesis, effect of capping agents, structural, optical and photoluminescence properties of ZnO nanoparticles. J Lumin **129**: 874–878

Spiller SC, Kaufman LS, Thompson WF, Briggs WR (1987) Specific mRNA and rRNA levels in greening pea leaves during recovery from iron stress. Plant Physiol **84**: 409–414

Stookey LL (1970) Ferrozine - a new spectrophotometric reagent for iron. Anal Chem **42**: 779–781

Stumm W, Sulzberger B (1992) The cycling of iron in natural environments: considerations based on laboratory studies of heterogeneous redox processes. Geochim Cosmochim Acta **56**: 3233–3257

Sun L, Song L, Zhang Y, Zheng Z, Liu D (2016) *Arabidopsis* PHL2 and PHR1 Act redundantly as the key components of the central regulatory system controlling

transcriptional responses to phosphate starvation. Plant Physiol **170**: 499–514

Syers JK, Johnston AE, Curtin D (2008) Efficiency of soil and fertilizer phosphorus use: reconciling changing concepts of soil phosphorus behaviour with agronomic information. FAO Fertil. Plant Nutr. Bull.

Takagi S, Nomoto K, Takemoto T (1984) Physiological aspect of mugineic acid, a possible phytosiderophore of graminaceous plants. J Plant Nutr **7**: 469–477

Terry N, Javier A (1986) Function of iron in chloroplasts. J Plant Nutr **9**: 609–646

Tilman D, Cassman KG, Matson PA, Naylor R, Polasky S (2002) Agricultural sustainability and intensive production practices. Nature **418**: 671–677

Tomasi N, Kretzschmar T, Espen L, Weisskopf L, Fuglsang AT, Palmgren MG, Neumann G, Varanini Z, Pinton R, Martinoia E, Cesco S (2009) Plasma membrane H^+-ATPase-dependent citrate exudation from cluster roots of phosphate-deficient white lupin. Plant, Cell Environ **32**: 465–475

Tomasi N, Weisskopf L, Renella G, Landi L, Pinton R, Varanini Z, Nannipieri P, Torrent J, Martinoia E, Cesco S (2008) Flavonoids of white lupin roots participate in phosphorus mobilization from soil. Soil Biol Biochem **40**: 1971–1974

Tsai HH, Schmidt W (2017) Mobilization of Iron by Plant-Borne Coumarins. Trends Plant Sci **22**: 538–548

United Nations (2017) World population prospects: the 2017 revision, key findings and advance tables.

Vert G, Grotz N, Dédaldéchamp F, Gaymard F, Guerinot L, Briat J-F, Curie C (2002) IRT1, an *Arabidopsis* transporter essential for iron uptake from the soil and for plant growth. Plant Cell **14**: 1223–1233

Vodyanitskii YN (2010) Iron hydroxides in soils: a review of publications. Eurasian Soil Sci **43**: 1244–1254

Walter A, Romheld V, Marschner H, Mori S (1994) Is the release of phytosiderophores in zinc-deficient wheat plants a response to impaired iron utilization? Physiol Plant **92**: 493–500

Wang P, Lombi E, Zhao FJ, Kopittke PM (2016) Nanotechnology: a new opportunity in plant sciences. Trends Plant Sci **21**: 699–712

Wang Y, Cheng Y, Ou K, Lin L, Liang J (2008) In vitro solubility of calcium , iron , and zinc in rice bran treated with phytase, cellulase, and protease. J Agric Food Chem **56**: 11868–11874

Wang Z, Ruan W, Shi J, Zhang L, Xiang D, Yang C, Li C, Wu Z, Liu Y, Yu Y, Shou H, Mo X, Mao C, Wu P (2014) Rice SPX1 and SPX2 inhibit phosphate starvation

responses through interacting with PHR2 in a phosphate-dependent manner. Proc Natl Acad Sci **111**: 14953–14958

Wang Z, Xie X, Zhao J, Liu X, Feng W, White JC, Xing B (2012) Xylem- and phloem-based transport of CuO nanoparticles in maize (*Zea mays* L.). Environ Sci Technol **46**: 4434–4441

Warzybok A, Migocka M (2013) Reliable reference genes for normalization of gene expression in cucumber grown under different nitrogen nutrition. PLoS One. doi: 10.1371/journal.pone.0072887

Wasaki J, Yonetani R, Kuroda S, Shinano T, Yazaki J, Fujii F, Shimbo K, Yamamoto K, Sakata K, Sasaki T, Kishimoto N, Kikuchi S, Yamagishi M, Osaki M (2003) Transcriptomic analysis of metabolic changes by phosphorus stress in rice plant roots. Plant Cell Environ **26**: 1515–1523

Yakhin OI, Lubyanov AA, Yakhin IA, Brown PH (2017) Biostimulants in plant science: a global perspective. Front Plant Sci. doi: 10.3389/fpls.2016.02049

Zanin L, Venuti S, Zamboni A, Varanini Z, Tomasi N, Pinton R (2017) Transcriptional and physiological analyses of Fe deficiency response in maize reveal the presence of *Strategy I* components and Fe/P interactions. BMC Genomics **18**: 154

Zhai G, Walters KS, Peate DW, Alvarez PJJ, Schnoor JL (2014) Transport of gold nanoparticles through plasmodesmata and precipitation of gold ions in woody poplar. Environ Sci Technol Lett **1**: 146–151

Zhang J, Liu B, Li M, Feng D, Jin H, Wang P, Liu J, Xiong F, Wang J, Wang H-B (2015) The bHLH transcription factor bHLH104 interacts with IAA-LEUCINE RESISTANT3 and modulates iron homeostasis in *Arabidopsis*. Plant Cell **27**: 787–805

Zhang T, Lu Y, Luo G (2013) Size adjustment of iron phosphate nanoparticles by using mixed acids. Ind Eng Chem Res **52**: 6962–6968

Zhang T, Xin D, Lu Y, Luo G (2014) Direct precipitation for a continuous synthesis of nanoiron phosphate with high purity. Ind Eng Chem Res **53**: 6723–6729

Zhou J, Jiao F, Wu Z, Li Y, Wang X, He X, Zhong W, Wu P (2008) *Os*PHR2 is involved in phosphate-starvation signaling and excessive phosphate accumulation in shoots of plants. Plant Physiol **146**: 1673–1686

Zocchi G, Cocucci S (1990) Fe uptake mechanism in Fe-efficient cucumber roots. Plant Physiol **92**: 908–911

ACKNOWLEDGEMENTS

This thesis, as all theses, is not only the result of individual experimental work, but also the result of the help of many people, without which this work would never have been accomplished as it is.
So, first, I would like to thank my Tutor, Prof. Zeno Varanini, for his guide and mentoring during these three years of PhD, and for critical thesis correction.
I also would like to thank Dr. Anita Zamboni, for her help in setting up experiments and guidelines in data analysis, and also her help in thesis correction.
A special thank goes also to FCP Cerea, for being framework of the Joint Project 2014 'UNIVR-FCP Cerea Nanofert' that I was enthusiastic to follow.
Thanks to Prof. Barbara Baldan (UNIPD) for her guide in TEM samples preparation, for TEM samples sectioning and TEM observations, and to UNIPD technicians.
I also would like to thank Prof. Flavia Guzzo, for her tips on roots sampling for TEM analysis.
I also thank Prof. Adolfo Speghini, for his tips and pieced of advice on nanostructures materials chemistry.
A thank goes also to Letizia, and Marelsa, that during their thesis and internship helped me performing experiments.
However, these three years of work were also full of lunches, coffee breaks and after-work moments full of exchanges of ideas, opinions, and joking, so thank to Paolo, Irene, Andrei, Simone, Daniele, Elisa, Giacomo, Flavio, Stefano, Lorenzo, Chiara, Marco, Mauro, Anna and Andrea, and all the people that I forgot to mention, but are also thanked.
Finally, I thank my family that supported me and encouraged me in the difficult moments of this path.

7 SUPPLEMENTARY TABLES AND FIGURES

Isotope	Element	Level 1	Level 2	Level 3	Level 4	Level 5	Level 6	Level 7	Level 8	Level 9	Level 10	Level 11	Level 12
11	**B**	0.2	0.4	0.8	1.6	3.2	6.4	12.8	25.6	51.2	102.4	204.8	409.6
23	**Na**	4	8	16	32	64	128	256	512	1024	2048	4096	8192
24	**Mg**	20	40	80	160	320	640	1280	2560	5120	10240	20480	40960
31	**P**	20	40	80	160	320	640	1280	2560	5120	10240	20480	40960
39	**K**	200	400	800	1600	3200	6400	12800	25600	51200	102400	204800	409600
44	**Ca**	100	200	400	800	1600	3200	6400	12800	25600	51200	102400	204800
55	**Mn**	0.4	0.8	1.6	3.2	6.4	12.8	25.6	51.2	102.4	204.8	409.6	819.2
56	**Fe**	0.5	1	2	4	8	16	32	64	128	256	512	1024
59	**Co**	0.01	0.02	0.04	0.08	0.16	0.32	0.64	1.28	2.56	5.12	10.24	20.48
63	**Cu**	0.05	0.1	0.2	0.4	0.8	1.6	3.2	6.4	12.8	25.6	51.2	102.4
66	**Zn**	0.2	0.4	0.8	1.6	3.2	6.4	12.8	25.6	51.2	102.4	204.8	409.6
78	**Se**	0.01	0.02	0.04	0.08	0.16	0.32	0.64	1.28	2.56	5.12	10.24	20.48
95	**Mo**	0.01	0.02	0.04	0.08	0.16	0.32	0.64	1.28	2.56	5.12	10.24	20.48

Table S1: Elemental composition of calibration curves points for ICP-MS analysis.

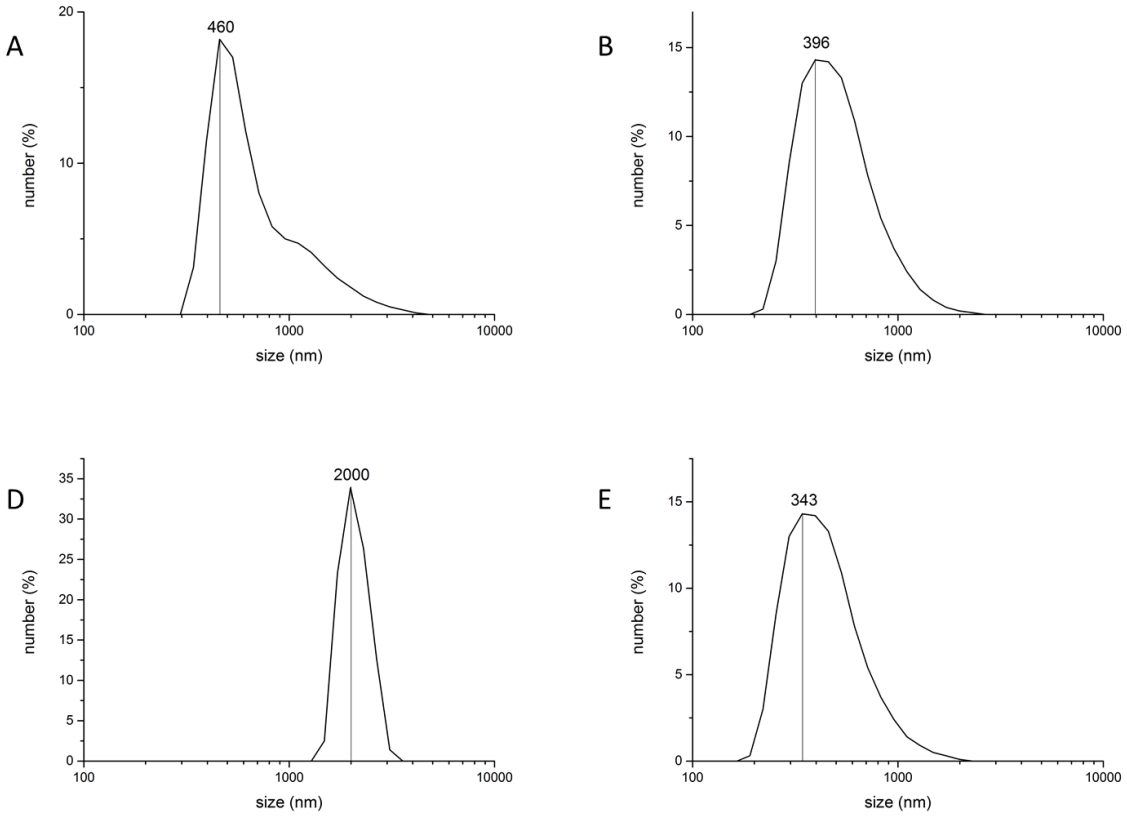

Figure S1: Particle size distribution plots for the sets of conditions A, B, D and E of batch synthesis.

Multi-elemental analysis of cucumber shoot

		C	-P	-P+NPs	-P+b
mg/gDW	Mg	7.23±0.78 a	7.50±1.51 a	7.20±0.72 a	7.36±0.80 a
	P	14.28±0.99 a	1.82±0.34 c	6.12±1.17 b	2.49±0.15 c
	K	54.19±7.13 ab	34.27±8.80 c	56.84±9.09 a	44.77±5.61 b
	Ca	61.98±4.85 a	56.77±11.00 ab	55.62±4.14 ab	50.43±3.11 b
µg/gDW	Mn	44.2±8.2 c	86.8±13.9 a	43.6±5.6 c	62.8±5.5 b
	Fe	182.3±39.0 a	211.4±74.4 a	204.8±106.9 a	255.6±55.4 a
	Cu	11.6±1.8 a	12.9±3.4 a	13.1±1.2 a	12.0±1.3 a
	Zn	100.5±13.1 a	66.8±16.0 bc	81.4±9.6 b	65.6±7.4 c

Table S2: Nutrients concentrations in plant tissues ± SD of three independent experiments with three plants (technical replicates) each. Lowercase letters indicate statistical significance of differences along the row determined with ANOVA (One-way ANOVA with Turkey's post hoc test, p<0.05).

		C	-Fe	-Fe+NPs	-Fe+b
mg/gDW	Mg	7.23±0.78 c	15.48±2.51 a	7.90±0.57 bc	9.35±0.50 b
	P	14.28±0.99 a	11.24±1.15 b	14.52±0.66 a	14.44±1.98 a
	K	54.19±7.13 ab	62.41±13.82 a	52.31±6.43 ab	51.24±4.53 b
	Ca	61.98±4.85 b	67.86±4.20 a	64.95±3.50 ab	67.23±4.69 ab
µg/gDW	Mn	44.2±8.2 c	257.1±76.3 a	72.7±15.2 c	132.7±18.7 b
	Fe	182.3±39.0 a	87.3±29.7 b	201.9±63.3 a	166.1±52.6 ab
	Cu	11.6±1.8 c	28.8±7.2 a	15.0±0.9 bc	18.2±3.0 b
	Zn	100.5±13.1 b	207.4±46.8 a	111.4±9.0 b	132.7±32.4 b

Table S3: Nutrients concentrations in plant tissues ± SD of three independent experiments with three plants (technical replicates) each. Lowercase letters indicate statistical significance of differences along the row determined with ANOVA (One-way ANOVA with Turkey's post hoc test, p<0.05).

		C	-P-Fe	-P-Fe+NPs	-P-Fe+b
mg/gDW	Mg	7.23±0.78 b	13.85±0.92 a	7.35±1.00 b	7.47±0.57 b
	P	14.28±0.99 a	2.20±0.26 c	4.67±0.78 b	2.11±0.18 c
	K	54.19±7.13 a	48.83±4.89 a	51.55±11.83 a	35.59±4.93 b
	Ca	61.98±4.85 ab	60.98±4.60 ab	58.62±7.41 b	64.72±6.86 a
µg/gDW	Mn	44.2±8.2 c	304.7±56.5 a	75.2±15.2 c	114.3±14.9 b
	Fe	182.3±39.0 a	92.6±34.5 c	137.6±32.9 b	125.2±24.5 bc
	Cu	11.6±1.8 c	30.4±2.8 a	15.6±2.6 b	18.2±1.5 b
	Zn	100.5±13.1 b	193.1±37.7 a	87.3±12.8 b	92.3±10.0 b

Table S4: Nutrients concentrations in plant tissues ± SD of three independent experiments with three plants (technical replicates) each. Lowercase letters indicate statistical significance of differences along the row determined with ANOVA (One-way ANOVA with Turkey's post hoc test, p<0.05).

Multi-elemental analysis of cucumber root

		C	-P	-P+NPs	-P+b
mg/gDW	Mg	2.77±0.42 a	2.68±0.23 a	2.78±0.53 a	2.95±0.50 a
	P	8.22±0.87 c	2.00±0.19 a	6.20±1.84 b	4.69±1.83 b
	K	101.02±14.12 a	92.52±4.27 a	99.40±16.44 a	102.72±22.50 a
	Ca	7.65±1.64 a	8.06±1.12 a	7.81±1.56 a	7.64±1.41 a
µg/gDW	Mn	17.0±5.2 b	80.1±22.0 a	25.8±17.7 b	35.2±13.2 b
	Fe	1188±224 a	1234±245 a	9463±4031 c	5972±2359 b
	Cu	12.7±7.2 a	13.0±4.2 a	15.4±5.2 a	14.0±3.2 a
	Zn	132.5±43.6 a	70.8±14.1 b	119.5± 62.4 ab	94.5±38.4 ab

Table S5: Nutrients concentrations in plant tissues ± SD of three independent experiments with three plants (technical replicates) each. Lowercase letters indicate statistical significance of differences along the row determined with ANOVA (One-way ANOVA with Turkey's post hoc test, p<0.05).

		C	-Fe	-Fe+NPs	-Fe+b
mg/gDW	Mg	2.77±0.42 a	2.46±0.67 a	2.80±0.36 a	2.72±0.62 a
	P	8.22±0.87 a	6.61±0.97 a	9.42±3.03 a	8.87±4.25 a
	K	101.02±14.12 ab	77.62±7.67 b	113.07±21.18 a	104.6±31.04 a
	Ca	7.65±1.64 a	9.60±2.80 a	8.03±1.43 a	8.41±1.33 a
µg/gDW	Mn	17.0±5.2 c	48.9±26.4 b	35.4±14.3 bc	86.8±39.6 a
	Fe	1188±224 bc	114±73 c	8109±2712 a	3070±2060 b
	Cu	12.7±7.2 c	399.2±195.7 a	53.9±21.4 bc	175.3±65.1 b
	Zn	132.5±43.6 b	543.9±242.8 a	179.1±60.3 b	378.8±109.9 a

Table S6: Nutrients concentrations in plant tissues ± SD of three independent experiments with three plants (technical replicates) each. Lowercase letters indicate statistical significance of differences along the row determined with ANOVA (One-way ANOVA with Turkey's post hoc test, p<0.05).

		C	-P-Fe	-P-Fe+NPs	-P-Fe+b
mg/gDW	Mg	2.77±0.42 a	2.88±1.56 a	2.71±0.35 a	2.77±0.72 a
	P	8.22±0.87 a	5.09±3.30 bc	6.84±1.34 ab	3.61±1.00c
	K	101.02±14.12 a	104.91±45.43 a	98.24±16.30 a	95.19±25.84 a
	Ca	7.65±1.64 a	10.28±2.81 b	8.07±1.69 ab	7.07±1.53 a
µg/gDW	Mn	17.0±5.2 b	116.9±61.8 a	31.0±9.1 b	88.1±18.5a
	Fe	1188±224 b	106±34 b	8109±2712 a	2918±1321 b
	Cu	12.7±7.2 b	236.4±119.3 a	62.3±29.2 b	87.2±39.4 b
	Zn	132.5±43.6 b	481.0±204.6 a	181.2±70.5 b	200.6±53.4 b

Table S7: Nutrients concentrations in plant tissues ± SD of three independent experiments with three plants (technical replicates) each. Lowercase letters indicate statistical significance of differences along the row determined with ANOVA (One-way ANOVA with Turkey's post hoc test, p<0.05).

Multi-elemental analysis of maize shoot

		C	-P	-P+NPs	-P+b
mg/gDW	Mg	2.92±0.18 a	2.54±0.21 b	2.74±0.23 ab	2.40±0.20 bc
	P	11.32±2.19 a	2.09±0.40 b	3.36±0.45 b	2.13±0.44 b
	K	92.05±9.69 a	81.65±8.34 a	82.60±5.42 a	84.37±11.76 a
	Ca	6.50±0.53 b	6.15±0.51 b	7.12±0.65 a	6.40±0.83 ab
µg/gDW	Mn	55.2±9.4 a	48.2±10.6 ab	47.7±5.0 ab	43.8±8.1 b
	Fe	134.0±12.5 b	148.1±26.8 b	251.4±65.9 a	176.4±65.5 b
	Cu	11.3±3.4 a	9.9±1.8 a	8.9±0.8 a	10.0±2.8 a
	Zn	75.5±13.4 a	78.5±16.1 a	75.2±11.3 a	75.5±19.4 a

Table S8: Nutrients concentrations in plant tissues ± SD of three independent experiments with three plants (technical replicates) each. Lowercase letters indicate statistical significance of differences along the row determined with ANOVA (One-way ANOVA with Turkey's post hoc test, p<0.05).

		C	-Fe	-Fe+NPs	-Fe+b
mg/gDW	Mg	2.92±0.18 b	3.59±0.47 a	3.03±0.31 b	3.31±0.40 ab
	P	11.32±2.19 a	17.01±2.93 b	9.65±1.65 a	11.40± 1.85 a
	K	92.05±9.69 a	87.84±11.17 a	87.84±9.81 a	86.72±10.2 a
	Ca	6.50±0.53 b	8.84±1.81 a	6.24±0.61 b	6.83±0.86 b
µg/gDW	Mn	55.2±9.4 c	133.4±22.6 a	59.6±9.0 c	86.0±9.9 b
	Fe	134.0±12.5 a	54.6±14.6 d	97.5±11.9 b	76.3±14.6 c
	Cu	11.3±3.4 c	25.2±4.3 a	15.0±1.9 c	21.0±2.9 b
	Zn	75.5±13.4 c	302.5±83.0 a	107.0±17.1 c	171.1±29.0 b

Table S9: Nutrients concentrations in plant tissues ± SD of three independent experiments with three plants (technical replicates) each. Lowercase letters indicate statistical significance of differences along the row determined with ANOVA (One-way ANOVA with Turkey's post hoc test, p<0.05).

		C	-P-Fe	-P-Fe+NPs	-P-Fe+b
mg/gDW	Mg	2.92±0.18 b	3.43±0.46 a	2.52±0.20 c	2.42±0.23 c
	P	11.32±2.19 a	3.87±0.60 b	3.30±0.51 bc	2.02±0.64 c
	K	92.05±9.69 a	90.45±10.97 a	80.82±9.97 a	79.07±15.65 a
	Ca	6.50±0.53 b	7.72±1.15 a	5.95±0.58 b	5.76±0.68 b
µg/gDW	Mn	55.2±9.4 b	153.7±27.1 c	57.2±13.9 b	59.2±10.7 b
	Fe	134.0±12.5 a	56.6±21.0 c	120.7±56.0 ab	85.4±6.8 bc
	Cu	11.3±3.4 b	25.8±7.0 a	13.2±1.3 b	13.1±1.6 b
	Zn	75.5±13.4 c	316.3±53.3 a	104.2±10.1 bc	114.4±9.7 b

Table S10: Nutrients concentrations in plant tissues ± SD of three independent experiments with three plants (technical replicates) each. Lowercase letters indicate statistical significance of differences along the row determined with ANOVA (One-way ANOVA with Turkey's post hoc test, p<0.05).

Multi-elemental analysis of maize roots

		C	-P	-P+NPs	-P+b
mg/gDW	Mg	2.69±0.46 b	2.94±0.46 ab	2.63±0.37 b	3.35±0.40 a
	P	3.74±0.79 a	1.37±0.34 c	2.94±0.54 b	1.65±0.44 c
	K	46.12±5.98 a	40.20±8.23 ab	37.30±4.40 b	37.06±4.18 b
	Ca	8.19±1.43 a	7.39±1.30 a	6.67±1.37 a	6.76±0.86 a
µg/gDW	Mn	350±088 a	250±45 b	254±43 b	239±65 b
	Fe	1031±435 b	810 ±163 b	6198±1345 a	1884±0.994 b
	Cu	28.1±20.1 a	14.6±3.3 ab	13.1±1.2 b	19.5±6.6 ab
	Zn	158.2±24.1 a	205.8±39.0 a	193.6±59.0 a	196.3±63.1 a

Table S11: Nutrients concentrations in plant tissues ± SD of three independent experiments with three plants (technical replicates) each. Lowercase letters indicate statistical significance of differences along the row determined with ANOVA (One-way ANOVA with Turkey's post hoc test, p<0.05).

		C	-Fe	-Fe+NPs	-Fe+b
mg/gDW	Mg	2.69±0.46 c	4.52±0.60 a	3.39±0.29 b	4.46±0.29 a
	P	3.74±0.79 b	5.25±1.05 a	4.15±0.58 ab	4.60±1.15 ab
	K	46.12±5.98 a	50.40±7.90 a	46.03±5.55 a	47.85±5.09 a
	Ca	8.19±1.43 a	8.18±1.36 a	8.84±1.13 a	8.87±1.12 a
µg/gDW	Mn	350±88 a	230±31 b	209±36 b	193±36 b
	Fe	1031 ±435 b	65±42 c	2263±765 a	351±127 c
	Cu	28.1±20.1 d	235.8±27.1 a	80.9±14.5c	147.6±22.1 b
	Zn	158.2±24.1 b	276.9±46.9 a	208.2±41.8 b	190.1±71.1 b

Table S12: Nutrients concentrations in plant tissues ± SD of three independent experiments with three plants (technical replicates) each. Lowercase letters indicate statistical significance of differences along the row determined with ANOVA (One-way ANOVA with Turkey's post hoc test, p<0.05).

		C	-P-Fe	-P-Fe+NPs	-P-Fe+b
mg/gDW	Mg	2.69±0.46 b	4.34±0.83 a	3.28±0.33 b	3.25±0.38 b
	P	3.74±0.79 a	1.65±0.35 c	2.39±0.28 b	1.64±0.38 c
	K	46.12±5.98 ab	48.73±6.06 a	43.75±6.15 ab	40.97±5.42 b
	Ca	8.19±1.43 a	7.07±1.38 a	8.09±0.94 a	7.34±1.16 a
µg/gDW	Mn	350±88 a	230±35 b	191±28 b	209±31 b
	Fe	1031±435 b	138±0.86 c	3004±517 a	744±346 b
	Cu	28.1±20.1 d	244.0±32.6 a	64.1±8.3 c	121.9±16.9 b
	Zn	158.2±24.1 c	267.2±62.3 a	236.7±51.8 ab	192.0±33.6 bc

Table S13: Nutrients concentrations in plant tissues ± SD of three independent experiments with three plants (technical replicates) each. Lowercase letters indicate statistical significance of differences along the row determined with ANOVA (One-way ANOVA with Turkey's post hoc test, p<0.05).

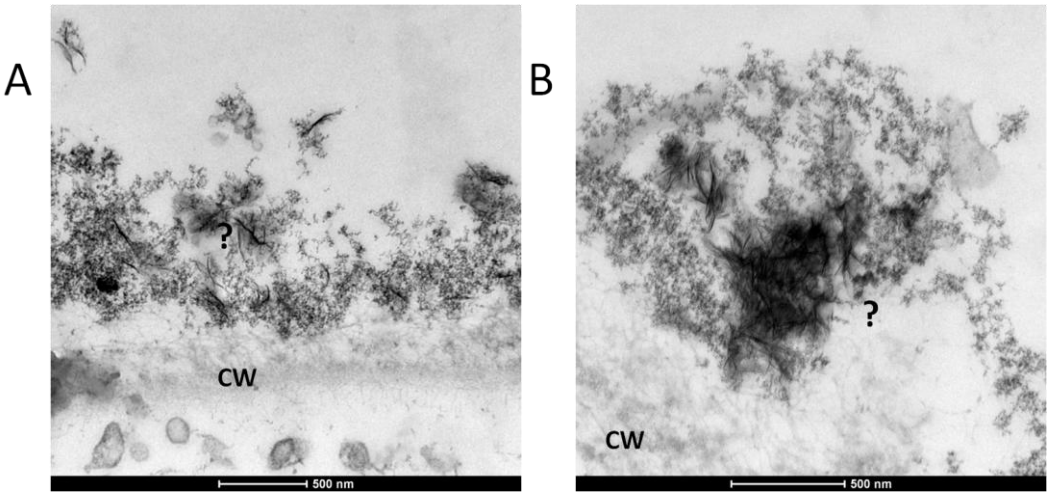

Figure S2: TEM observation of a cross section of a cucumber plant grown with $FePO_4$ NPs as P source. CW: cell wall; ?: unexpected and unknown nano-sized black laths.

ESEM-EDAX analysis of –P+NPs treated cucumber roots, Report S1

EXAD TEAM

Area 1

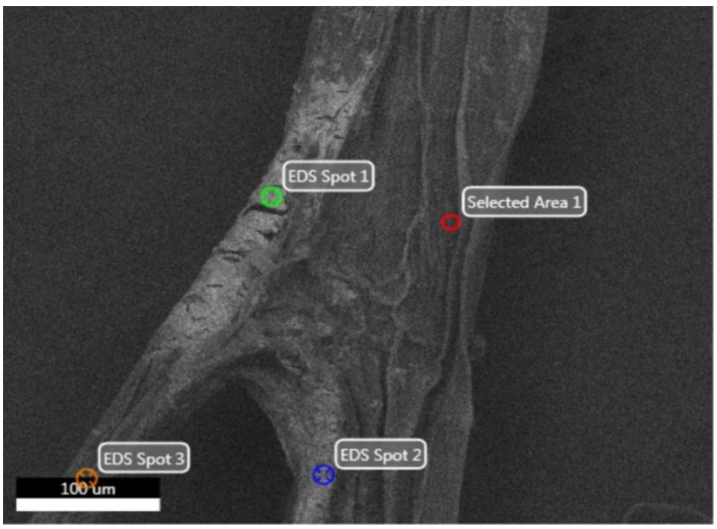

kV: 20	Mag: 300	Takeoff: 48.7	Live Time(s): 48.4	Amp Time(μs): 7.68	Resolution (eV): 129.3

Selected Area 1

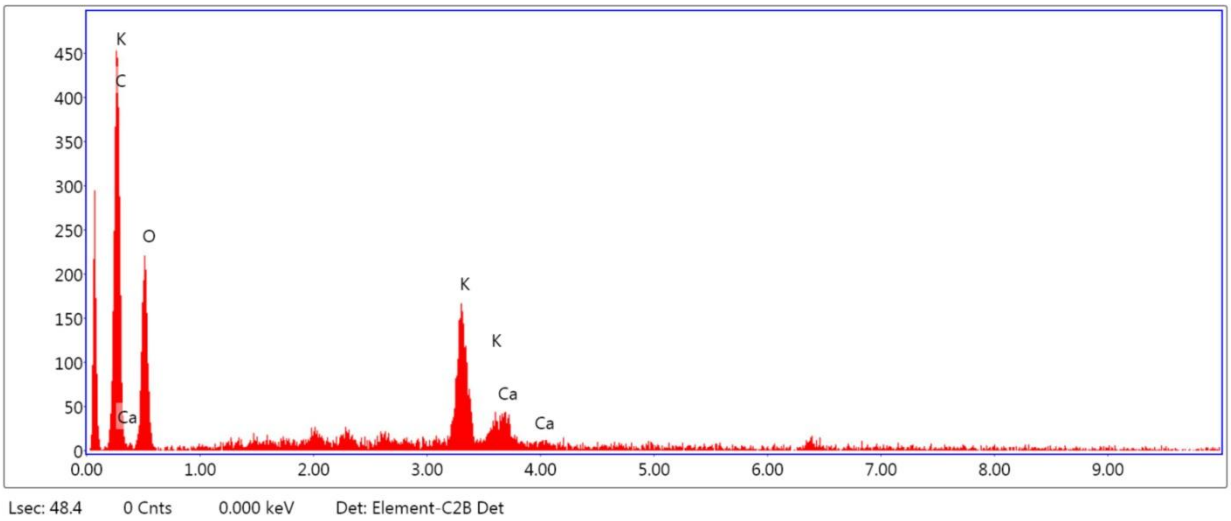

eZAF Smart QuantResult

Element	Weight %	Atomic %	Net Int.	Error %	Kratio	Z	R	A	F
C K	32.79	45.15	47.88	7.75	0.2049	1.0624	0.9643	0.5879	1.0000
O K	43.37	44.83	27.78	12.63	0.0759	1.0170	0.9851	0.1721	1.0000
K K	17.46	7.38	37.11	4.80	0.1557	0.8578	1.0569	1.0119	1.0271
CaK	6.38	2.63	10.62	9.28	0.0540	0.8734	1.0612	0.9538	1.0153

kV: 20	Mag: 300	Takeoff: 48.7	Live Time(s): 48.4	Amp Time(μs): 7.68	Resolution (eV): 129.3

EDS Spot 1

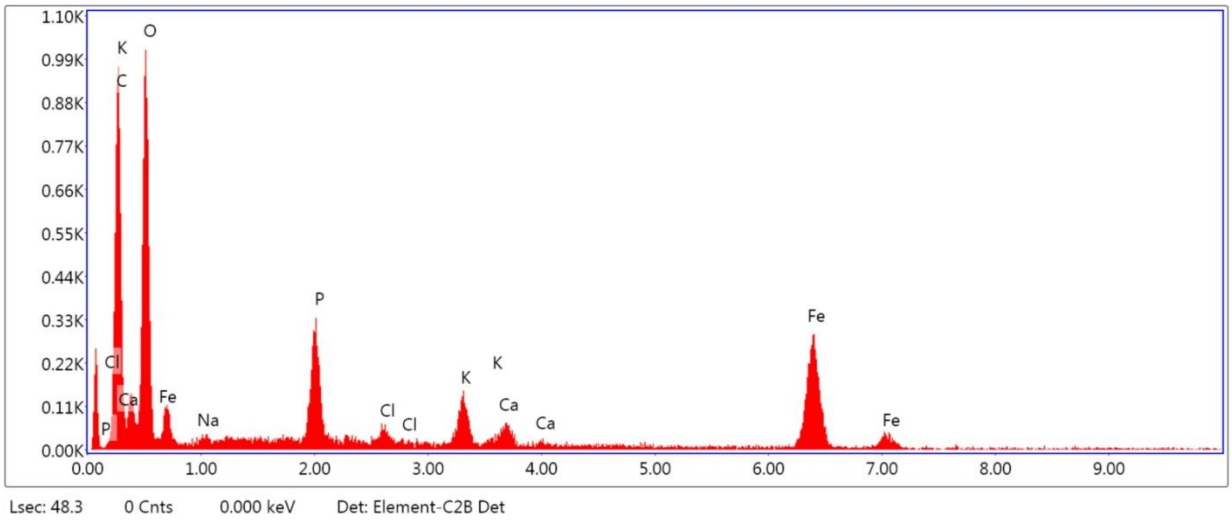

eZAF Smart QuantResult

Element	Weight %	Atomic %	Net Int.	Error %	Kratio	Z	R	A	F
C K	27.46	43.29	75.31	12.35	0.0886	1.1024	0.9409	0.2926	1.0000
O K	34.59	40.93	132.56	9.62	0.0996	1.0570	0.9631	0.2725	1.0000
NaK	1.03	0.85	4.05	27.10	0.0031	0.9620	0.9900	0.3142	1.0021
P K	5.66	3.46	54.48	5.71	0.0438	0.9265	1.0187	0.8250	1.0126
ClK	0.85	0.45	7.75	21.13	0.0072	0.8994	1.0308	0.9088	1.0292
K K	3.23	1.56	25.46	10.82	0.0294	0.8956	1.0416	0.9663	1.0516
CaK	1.73	0.81	11.66	17.13	0.0163	0.9122	1.0465	0.9718	1.0659
FeK	25.46	8.63	77.33	4.15	0.2173	0.8147	1.0680	1.0071	1.0403

kV: 20	Mag: 300	Takeoff: 48.7	Live Time(s): 48.4	Amp Time(μs): 7.68	Resolution (eV): 129.3

EDS Spot 2

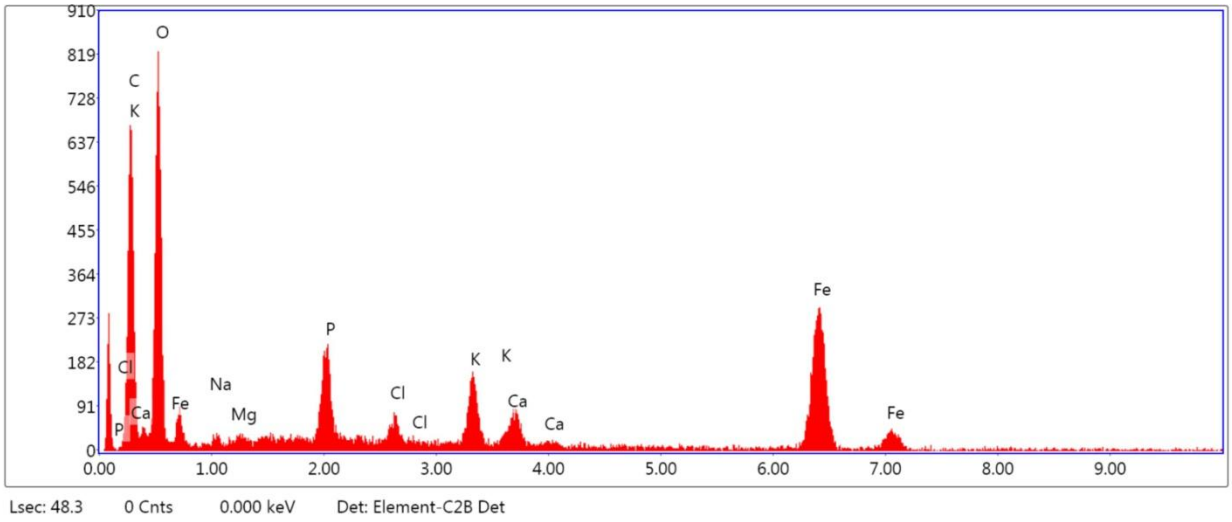

eZAF Smart QuantResult

Element	Weight %	Atomic %	Net Int.	Error %	Kratio	Z	R	A	F
C K	23.10	39.94	54.24	11.50	0.0723	1.1243	0.9283	0.2784	1.0000
O K	30.19	39.19	103.63	9.82	0.0882	1.0788	0.9512	0.2709	1.0000
NaK	0.90	0.82	2.98	33.04	0.0026	0.9825	0.9790	0.2930	1.0020
MgK	0.42	0.36	2.50	44.35	0.0018	1.0000	0.9871	0.4336	1.0036
P K	4.64	3.11	39.19	6.55	0.0357	0.9470	1.0088	0.8011	1.0137
ClK	1.42	0.83	11.52	18.12	0.0121	0.9195	1.0215	0.8995	1.0312
K K	4.42	2.35	31.28	8.47	0.0409	0.9158	1.0328	0.9585	1.0536
CaK	2.83	1.47	17.10	11.59	0.0271	0.9329	1.0380	0.9616	1.0657
FeK	32.08	11.93	87.39	3.67	0.2782	0.8338	1.0614	1.0036	1.0361

kV: 20	Mag: 300	Takeoff: 48.7	Live Time(s): 48.4	Amp Time(μs): 7.68	Resolution (eV): 129.3

EDS Spot

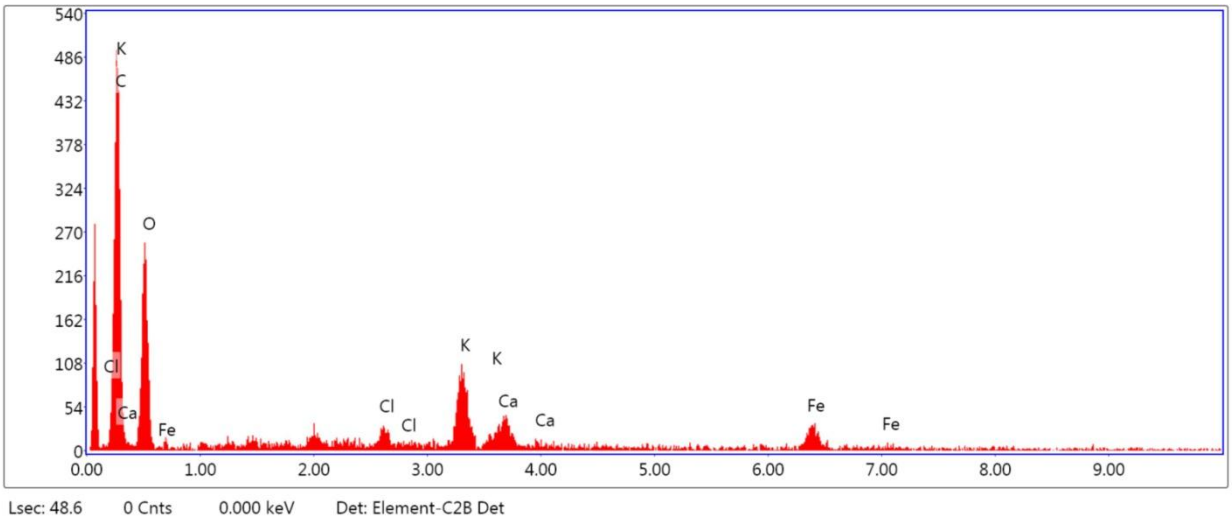

eZAF Smart QuantResult

Element	Weight %	Atomic %	Net Int.	Error %	Kratio	Z	R	A	F
C K	38.44	52.53	52.13	8.87	0.1906	1.0656	0.9613	0.4654	1.0000
O K	37.59	38.56	32.04	12.17	0.0748	1.0204	0.9823	0.1952	1.0000
ClK	1.39	0.64	4.24	26.87	0.0122	0.8654	1.0452	0.9700	1.0439
K K	8.90	3.73	22.20	6.71	0.0796	0.8614	1.0550	0.9995	1.0392
CaK	4.39	1.80	8.94	11.23	0.0388	0.8772	1.0594	0.9756	1.0339
FeK	9.30	2.73	8.87	11.61	0.0774	0.7824	1.0779	1.0054	1.0586